Radiation-matter oscillations and spectral line narrowing in field-correlated four-wave mixing. I. Theory

M. A. Dugan and A. C. Albrecht
Department of Chemistry, Baker Laboratory, Cornell University, Ithaca, New York 14853-1301
(Received 11 May 1990)

The theoretical basis for new signal transients and spectral features generated in field-correlated four-wave mixing spectroscopies is developed. Special attention is given to those signal responses that are sensitive to phase or amplitude correlation among the input driving fields, and not simply their intensity correlation. Thus the cases of incoherent broadband excitation and of coherent short-pulsed excitation will be discussed and compared. Applications to the coherent Raman spectroscopies, both electronically nonresonant and full resonant, are analyzed. Novel interferometric oscillatory behavior is exposed in terms of radiation-matter detuning beats and matter-matter bilevel and trilevel quantum beats. In addition, new resonances are found that have submaterial linewidths and detuning parameters that lock onto the mode frequency of the driven chromophore. These spectral features are members of a class of bichromophore resonant line shapes arising from nonlinear mixing with correlated driving fields. Analytic results are presented and modeled to anticipate experimental results presented in the following paper [Phys. Rev. A **43**, 3922 (1991)].

INTRODUCTION

Four-wave mixing (4WM) spectroscopies prove to be a versatile probe of molecular spectra and dynamics in both the condensed and the gas phase.[1-11] Actually at the signal level 4WM is an eight-field mixing process involving four conjugate field pairs (four photons). In general, for arbitrary weak $n+1$ wave mixing, there are $n!2^n$ channels, variously resonant, that together generate the macroscopic polarization, so that a given measured response may reflect complicated interferences among these different amplitude components and, accordingly, be rich in information. At the same time, the amplitude and phase properties of the fields that are being mixed by a nonlinear medium are influential in determining the response. Ultrashort coherent light pulses and long, incoherent, light pulses have been used in several laboratories to record transient oscillatory behavior, as well as sharp spectral features, in various 4WM measurements. Damped sum and difference beating has been seen involving purely material oscillators,[7,12-18] purely radiation oscillators,[7,19,21] and hybrid radiation-matter oscillators.[19-24] Their proper interpretation can provide new insight into the nonlinear mixing process and the associated material relaxation dynamics.

Considerable theoretical work exists regarding material relaxation on short-time scales and how the amplitude and phase properties of the driving fields can expose and even influence such dynamics.[25-35] In one extreme, transform limited (coherent) fields are used to permit easy deconvolution from the signal of the purely field-dependent contribution (the coherent peak). A more refined approach consists of careful phase and amplitude tailoring of optical pulses to enhance certain nonlinear cross sections, while suppressing others, leading to a more easily interpretable material response.[36-38] At the other extreme, much effort, both in theory and experiment, has been given to the understanding of nonlinear optical processes driven by incoherent excitation fields. Such noise fields, characterized by a time-bandwidth product that is orders of magnitude greater than the theoretical bandwidth limit, have been shown capable of sub-pulse-width timing (with accumulation) in various optical mixing experiments.[39-42] Incoherent excitation introduces new resonances as well as additional broadening mechanisms not seen with coherent (transform limited) fields.[24,43-45]

4WM and related nonlinear optical techniques, so valuable in probing the fundamentals of radiation-matter interaction, also offer great potential for applications in the area of optical data processing, storage, and retrieval.[46] Of particular importance in communications technology is the application of such phase-sensitive nonlinear processes in the generation of squeezed states of the radiation field.[47-49] Thus the development of theoretical models consistent with experimental results, in whatever context, can only improve nonlinear optical processes as analytic techniques and facilitate in the design of integrated optical circuitry.

Recently a subclass of new 4WM transients has been reported from this laboratory[23] in coherent Raman spectroscopies [both Stokes, coherent Stokes Raman scattering (CSRS), and anti-Stokes, coherent anti-Stokes Raman scattering (CARS) processes] using incoherent light. In these experiments two incoherent nanosecond light beams, derived from a single broadband dye laser pulse, are relatively delayed by time τ, and then simultaneously mixed in a nonlinear medium with a tunable narrow-band field. The narrow-band field is displaced in frequency from that of the broadband fields by an amount that corresponds to a near-resonant Raman vibration. Strong terahertz oscillations appear in the interferogram as long as the CSRS or the CARS fourth wave, as well as the narrow-band input field, are kept spectrally sharp to well

within the Raman linewidth. In this limit, these radiation-matter detuning oscillations carry both precise vibrational memory and Raman frequency information. In the present work (I), we present the general basis in theory of these new signal responses. The setting is within a general perturbative treatment of three-color 4WM interferometry in which the fields may be arbitrarily phase or amplitude correlated, but where the "chromophores" (our basic scattering unit) are uncoupled in their absence. The previous analysis[23] is generalized here to include fully resonant scattering in mixtures of chromophores possessing different Bohr frequencies and linewidths. The theory is also extended to include finite-bandwidth effects for all of the intervening fields. For a system of closely spaced electronic or vibrational resonances that are spectrally embraced by the broadband field, the signals vary with τ as a superposition of detuning oscillations, each detuned from a given Bohr frequency and damped by the corresponding dephasing time. By increasing the bandwidth of the signal field or the nondegenerate field, these individual transients damp more quickly in τ, giving rise to a much attenuated oscillatory behavior that reflects interferences between inter- and intrachromophore states as well as other detuning beats. Such oscillations are seen to decay in time with an effective dephasing rate characterized by the coherence loss of all the superposed material and radiation modes.

For the case of incoherent excitation in the coherent Raman spectroscopies, predictions are made of new spectral features having sub-Raman linewidths and which at the same time precisely identify the Raman mode frequencies of the chromophore(s). The realization of such resonances, both in the electronic ground and electronic excited states, will make possible a particularly accurate decoding of complex multicomponent lines into their individual frequency components. At present, experimental verification of such narrowed resonances has been obtained for ground-state coherent Raman scattering. This is reported in the following paper, II, where other examples of the new radiation-matter features predicted in this theory are given.

This paper is organized as follows. A general theoretical development of parametric 4WM will be outlined in Sec. I. We leave the reader with abundant (though incomplete) references to the literature for details. The 4WM signal transients presented here are in some sense weak-field Rabi oscillations. Therefore, to simplify the theoretical development, a perturbative approach, with respect to the matter-radiation coupling, will be used. The nonconservation of the trace of the density matrix, usually characteristic of a perturbation approach, can lead to artifacts.[50] The signal features discussed here survive this approximation, for they are confirmed experimentally. Strong-field effects, although interesting, are not essential to the interpretation of these signals. Recently, Stehle[51] has given a generalized quantum-mechanical account of Rabi oscillatory behavior showing its occurrence at all orders in the matter-radiation interaction.

In Sec. II, the dependence of the susceptibilities on the coherent properties of the input fields will be discussed, distinguishing between the two cases of coherent and incoherent excitation, the former referring to fields whose coherence time closely resembles the pulse width. Time-domain interferometry with coherent driving fields allows for a distinct time ordering between the exciting and probing steps in the evolution of the scattering amplitudes (the polarization amplitudes). Measurements with incoherent light, however, involve interferometric delays greater than the coherence times, which are typically 100–200 fs, but much less than the pulse widths, which are typically 10 ns, offering a sensitivity for accumulated material responses over a large dynamic range.

Analytic applications of the theory to both electronically resonant and nonresonant coherent Raman scattering in Sec. III is followed in Sec. IV by model calculations and a brief discussion of the physics that underlies the theory. In light of this discussion, other closely related 4WM spectroscopies will be considered. Experimental methods and results will be presented in the following paper (II) where the merits of these experiments for probing condensed-phase dynamics are illustrated and discussed.

I. COHERENT 4WM SCATTERING WITH LIGHT HAVING ARBITRARY PHASE AND AMPLITUDE PROPERTIES

The perturbative theory of four-wave mixing is taken from its most general starting point at eighth order in fields, including detection, to a form that is suitable for discussing 4WM scattering from spatially uncorrelated chromophores. Thus phase-matched scattering involving as many as eight chromophores (Sec. I A) is reduced, in Sec. I B, to a "bichromophore" model applicable to 4WM in an amorphous sample of uncoupled chromophores which are pairwise phase and amplitude dressed by the driving fields.

A. Parametric four-photon processes with detection

Here we outline the theory of interferometric measurements in different 4WM spectroscopies. The aim is to expose the effects of field correlation in such experiments. In general, weak-field four-photon processes such as 4WM with spatial and temporal correlation among the chromophores appears at eighth order in the radiation-matter interaction operators.[52,53] Initially, the signal can be written as

$$S^{(8)}=\mathrm{Tr}[\hat{S}\,\hat{\rho}^{(8)}(t)]\ , \tag{1.1}$$

where $\hat{S}$, an operator representing the measurement process, is given by

$$\hat{S}=\frac{d\hat{N}_D}{dt}=i[\hat{N}_D,\hat{H}]\ . \tag{1.2}$$

$\hat{N}_D$ is written as a normal ordering of the detector creation annihilation operators representing a photocount at time t,[54]

$$\hat{N}_D = \sum_{\alpha_D} \hat{b}^{\dagger}_{\alpha_D} \hat{b}_{\alpha_D} \ . \tag{1.3}$$

Here α_D and D represent the active absorbers of the detector and the detected field mode(s), respectively. This field is derived from the generated signal field which is given as a superposition of individual signal fields S, each originating on a given chromophore α_S ($\tilde{V}^{\pm}_S = \sum_{\alpha_S} \tilde{V}^{\pm}_{\alpha_S}$). The total Hamiltonian in Eq. (1.2) can be partitioned as $\hat{H} = \hat{H}_M + \hat{H}_B + \hat{H}_R + \hat{H}_D + \tilde{H}_{MB} + \tilde{H}_{MR} + \hat{H}_{DR}$, where $\hat{H}_M$, $\hat{H}_B$, $\hat{H}_R$, and $\hat{H}_D$ represent the chromophore, bath, radiation, and detector Hamiltonians, respectively. Coupling between the chromophore-bath and chromophore-radiation subspaces is determined by the stochastic interaction Hamiltonians $\tilde{H}_{MB}$ and $\tilde{H}_{MR}$. Projection of the modes of the signal subspace onto the detector subspace is accomplished by the Hamiltonian $\hat{H}_{DR}$. In the dipole approximation, $\tilde{H}_{MR}$ can be written as

$$\tilde{H}_{MR}(t) = \sum_{\lambda,\alpha_\lambda} [\tilde{V}^{+}_{\alpha_\lambda}(t) + \tilde{V}^{-}_{\alpha_\lambda}(t)] \ , \tag{1.4}$$

where (in Hz)

$$\begin{aligned} \tilde{V}^{+}_{\alpha_\lambda}(t) &= \left[iC_\lambda \left[\sum_{\zeta=\pm} \hat{\boldsymbol{\mu}}_{\alpha_\lambda} \cdot \mathbf{e}^{\zeta}_{\lambda} \right] \hat{a}_\lambda \right] \tilde{E}_\lambda(\mathbf{r}_{\alpha_\lambda}, t) e^{i(\mathbf{k}_\lambda \cdot \mathbf{r}_{\alpha_\lambda} - \omega_\lambda t)} \\ &= \hat{v}^{+}_{\alpha_\lambda} E^0_\lambda \tilde{\epsilon}_\lambda(\mathbf{r}_{\alpha_\lambda}, t) e^{i(\mathbf{k}_\lambda \cdot \mathbf{r}_{\alpha_\lambda} - \omega_\lambda t)} \ , \\ C_\lambda &= \left[\frac{\omega_\lambda}{2\epsilon_0 \hbar L^3} \right]^{1/2} \ , \end{aligned} \tag{1.5}$$

with $\tilde{V}^{-}_{\alpha_\lambda} = (\tilde{V}^{+}_{\alpha_\lambda})^{\dagger}$. In general, α_λ associates field λ with chromophore α, located at the vector position $\mathbf{r}_{\alpha_\lambda}$. The dipole operator for chromophore α_λ is $\hat{\boldsymbol{\mu}}_{\alpha_\lambda}$ and $\hat{a}_\lambda$ ($\hat{a}^{\dagger}_\lambda$) is the annihilation (creation) operator for the λth radiation mode. Box normalization is assumed and a sum over the two possible polarization states of a given field, unit vector $\mathbf{e}^{\zeta}_{\lambda}$ with $\zeta = \pm$, is indicated. Partitioning of the radiation-matter interaction into an operator part $\hat{v}^{\pm}_{\alpha_\lambda}$, a dimensioned field strength constant E^0_λ, a dimensionless stochastic space-time field function $\tilde{\epsilon}_\lambda(r_{\alpha_\lambda}, t)$, and a rapidly oscillating space-time phase factor is done to aid in the following theoretical development. The sum over λ in Eq. (1.4) consists of the three input modes ($\lambda = 1,2,3$) and the generated signal mode(s) S. Similar to Eq. (1.5), we can construct the photocathode detector field operator (the case $\lambda = D$), $\hat{H}_{DR} = \hat{V}^{+}_D + \hat{V}^{-}_D$. Here the chromophore dipole operator $\hat{\boldsymbol{\mu}}_{\alpha_\lambda}$ is replaced with the corresponding operator for the detector absorbers (photocathode) $\hat{\boldsymbol{\mu}}_{\alpha_D}$, assumed linear in the $\hat{b}_{\alpha_D}$ and $\hat{b}^{\dagger}_{\alpha_D}$ operators. In the simplest case, the detected field states can be considered to be a subset of the states defining the generated multimode signal field. In the general case, the detected field may be derived from the generated signal field through arbitrary mode conversion (e.g., frequency conversion with a gating field). Now Eq. (1.1) with Eqs. (1.2) and (1.3) (using $[\hat{b}_{\alpha_D}, \hat{b}^{\dagger}_{\alpha'_D}] = \delta_{\alpha_D \alpha'_D}$) gives

$$S^{(8)} = \mathrm{Tr}_{M,R,B,D} \left[\sum_{\alpha_D} (\hat{V}^{+}_{\alpha_D} - \hat{V}^{-}_{\alpha_D}) \hat{\rho}^{(8)}(t) \right] . \tag{1.6}$$

Generally, the detector field is derived from the generated signal field through use of the convolution theorem. This convolution is most naturally considered in the nonlinear response function developed below. $\hat{V}^{\pm}_{\alpha_D}$ can be written

$$\hat{V}^{\pm}_{\alpha_D} = \hat{v}^{\pm}_{\alpha_D} E^0_D \tilde{\epsilon}_D(\mathbf{r}_{\alpha_D}, t) e^{\pm i(\mathbf{k}_D \cdot \mathbf{r}_{\alpha_D} - \omega_D t)} \ , \tag{1.7}$$

where the field dependence of the operator $\hat{V}^{\pm}_{\alpha_D}$ contains products of the form $\hat{a}_D(\hat{a}_S + \hat{a}^{\dagger}_S)$ and its adjoint.

Using nonlinear response theory, the density operator, eighth order in the field-matter interaction $\tilde{H}_{MR}$ (for $\lambda = 1$, 2, 3, and S), can be written as

$$\hat{\rho}^{(8)}(t) = \int_{-\infty}^{t} dt_1 \int_{-\infty}^{t_1} dt_2 \cdots \int_{-\infty}^{t_7} dt_8 \hat{G}(t,t_1) \tilde{L}_{MR}(t_1) \hat{G}(t_1,t_2) \tilde{L}_{MR}(t_2) \cdots \hat{G}(t_7,t_8) \tilde{L}_{MR}(t_8) \hat{G}(t_8, -\infty) \hat{\rho}(-\infty) \ , \tag{1.8}$$

Here use is made of the Liouville notation.[55] The tetradic propagator $\hat{G}$ and the interaction Liouvillians $\tilde{L}_{MR}$ and $\hat{L}_{DR}$ are given as

$$\hat{G}(t_m, t_n) = \mathbf{T} \exp \left[-i \int_{t_n}^{t_m} dt' [\hat{L}_0 + \tilde{L}_{MB}(t') + \hat{L}_{DR}(t')] \right] , \tag{1.9}$$

$$\tilde{L}_{MR}(t) = [\tilde{H}_{MR}(t), \cdot] \ , \quad \hat{L}_{DR}(t) = [\hat{H}_{DR}(t), \cdot] \ , \tag{1.10}$$

with $\hat{L}_0 = [(\hat{H}_M + \hat{H}_B + \hat{H}_D), \cdot]$ and $\mathbf{T}$ representing a time-ordering operator.

In the time evolution of the scattering represented by the eighth-order density operator, all possible time orderings of the four fields (and their conjugates), including the signal field, are permitted. Defining the propagators $\hat{G}(t)$ to include the detector signal operator accounts for the spectral decomposition step in the measurement process. It acts automatically at the amplitude level, prior and up to the moment of the photoelectric detection step denoted by the operator $\hat{S}$ in Eq. (1.1). Available to act at all time intervals, it generates terms that survive the tracing in Eq. (1.6) when it acts at those steps where the signal field S and its conjugate are produced. Physically, propagation under the action of $\hat{L}_{\mathrm{DR}}$ represents any spectral filtering, frequency converting, or phase shifting (e.g., homodyning or heterodyning) of the generated signal field. Such a detector response propagator is essential when probing material or radiation responses that average to zero in white quadratic detection.

Equation (1.6) serves as a general starting equation for all four-photon processes (eight fields in quadrature pairs

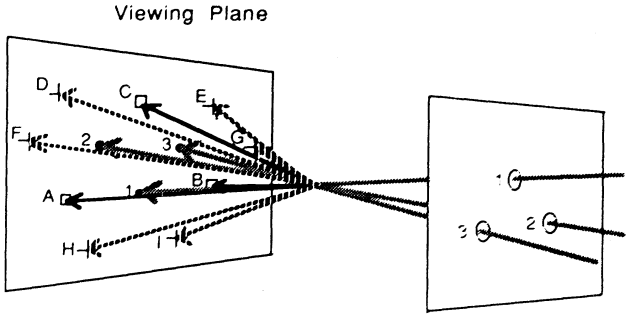

FIG. 1. Phase-matching diagram using the folded-box geometry. In general, three input beams with wave vectors k_1, k_2, and k_3 (labeled 1, 2, and 3) interact in a nonlinear medium generating a variety of spatially distinct signal beams. Three of these beams (solid lines), represented by the squares and labeled A, B, and C on the viewing plane, are dependent on all three input fields and satisfy the phase matching given by $\mathbf{k}_A=\mathbf{k}_1+\mathbf{k}_2-\mathbf{k}_3$, $\mathbf{k}_B=\mathbf{k}_1-\mathbf{k}_2+\mathbf{k}_3$, and $\mathbf{k}_C=-\mathbf{k}_1+\mathbf{k}_2+\mathbf{k}_3$. (The crosses (+) on the viewing plane represent signals from the two-beam fourth waves (dashed lines) where one input beam contributes two of three input fields to the mixing process. These signal beams labeled D–I satisfy the phase matching given by $\mathbf{k}_D=2\mathbf{k}_2-\mathbf{k}_2$, $\mathbf{k}_E=2\mathbf{k}_3-\mathbf{k}_1$, $\mathbf{k}_F=2\mathbf{k}_2-\mathbf{k}_3$, $\mathbf{k}_G=2\mathbf{k}_3-\mathbf{k}_2$, $\mathbf{k}_H=2\mathbf{k}_1-\mathbf{k}_3$, and $\mathbf{k}_I=2\mathbf{k}_1-\mathbf{k}_2$. Any one of the input beams can generate a 4WM signal by either acting alone (three times) or acting once upon joining a second beam that acts self-conjugately. Finally, of the several sum frequency signals there are the third-harmonic fields that copropagate with each one of the three input beams.

summed over all possible permutations). Experimentally, one may choose to study a subclass of mixing channels by selecting a particular parametric or phase matched component. Figure 1 displays the possible spatially coherent fourth waves $\mathbf{k}_S^i$ generated in quasidegenerate 4WM involving only two (+) or all three (□) of the input beams $\mathbf{k}_1$, $\mathbf{k}_2$, and $\mathbf{k}_3$. While establishing the basis for momentum conservation in the scattering processes, phase matching serves as a Fourier filter in selecting a certain combination of field operators that generate the material polarization. Several authors have noted the multiparticle nature of parametric spectroscopies. These require at least a two-chromophore scattering unit to retain spatial phase information of the input fields.[28,52,53] In fact, each of the eight field operators can act on every chromophore within the interaction volume. The enumeration of such field-chromophore entities has been accomplished by identifying the chromophore upon which the field λ acts as α_λ (or β_λ, $\lambda=1,2,3,S$). Because at the signal level all fields act conjugately, we can always prescribe a set of four field phases $\{\xi_\lambda\}$ together with the conjugate set $\{-\xi_\lambda\}$. Here $\xi_\lambda=\pm$ and thus distinguishes the operator (for field λ) from its adjoint, or a complex variable related to field λ from its conjugate. Thus without loss of generality let the set $\{\xi_\lambda\}$ be associated with the chromophore set $\{\alpha_\lambda\}$ and the conjugate set $\{-\xi_\lambda\}$, with the chromophore set $\{\beta_\lambda\}$. In principle, a given chromophore set can consist of as many as four spatially distinct chromophores of like or unlike chemical composition (when only one field acts on each chromophore), or as few as one distinct chromophore (when all four fields act on one chromophore). The spatial phase factor for each field [see in Eq. (1.5)] accumulates to eighth order via Eq. (1.8) to produce the generalized spatial phase factor that controls phase matching. In the present notation one obtains

$$F(\{k_\lambda\},\{r_{\alpha_\lambda}\}-\{r_{\beta_\lambda}\})=\prod_\lambda \exp[i\xi_\lambda\mathbf{k}_\lambda\cdot(\mathbf{r}_{\alpha_\lambda}-\mathbf{r}_{\beta_\lambda})]\ . \tag{1.11}$$

For any prescribed set $\{\xi_\lambda\}$, all phase-matching constraints on the signal appear through Eq. (1.11). For the special case where all eight field operators (four quadrature pairs) were to intervene on single chromophore, all position vectors would be identical and there is exact cancellation in the spatial phase of the superposition field. Phase matching is trivially automatic. The directionality of emission in such a case is then determined by the orientational average of the transition tensor on the chromophore coupled to the eight specified field polarization unit vectors. Maximum nontrivial phase constraints on the signal are derived from chromophore sets $\{\alpha_\lambda\}$ and $\{\beta_\lambda\}$ for which $\alpha_\lambda\neq\beta_\lambda$ for all λ. This extreme condition ensures that $\mathbf{r}_{\alpha_\lambda}-\mathbf{r}_{\beta_\lambda}\neq\mathbf{0}$ for all λ, and is the basis for further conceptual development. Nontrivial phase-matching constraints are partially lost as soon as even one conjugate pair of fields acts on a single chromophore (giving $\mathbf{r}_{\alpha_\lambda}-\mathbf{r}_{\beta_\lambda}=\mathbf{0}$ for some λ).

For phase-matched four-photon scattering under arbitrary spatial and temporal correlation (introduced either through spatial ordering of the chromophores or through the radiation-matter Hamiltonian) Eq. (1.6) can be expressed as an eight-field, eight-chromophore correlation function. Such a multifield, multichromophore correlator description will be subject to the definition of the zeroth-order state basis, and when applied to Eq. (1.5), must comply with the dipole approximation. This latter constraint requires that the spatial extent of the states of the individual chromophore be small compared to the wavelengths of the interacting fields. (The effects of quadrupolar and higher-order terms in nonlinear-response theory has recently been treated by Knoester and Mukamel.[56])

The chromophore notation is formally introduced into the matter Hamiltonians H_M, $\hat{H}_B$, and $\tilde{H}_{MB}$:

$$\hat{H}_M+\hat{H}_B+\tilde{H}_{MB}(t)=\sum_\alpha\left[\hat{H}_\alpha+\hat{H}_{B_\alpha}+\tilde{H}_{\alpha B_\alpha}(t)+\sum_{\alpha,\beta}\hat{V}_{\alpha\beta}\right]. \tag{1.12}$$

$\hat{H}_\alpha$ ($\hat{H}_\beta$) are the chromophore Hamiltonians. $\tilde{H}_{\alpha B_\alpha}$ ($\tilde{H}_{\beta B_\beta}$) couples the chromophore α (β) with its individual bath subspace. They are responsible for the relaxation of the optically prepared states. Interchromophore coupling is described by $\hat{V}_{\alpha\beta}$. For the present discussion,

however, we choose to define the chromophore such that its zeroth-order state basis is diagonal in $\hat{H}_\alpha$ ($\hat{H}_\beta$), regardless of its monomeric or oligometric molecular construction. We thus take $\hat{V}_{\alpha\beta}=0$ by definition and regard any remnant interchromophore coupling as subsumed in $\tilde{H}_{\alpha\beta_\alpha}$ ($\tilde{H}_{\beta B_\beta}$).

In materials thus built of independent chromophores, the eighth-order expression for the signal [Eq. (1.6)] factors into one containing a product of two fourth-order density operators. Thus

$$S^{(8)}=\mathrm{Tr}_{R,D}\left[\left[\sum_{\{\alpha_\lambda\}\{\beta_\lambda\}}[F(\{k_\lambda\},\{r_{\alpha_\lambda}\}-\{r_{\beta_\lambda}\})\langle\hat{\rho}^{(4)+}_{\{\alpha_\lambda\}}(\mathbf{r}_{\alpha_\lambda},t)\rangle_{\{\alpha_\lambda\}}\langle\hat{\rho}^{(4)-}_{\{\beta_\lambda\}}(\mathbf{r}_{\beta_\lambda},t)\rangle_{\{\beta_\lambda\}}+\text{H.a.}]\hat{\rho}_{\mathrm{RD}}\right]\right] \tag{1.13}$$

in which $\hat{\rho}^{(4)+}_{\{\alpha_\lambda\}}$ (and $\hat{\rho}^{(4)-}_{\{\beta_\lambda\}}$) are density operators (discussed further below), fourth-order in the intervening fields, each representing a set of up to four chromophores (H.a. denotes the Hermitian adjoint). In writing Eq. (1.13), separability of the initial density operator $\hat{\rho}(-\infty)$ with respect to the M, B, and $R(D)$ subspaces is assumed. Each of the fourth-order terms contains an intervention from the S mode(s) operator at some point during the time evolution where it is promptly convolved with the detector response propagator. A given phase-matching prescription fixes the Fourier components $\{\xi_\lambda\}$ in $\hat{\rho}^{(4)+}_{\{\alpha_\lambda\}}$, and necessarily fixes the set $\{-\xi_\lambda\}$ appearing in $\hat{\rho}^{(4)-}_{\{\beta_\lambda\}}$. The choice of a set $\{\xi_\lambda\}$ fixes the $\pm$ superscripts of the fourth-order density operators. Once traced over the matter states (bath and chromophore) as indicated by the brackets ($\langle\ \rangle_{\{\alpha_\lambda\}}$) these fourth-order operators remain as tetradic operators with respect to the radiation subspace. Thus the radiation-averaged quantities must be calculated at quadrature in the fields (eighth order). In general, we have eight unconstrained sums involving chromophore sets $\{\alpha_\lambda\}$ and $\{\beta_\lambda\}$. Simplification to the conventional bichromophore model will be introduced in Sec. I B.

Equation (1.13) serves as a fully quantized expression for the signal measured in 4WM and, through the detector propagator, allows for general detection, the simplest case being frequency resolution in the signal. Saturation effects, in this limit (small-flip-angle limit), are accounted for by allowing the signal field to build up from, and feed back into, the mixing process via the fourth-order term. However, the trace of the density matrix would have to be explicitly conserved to avoid artifacts.[50] Analogous to the development in Ref. 53, we will only be concerned with the "seeding" events of the mixing process by allowing the initial signal mode(s) to be produced by the vacuum operator ($|\mathrm{vac}\rangle_{s\,s}\langle\mathrm{vac}|$). At the seeding level, signal contributions arise from the amplitude level terms in which the vacuum blackbody operator $\tilde{V}^{\pm}_S(t)$ discharges the induced dipoles (superposition states) generated at orders up to and including third order in the incident fields. The vacuum blackbody operator possesses all possible wave vectors and frequencies (k_S,ω_S) defined by the set of mode indices $\{S\}$. For a given phase matching (defined by the experiment), only a certain subgroup of zero-point radiation modes will experience gain from these four-photon parametric scattering channels. Such gain has a strict spatial directionality determined by the sum over chromophores α_λ and β_λ in Eq. (1.13). The fully quantum-mechanical development allows for the zero-point field to intervene at any order in the evolution to fourth order. However, only a subclass of these scattering channels exists where the vacuum operator resonantly discharges an induced dipole such as in a Raleigh-type process. The much weaker, nonresonant vacuum intervention is the analogous Raman-type process. For a scattering channel where only superposition states are generated up to fourth order (general three- or four-color 4WM), the zero-point field can resonantly intervene only at fourth order. That is, it acts to collapse the complete third-order polarization. For the remaining development, the vacuum black body seeding intervention is taken at fourth order where it is assumed not to introduce correlation among the frequency components of the signal field other than that conveyed through the third-order polarization amplitudes that generate it.

Since the detector propagator containing $\hat{L}_{DR}$ acts only on the signal mode(s) of the radiation subspace, it can be factored from the material related propagators [$\hat{G}(t)$] and labeled separately as the detector response operator $\hat{R}_D(t)$. With $\hat{V}^{\pm}_S$ acting last in the time sequence, and at room temperature only able to discharge in one direction any material optical coherent state built by $\hat{\rho}^{(3)}$, $\hat{\rho}^{(4)}$ at time t can be expressed in terms of the time convolution of $\hat{R}_D(t)$ with $\langle\hat{V}^{\pm}_S\hat{\rho}^{(3)}\rangle_{\{\alpha_\lambda\}}$. This term, stripped of the spatial phase factors of all four fields and the temporal phase of the signal field, shall be called simply $\hat{p}^{(3)}_{\{\alpha_\lambda\}}$—an "electric dipole operator." [See Eq. (1.5) for phase factors and the dipole operator $\hat{\mu}$ from which its name is derived.] The detected signal at ω_S, Eq. (1.13) can now be written as

$$S^{(8)}=\sum_{\{\alpha_\lambda\},\{\beta_\lambda\}}F(\{k_\lambda\},\{r_{\alpha_\lambda}\}-\{r_{\beta_\lambda}\})$$

$$\times\int_{-\infty}^{t}dt'\int_{-\infty}^{t}ds'\langle\hat{R}_D(t-t')\hat{R}^{\dagger}_D(t-s')e^{i\omega_S(t'-s')}\langle\hat{p}^{(3)}(\{r_{\alpha_\lambda}\},t')\rangle_{\{\alpha_\lambda\}}\langle\hat{p}^{(3)\dagger}(\{r_{\beta_\lambda}\},s')\rangle_{\{\beta_\lambda\}}\rangle_{R,D}\ . \tag{1.14}$$

More specifically, $\hat{p}^{(3)}_{\{\alpha_\lambda\}}$ in (hz) is the electric dipole moment operator developed at time t' on chromophore α_S as a result of the previous action of the incident fields ($\lambda=1,2,3$) on chromophores α_1, α_2, and α_3. $\langle\ \rangle_{R,D}$ represents the average over the radiation and the detector subspaces [from $\mathrm{Tr}_{R,D}$ in Eq. (1.13)].

In one typical class of experiments the signal, first subjected to the detector response, is then integrated over real time at the photocathode. It is usually measured as a function of the delay in time τ of one of the input fields (e.g., k_1,ω_1) relative to the other two ($k_2,\omega_2;k_3,\omega_3$). One is interested, therefore, in the full time integral over $S^{(8)}(t)$. Towards this end it is useful to replace the detector response operator $\hat{R}_D(t)$ by the Fourier transform operator of its complex spectral density $j_D(\omega'_S)$, where

$$\hat{R}_D(t)=\int_{-\infty}^{\infty} d\omega_S j_D(\omega_S) e^{-i\omega_S t} . \tag{1.15}$$

Equations (1.14) and (1.15) give

$$\begin{aligned} I(\omega_S;\tau)&=\int_{-\infty}^{\infty} dt\, S^{(8)} \\ &=\int_{-\infty}^{\infty} d\omega'_S J_D(\omega'_S) \\ &\quad\times\int_{-\infty}^{\infty} dt' \int_{-\infty}^{\infty} ds' e^{i(\omega_S+\omega'_S)(t'-s')} \\ &\quad\times\mathcal{C}(t',s';\tau) , \end{aligned} \tag{1.16}$$

where $J_D(\omega'_S)=|j_D(\omega'_S)|^2$ and the so-called "polarization correlator" is given as

$$\begin{aligned} \mathcal{C}(t',s';\tau)=&\sum_{\{\alpha_\lambda\},\{\beta_\lambda\}} F(\{k_\lambda\},\{r_{\alpha_\lambda}\}-\{r_{\beta_\lambda}\}) \\ &\times\langle\langle\hat{p}^{(3)}(r_{\{\alpha_\lambda\}},t';\tau)\rangle_{\{\alpha_\lambda\}} \\ &\times\langle\hat{p}^{(3)\dagger}(r_{\{\beta_\lambda\}},s';\tau)\rangle_{\{\beta_\lambda\}}\rangle_R . \end{aligned} \tag{1.17}$$

At the other experimental extreme we propose a type of "white" detection where $\hat{R}_D(t-t') \propto \delta(t-t')\sum_S |S\rangle\langle S|$ and Eq. (1.14) becomes simply

$$I(t;\tau)=\int_{-\infty}^{\infty} d\omega_S S^{(8)}=\mathcal{C}(t;\tau) . \tag{1.18}$$

B. Spatial and temporal field-matter correlation and the bichromophore model

Long-time signal averaging with spectral resolution of the generated fourth wave is fundamental in many applications, including our own, so we proceed from Eq. (1.16). Here the dipole operator $\hat{p}^{(3)}$ [in Eq. (1.17)] built from polarization on chromophore set $\{\alpha_\lambda\}$ is taken at time t', while that on chromophore β_S from $\{\beta_\lambda\}$ is taken at time s', independent of t'. Equation (1.16) [with Eq. (1.17)] is the starting equation for calculating frequency-resolved interferograms generated from incoherent as well as from coherent broadband 4WM. The two radiation-space operators, $\langle\hat{p}^{(3)}\rangle$ from $\{\alpha_\lambda\}$ and $\langle\hat{p}^{(3)\dagger}\rangle$ from $\{\beta_\lambda\}$, are coupled by field correlation so that averaging over the radiation subspace $\langle\ \rangle_R$ cannot lead to a simple product, even though the chromophores themselves are, by definition, otherwise uncoupled. The radiation-subspace average is actually a two-part average, a quantum-mechanical one involving the $\{\hat{a}^{\xi_\lambda}_\lambda\}$ and a classical average involving the stochastic space-time field functions $\{\bar{\epsilon}^{\xi_\lambda}_\lambda(\mathbf{r}_{\alpha_\lambda},t)\}$ [see Eq. (1.5)]. To expose these two kinds of radiation-space quantities let us express the dipole operator in terms of a nonlinear material response operator and the stochastic field functions:

$$\begin{aligned} &\langle\hat{p}^{(3)}(\{r_{\alpha_\lambda}\},t;\tau)\rangle_{\{\alpha_\lambda\}} \\ &=\prod_{\lambda=1}^{3}(E^0_\lambda)^{\xi_\lambda}\int_{-\infty}^{t} dt_1\int_{-\infty}^{t_1} dt_2\int_{-\infty}^{t_2} dt_3\hat{\Pi}_{1,2,3}\langle\hat{R}^{(3)}_{\{\alpha_\lambda\}}(t,(\mathbf{e}_1,t_1),(\mathbf{e}_2,t_2),(\mathbf{e}_3,t_3))\rangle_{\{\alpha_\lambda\}} \\ &\quad\times\bar{\epsilon}^{\xi_1}_1(\mathbf{r}_{\alpha_1},t_1-\tau)\bar{\epsilon}^{\xi_2}_2(\mathbf{r}_{\alpha_2},t_2)\bar{\epsilon}^{\xi_3}_3(\mathbf{r}_{\alpha_3},t_3) \end{aligned} \tag{1.19}$$

[and analogously for $\langle\hat{p}^{(3)\dagger}(\{r_{\beta_\lambda}\},t;\tau)\rangle_{\{\beta_\lambda\}}$]. $\hat{\Pi}$ represents a permutation operator over all possible time orderings of the three fields. The quantum-mechanical field operators $\{\bar{\alpha}^{\xi_\lambda}_\lambda\}$ are hidden in the nonlinear-response operator $\hat{R}^{(3)}_{\{\alpha_\lambda\}}(t)$; the $\{\bar{\epsilon}^{\xi_\lambda}_\lambda\}$ appear explicitly.

All relevant information concerning the microscopic material dynamics is contained in the third-order nonlinear-response operator $\hat{R}^{(3)}_{\{\alpha_\lambda\}}(t)$ after it has been reduced to an operator only in the radiation subspace $\langle\hat{R}^{(3)}_{\{\alpha_\lambda\}}(t)\rangle_{\{\alpha_\lambda\}}$. Before returning to the issue of field correlation at the signal level, we express this reduction in more detail. The reduction over the space of $\{\alpha_\lambda\}$ includes both a trace over the chromophore basis and one over the bath basis $\{B_{\alpha_\lambda}\}$ that is relevant to the chromophore set $\{\alpha_\lambda\}$. Tracing over the chromophore basis leaves (in matrix form)

$$\begin{aligned} &\langle\hat{R}^{(3)}_{\{\alpha_\lambda\}}(t,(\mathbf{e}_1,t_1),(\mathbf{e}_2,t_2),(\mathbf{e}_3,t_3))\rangle_{\{\alpha_\lambda\}} \\ &=\sum_{i,j,k,l}\sum_{m,n,o,p}\sum_{q,r,s,t}\sum_{g}\langle(\hat{v}^{\xi_S}_{\alpha_S})_{ij}\tilde{G}^{\alpha_1}_{ij,kl}(t,t_1)\hat{L}^{\xi_1}_{kl,mn}(t_1)\tilde{G}^{\alpha_2}_{mn,op}(t_1,t_2)\hat{L}^{\xi_2}_{op,qr}(t_2)\tilde{G}^{\alpha_3}_{qr,st}(t_2,t_3)\hat{L}^{\xi_3}_{st,gg}(t_3)\rangle_{\{B_{\alpha_\lambda}\}} \end{aligned} \tag{1.20}$$

in which the commutator operator

$$\hat{L}^{\xi_\lambda}_{kl,mn}(t)\cdot = \delta_{ln} e^{-\xi_\lambda i\omega_\lambda t}(\hat{v}^{\xi_\lambda}_{\alpha_\lambda})_{km}\cdot - \cdot(\hat{v}^{\xi_\lambda}_{\alpha_\lambda})_{nl}\delta_{km} e^{-\xi_\lambda i\omega_\lambda t} , \tag{1.21}$$

where the

$$(\hat{v}^{\xi_\lambda}_{\alpha_\lambda})_{km}\cdot = C_\lambda \left[\sum_{\xi=\pm} \boldsymbol{\mu}^{\alpha_\lambda}_{km}\cdot\boldsymbol{\epsilon}^{\xi_\lambda} \right] \hat{a}^{\xi_\lambda}\cdot \tag{1.22}$$

contain the (previously hidden) field operators $\{\hat{a}^{\xi_\lambda}_\lambda\}$ that, at signal level, are subject to the quantum-mechanical part of the field averaging. In this limit, dynamical evolution of the optically prepared single-chromophore state is governed by the field-free propagators $\tilde{G}^{\alpha_\lambda}(t)$ for chromophore α_λ. Since by definition the chromophores are uncoupled with respect to $\hat{H}_M$ and $\tilde{H}_{MB}$, the bath average $\langle\ \rangle_{\{B_{\alpha_\lambda}\}}$ over the three propagators reduces to a product of independent averages, each associated with propagation on an individual chromophore.

We now return to the classical part of the field averaging. When Eq. (1.19) is inserted into Eq. (1.17) a six-field classical correlation function appears upon averaging over spatial and temporal fluctuations of the input radiation fields $\{\bar{\epsilon}^{\xi_\lambda}_\lambda\}$, $\lambda=1,2,3$. In general, such field coherence, responsible for correlating the two dipole operators in Eq. (1.17), cannot be factored into its separate spatial and temporal parts. However, to simplify the discussion, the fields are taken to be "cross spectrally pure" to allow the factorization of the field correlation into independent spatial and temporal correlators.[54] The six-order field correlator is now written as

$$\langle \bar{\epsilon}^{\xi_1}_1(\mathbf{r}_{\alpha_1},t_1-\tau)\bar{\epsilon}^{\xi_2}_2(\mathbf{r}_{\alpha_2},t_2)\bar{\epsilon}^{\xi_3}_3(\mathbf{r}_{\alpha_3},t_3)\bar{\epsilon}^{-\xi_1}_1(\mathbf{r}_{\beta_1},s_1-\tau)\bar{\epsilon}^{-\xi_2}_2(\mathbf{r}_{\beta_2},s_2)\bar{\epsilon}^{-\xi_3}_3(\mathbf{r}_{\beta_3},s_3)\rangle_R$$
$$= \Phi(\{\mathbf{r}_{\alpha_\lambda}\},\{\mathbf{r}_{\beta_\lambda}\})\Gamma^{(3,3)}(t_1-\tau,t_2,t_3,s_1-\tau,s_2,s_3) , \tag{1.23}$$

where $\Gamma^{(3,3)}$, space independent, is just the full $\{\bar{\epsilon}^{\xi_\lambda}_\lambda\}$ correlator integrated over space. (The space integral on Φ gives unity.) $\Phi(\{\mathbf{r}_{\alpha_\lambda}\},\{\mathbf{r}_{\beta_\lambda}\})$ is the pure-space field correlation function. This factorization of the field space-time correlation allows for the independent evaluation of the spatial and temporal dependence of the polarization correlator, Eq. (1.17), giving

$$\mathcal{C}(t',s';\tau) = \left[\prod_{\lambda=1}^{3} |E^0_\lambda|^2 \right] \Xi(\{\mathbf{k}_\lambda\})\mathfrak{S}(t',s';\tau) \tag{1.24}$$

in which the spatial field correlator becomes intimately coupled to the generalized phase function, Eq. (1.11), through the eightfold unconstrained summation over chromophores:

$$\Xi(\{\mathbf{k}_\lambda\}) = \sum_{\{\alpha_\lambda\},\{\beta_\lambda\}} F(\{\mathbf{k}_\lambda\},\{\mathbf{r}_{\alpha_\lambda}\}-\{\mathbf{r}_{\beta_\lambda}\})\Phi(\{\mathbf{r}_{\alpha_\lambda}\},\{\mathbf{r}_{\beta_\lambda}\}) , \tag{1.25}$$

and the temporal field correlator becomes coupled to the material response through two sets of linked threefold time integrals:

$$\mathfrak{S}(t',s';\tau) = \int_{-\infty}^{t'} dt_1 \int_{-\infty}^{t_1} dt_2 \int_{-\infty}^{t_2} dt_3 \int_{-\infty}^{s'} ds_1 \int_{-\infty}^{s_1} ds_2 \int_{-\infty}^{s_2} ds_3 \Gamma^{(3,3)}(t_1-\tau,t_2,t_3,s_1-\tau,s_2,s_3)$$
$$\times \langle \hat{\Pi}_{1,2,3} \langle \hat{R}^{(3)}_{\{\alpha_\lambda\}}(t',(\mathbf{e}_1,t_1),(\mathbf{e}_2,t_2),(\mathbf{e}_3,t_3)) \rangle_{\{\alpha_\lambda\}} \hat{\Pi}_{1,2,3} \langle \hat{R}^{(3)\dagger}_{\{\beta_\lambda\}}(s',(\mathbf{e}_1,s_1),(\mathbf{e}_2,s_2),(\mathbf{e}_3,s_3)) \rangle_{\{\beta_\lambda\}} \rangle_R . \tag{1.26}$$

It is convenient to replace each of the eight chromophore summations in Eq. (1.25) by the volume normalized integral over the position coordinate of the chromophore. Thus we now write for the spatial correlator [Eq. (1.25)]

$$\Xi(\{\mathbf{k}_\lambda\}) = \frac{N_{\alpha_1}}{V}\int d\mathbf{r}_{\alpha_1} \frac{N_{\alpha_2}}{V}\int d\mathbf{r}_{\alpha_2} \cdots \frac{N_{\beta_S}}{V}\int d\mathbf{r}_{\beta_S} F(\{\mathbf{k}_\lambda\},\{\mathbf{r}_{\alpha_\lambda}\}-\{\mathbf{r}_{\beta_\lambda}\})\Phi(\{\mathbf{r}_{\alpha_\lambda}\},\{\mathbf{r}_{\beta_\lambda}\}) . \tag{1.27}$$

A change of variables from chromophore position vectors $(\{\mathbf{r}_{\alpha_\lambda}\},\{\mathbf{r}_{\beta_\lambda}\})$ to position vectors $\{\mathbf{r}_{\alpha_\lambda}\}$ and relative position vectors $(\{\mathbf{r}_{\alpha_\lambda}\}-\{\mathbf{r}_{\beta_\lambda}\}\equiv\{\mathbf{r}_{\alpha_\lambda,\beta_\lambda}\})$ is useful when the spatial correlation function depends only on relative positions of the chromophores. Integration over the four chromophore coordinates $\{\mathbf{r}_{\alpha_\lambda}\}$ leaves simply V^{-4} to give

$$\Xi(\{\mathbf{k}_\lambda\}) = \frac{N_{\alpha_1}N_{\alpha_2}\cdots N_{\beta_S}}{V^4}\int d\mathbf{r}_{\alpha_1\beta_1}\int d\mathbf{r}_{\alpha_2\beta_2}\cdots\int d\mathbf{r}_{\alpha_S\beta_S} F(\{\mathbf{k}_\lambda\},\{\mathbf{r}_{\alpha_\lambda,\beta_\lambda}\})\Phi(\{\mathbf{r}_{\alpha_\lambda,\beta_\lambda}\}) . \tag{1.28}$$

1. The bichromomohore model and spatial correlation

There exists a (large) subset of experiments, specified by their phase-matching constraints [via $\{\xi_\lambda\}$ and Eq. (1.11)] and the nature of correlation among the fields, such that field-induced correlation can take place neither within the set $\{\alpha_\lambda\}$ nor within the set $\{\beta_\lambda\}$. (In such a case field-induced correlation is absent even when all four fields act on one chromophore.) For this kind of phase matching either the four fields acting on $\{\alpha_\lambda\}$ (and their conjugates on $\{\beta_\lambda\}$) are simply mutually uncorrelated, or, if not, only high-frequency multichromophore correlators appear. These vanish on cycle averaging. In such circumstances third-order polarization can develop only among the eigenstate of a single chromophore so that we set $\{\alpha_\lambda\}\rightarrow\alpha$ ($\{\beta_\lambda\}\rightarrow\beta$), $\{\mathbf{r}_{\alpha_\lambda}\}\rightarrow\mathbf{r}_\alpha$ ($\{\mathbf{r}_{\beta_\lambda}\}\rightarrow\mathbf{r}_\beta$), and ($\{\mathbf{r}_{\alpha_\lambda,\beta_\lambda}\}\rightarrow\mathbf{r}_{\alpha,\beta}$). The eightfold sum on chromophores in Eq. (1.14) (and beyond) now reduces to a simple double sum, one over α, the other over β. Thus the absence of any radiation-induced correlation across a multichromophore set $\{\alpha_\lambda\}$ (or $\{\beta_\lambda\}$) causes all terms in the eightfold sum to vanish, but for those that correspond to full third-order polarizations on single chromophores (α and β). This is termed the two-chromophore or the "bichromophore" model. Having lost a sixfold summation (and the corresponding V^3 from center-of-mass integrations), and $\Xi(\{\mathbf{k}_\lambda\})$ function [Eq. (1.28)] now becomes simply

$$\Xi(\Delta\mathbf{k})=\frac{N_\alpha N_\beta}{V}\int d\mathbf{r}_{\alpha,\beta}F(\Delta\mathbf{r}\cdot\mathbf{r}_{\alpha,\beta})\Phi(\mathbf{r}_{\alpha,\beta})\ , \tag{1.29}$$

where

$$F(\{\mathbf{k}_\lambda\},\{\mathbf{r}_{\alpha_\lambda,\beta_\lambda}\})\rightarrow F\left[\sum_\lambda(\xi_\lambda\mathbf{k}_\lambda\cdot\mathbf{r}_{\alpha,\beta})\right]=F(\Delta\mathbf{k}\cdot\mathbf{r}_{\alpha,\beta})\left[\Delta\mathbf{k}=\sum_\lambda\xi_\lambda\mathbf{k}_\lambda\right].$$

If the field spatial correlation function in terms of the chromophore separation $\Phi(\{\mathbf{r}_{\alpha,\beta}\})$ is taken to depend only on the magnitude, $r_{\alpha,\beta}$ scaled by a correlation distance l_c, we might write

$$\Phi(r_{\alpha,\beta})\propto e^{-r_{\alpha,\beta}/l_c}\ . \tag{1.30}$$

The spatial integral in Eq. (1.29) can be performed to produce a polarization correlator that depends on the phase mismatch (Δk). Such a phase-matching function is given by

$$\begin{aligned}\Xi(\Delta\mathbf{k})&=\frac{2\pi N_\alpha N_\beta}{V}\int_0^R dr\,r^2e^{(-r/l_c)}\int_0^\pi d\theta\sin(\theta)e^{[i\Delta kr\cos(\theta)]}\\&=\frac{4\pi N_\alpha N_\beta}{\Delta kV}\left\{\frac{l_c^3\Delta k}{[1+(l_c\Delta k)^2]^2}+Re^{(-R/l_c)}\frac{l_c\sin(\Delta kR)-\Delta kl_c^2\cos(\Delta kR)}{1+(\Delta kl_c)^2}\right.\\&\left.+l_c^2e^{(-R/l_c)}\frac{[1-(\Delta kl_c)^2]\sin(\Delta kR)-2\Delta kl_c\cos(\Delta kR)}{[1+(\Delta kl_c)^2]^2}\right\}.\end{aligned} \tag{1.31}$$

The upper limit (R) of the spatial integral is determined by the overlap of the incident fields. As the characteristic coherence length l_c increases, the signal becomes more sharply peaked about $\Delta k=0$. For arbitrary correlation lengths and an exponential form for the correlation, the signal dependence on Δk will be determined by Eq. (1.31). More generally, one must convolve the multichromophore spatial phase function $[F(\{\mathbf{k}_\lambda\},\{\mathbf{r}_{\alpha_\lambda,\beta_\lambda}\})]$ with the spatial correlator of the field $[\Phi(\{\mathbf{r}_{\alpha\lambda}\},\{\mathbf{r}_{\beta_\lambda}\})]$. (Analogously, any breakdown of the uncoupled chromophore model that leads to their long-range spatial correlation will likewise influence the dependence of the signal on the phase mismatch Δk.[52,53])

Since the 4WM experiments to be analyzed in Sec. III all fall within the bichromophore model, it is retained in all further development. Furthermore, we consider only the dependence of the signal on the temporal part of the field correlation where material memory can prolong the interference among correlated fields. By definition material spatial coherence due to $\hat{H}_M$ and $\hat{H}_{MB}$ alone appears only within a chromophore, whose extent must not exceed a small fraction of the wavelength of the fields (the dipole approximation). Any spatial correlation in the scattering process beyond that inherent in the incident fields (discussed above) is neglected. A reduced description of the field correlation function then follows upon integrating over the spatial dependencies in Eq. (1.31). [In general, though, the space-time factoring of the field correlator in Eq. (1.23) is only approximate.]

2. The bichromophore model and time correlation

We return now to the field time correlator $\Gamma^{(3,3)}(t)$ [Eq. (1.23)] and see how through it the amplitude and phase structure of the excitation fields can bring about correlation among the chromophores in the polarization correlator of Eqs. (1.24) and (1.26). First, a characteristic time (coherence time τ_c) associated solely with the fields, and defining the short-time signal component, can be defined through $\Gamma^{(3,3)}(t)$. [This is equivalent to the assumption of an infinitely rapid material response $G(t-t')\propto\delta(t-t')$.] Thus the temporal field correlator, written as an ensemble average in Eq. (1.23), can be rewritten here in terms of a time average as

$$\Gamma^{(3,3)}(\tau)=\lim_{T\to\infty}\frac{1}{2T}\int_{-T}^{+T}dt\,\tilde{\epsilon}_1^{\xi_1}(t-\tau)\tilde{\epsilon}_2^{\xi_2}(t)\tilde{\epsilon}_3^{\xi_3}(t)\times\tilde{\epsilon}_1^{-\xi_1}(-\tau)\tilde{\epsilon}_2^{-\xi_2}(0)\tilde{\epsilon}_3^{-\xi_3}(0)\ . \tag{1.32}$$

In general, the equivalence between Eqs. (1.23) and (1.32) represents ergodic fields. The absence of space coordinates in $\tilde{\epsilon}_\lambda^{\xi_\lambda}$ implies integration over Φ. Equation (1.32) follows by the stationarity assumption where $t=t'-s'$. Using the normalization condition introduced by Glauber, a normalized temporal field correlator can be given as

$$\gamma^{(3,3)}(\tau)=\Gamma^{(3,3)}(\tau)\left[\prod_{\lambda=1}^{6}\Gamma_\lambda^{(1,1)}(0)\right]^{-1/2}. \tag{1.33}$$

A coherence time τ_c of the superposition field is now defined by integrating the normalized correlator with respect to the delay parameter τ:

$$\tau_c=\int_{-\infty}^{\infty}d\tau|\gamma^{(3,3)}(\tau)|^2\ . \tag{1.34}$$

For systems possessing response times greater than τ_c, time ordering of the field interventions becomes important. The temporal correlation function, for a given time ordering, can be expressed as the Fourier transform of the spectral correlation function $J(\omega)$ (a sixth-order field spectral density):

$$\Gamma^{(3,3)}(t_1-\tau,t_2,t_3,s_1-\tau,s_2,s_3)=\int_{-\infty}^{\infty}d\omega_1'\int_{-\infty}^{\infty}d\omega_2'\cdots\int_{-\infty}^{\infty}d\omega_3''J(\omega_1',\omega_2',\omega_3',\omega_1''\omega_2'',\omega_3'')\times e^{i\xi_1(\omega_1'-\omega_1'')\tau}\exp\left[-i\sum_{i=1}^{3}\xi_i(\omega_i't_i-\omega_i''s_i)\right] \tag{1.35}$$

Assuming stationarity of the optical fields, the resonant frequency condition $\sum_i\xi_i\omega_i=0$ must hold. Thus the stationary six-field spectral correlation function can be defined as

$$J(\omega_1',\omega_2',\omega_3',\omega_1'',\omega_2'',\omega_3'')=\langle\tilde{\epsilon}_1^{\xi_1}(\omega_1')\tilde{\epsilon}_2^{\xi_2}(\omega_2')\tilde{\epsilon}_3^{\xi_3}(\omega_3')\tilde{\epsilon}_1^{-\xi_1}(\omega_1'')\tilde{\epsilon}_2^{-\xi_2}(\omega_2'')\tilde{\epsilon}_3^{-\xi_3}(\omega_3'')\rangle\delta(\omega_1'+\omega_2'+\omega_3'-\omega_1''-\omega_2''-\omega_3'')\ , \tag{1.36}$$

where $\tilde{\epsilon}_\lambda^{\xi_\lambda}(\omega_\lambda)$ is the Fourier transform of the temporal field function $\tilde{\epsilon}_\lambda^{\xi_\lambda}(t)$. In the time domain, this is equivalent to the time translational invariance of the temporal correlation function.[54]

Making use of Eq. (1.26) for the bichromophore case with Eq. (1.35) for $\Gamma^{(3,3)}$, the polarization correlator [Eq. (1.24), with Eq. (1.26)] can be written as

$$\begin{aligned}\mathcal{C}(t',s';\tau)=&\left[\prod_{\lambda=1}^{3}|E_\lambda^0|^2\right]\frac{\Xi(\Delta\mathbf{k})}{N_\alpha N_\beta}\\&\times\int_{-\infty}^{\infty}d\omega_1'\int_{-\infty}^{\infty}d\omega_2'\cdots\int_{-\infty}^{\infty}d\omega_3''J(\omega_1',\omega_2',\omega_3',\omega_1'',\omega_2'',\omega_3'')e^{i\xi_1(\omega_1'-\omega_1'')\tau}\exp\left[-i\sum_{i=1}^{3}\xi_i(\omega_i't'-\omega_i''s')\right]\\&\times\langle\hat{\chi}^{(3)}_{S,1,2,3}(\xi_S(\omega_S-\omega_S');\xi_1(\omega_1-\omega_1'),\xi_2(\omega_2-\omega_2'),\xi_3(\omega_3-\omega_3'))\\&\times\hat{\chi}^{(3)\dagger}_{S,1,2,3}((\xi_S(\omega_S-\omega_S');\xi_1(\omega_1-\omega_1''),\xi_2(\omega_2-\omega_2''),\xi_3(\omega_3-\omega_3'')))\rangle_R\ ,\end{aligned} \tag{1.37}$$

where the generalized third-order macroscopic susceptibility (an operator in the radiation subspace) is written in terms of the reduced temporal response operator [Eq. (1.20)] via Fourier transformation:

$$\begin{aligned}&\hat{\chi}^{(3)}_{S,1,2,3}(\xi_S(\omega_S-\omega_S');\xi_1(\omega_1-\omega_1'),\xi_2(\omega_2-\omega_2'),\xi_3(\omega_3-\omega_3'))\\&=N_\alpha\int_0^\infty d\tau_1\int_0^\infty d\tau_2\int_0^\infty d\tau_3\hat{\Pi}_{1,2,3}\langle\hat{R}^{(3)}_\alpha((\mathbf{e}_1,t'-\tau_1),(\mathbf{e}_2,t'-\tau_1-\tau_2),(\mathbf{e}_3,t'-\tau_1-\tau_2-\tau_3))\rangle_{\alpha,B_\alpha}\\&\quad\times e^{-i(\xi_1\omega_1'+\xi_2\omega_2'+\xi_3\omega_3')\tau_1}e^{-i(\xi_2\omega_2'+\xi_3\omega_3')\tau_2}e^{-i\xi_3\omega_3'\tau_3}\ .\end{aligned} \tag{1.38}$$

Here the change of variables from field intervention times t_i to intervals between field interventions $\tau_i=t_{i-1}-t_i$ has been utilized. Permutation of the temporal ordering of the fields via $\hat{\Pi}_i$ effectively permutes the frequencies (ω_i,ω_i') with respect to the time intervals τ_i to allow for all possible histories of time evolution.

3. *The bichromophore model and matter-bath stochastic processes*

The averaging of the response operator over the chromophore bath [B_α in Eq. (1.38)] is now associated with one chromophore and can be simplified by taking the sto-

chastic part ($\tilde{B}_\alpha$) of the material-bath interaction $\tilde{H}_{MB}(t)=\tilde{H}_{\alpha B_\alpha}(t)$, to be diagonal (elastic) in the basis of $\hat{H}_\alpha$.[57,58] Any state-changing (inelastic) process can be incorporated through the phenomenological addition of a damping constant. Therefore the following form for $\tilde{H}_{\alpha B_\alpha}(t)$ is implemented here:

$$\tilde{H}_{\alpha B_\alpha}(t)=\sum_{i,j}\left\{\sum_k[\gamma'_k(|i\rangle\langle k|+|k\rangle\langle i|)+\gamma'_{jk}(|j\rangle\langle k|+|k\rangle\langle j|)]+\delta\omega_{ij}(t)(|i\rangle\langle i|+|j\rangle\langle j|)\right\} \tag{1.39}$$

and similarly for $\tilde{H}_{\beta B_\beta}$. For a given time ordering of the input fields, the third-order nonlinear response operator [Eq. (1.20) for the multichromophore case $\{\alpha_\lambda\}$, or Eq. (1.38) for $\{\alpha_\lambda\}\rightarrow\alpha$] represents eight ($2^3$) different scattering channels (or Liouville space pathways of Ref. 27), $\hat{R}_\alpha^{(3)}(t)=\sum_{q=1}^{8}\hat{R}_\alpha^{(3)}(t)_q$ for $q=1-8$. Such channels are defined by fixing the action of each field operator in terms of its bra- or ket-side intervention. In general, for every unique channel, $\hat{R}_\alpha^{(3)}(t)_q$, the material states being driven actually can change in time if the third-order polarization is allowed to build up (or to accumulate) over times exceeding the characteristic time needed for transfer away from the initially prepared states. In this case, the states on chromophore α available for polarization constitute an open set, not restricted to a simple closed set of four levels. Thus the product of four dipole moment matrix elements, contained in $\hat{R}_\alpha^{(3)}(t)$, need not be joined by common material states. The mixing of different states in the development of the polarization is represented by the off-diagonal elements of the material propagators in the chromophore basis $[G_{ij,kl}(t)]$. This contrasts with scattering confined to a closed four-level system or to a multilevel system with excitation times short compared to interstate transfer times. Although processes such as interferences among different material superposition states, or transfer in general [represented by $G_{ij,kl}(t)$], may constitute important contributions to the material response (particularly if allowed to accumulate), their inclusion here would only complicate the following development. Therefore only diagonal elements of the material propagators will be considered $[G_{ij,ij}(t)]$. Thus for the qth channel, the reduced material response operator at time t can be expressed as a product of its phase factor, a reduced, phase-free, inelastic response operator $\langle\hat{K}_q^\alpha\rangle_{B_\alpha}$, and the (elastic) stochastic function F_q^α:

$$\langle\hat{R}_\alpha^{(3)}(t,(\mathbf{e}_1,t_1),(\mathbf{e}_2,t_2),(\mathbf{e}_3,t_3))_q\rangle_{\alpha,B_\alpha}=e^{-i(\xi_1\omega_1+\xi_2\omega_2+\xi_3\omega_3)t}\times\langle\hat{K}_q^\alpha(t,t_1,t_2,t_3)\rangle_{B_\alpha}F_q^\alpha(t,t_1,t_2,t_3)\,, \tag{1.40}$$

where

$$\langle\hat{K}_q^\alpha(t,t_1,t_2,t_3)\rangle_{B_\alpha}=\sum_{m,f,n,g}^{\alpha}\hat{v}_{fn}^{\xi_S}\hat{v}_{mf}^{\xi_1}\hat{v}_{gm}^{\xi_2}\hat{v}_{ng}^{\xi_3}e^{i(\omega_{ng}^\alpha+\xi_3\omega_3+i\gamma_{ng}^\alpha)(t_2-t_3)}\times e^{i(\omega_{mn}^\alpha+\xi_2\omega_2+\xi_3\omega_3+i\gamma_{mn}^\alpha)(t_1-t_2)}e^{i(\omega_{fn}^\alpha+\xi_1\omega_1+\xi_2\omega_2+\xi_3\omega_3+i\gamma_m^\alpha)(t-t_1)}\,, \tag{1.41}$$

and the stochastic function is

$$F_q^\alpha(t,t_1,t_2,t_3)=\left\langle\exp\left[i\int_{t_1}^{t}d\tau\,\delta\omega_{fn}^\alpha(\tau)\right]\times\exp\left[i\int_{t_2}^{t_1}d\tau'd\omega_{mn}^\alpha(\tau')\right]\times\exp\left[i\int_{t_3}^{t_2}d\tau''d\omega_{ng}^\alpha(\tau'')\right]\right\rangle_{\bar{B}_\alpha}. \tag{1.42}$$

where the f, m, n, and g labels on $F_q^\alpha(t)$ have been suppressed. The bracketed quantity $\langle\ \rangle_{B_\alpha}$ represents the average over the degrees of freedom of the α the chromophore bath. In the absence of "pure dephasing" $F_q^\alpha=1$.

In Eq. (1.41), the damping constants are given by $\gamma_{ij}=\sum_k\{\gamma'_{ik}+\gamma'_{jk}\}$. In ordered media when rotational averaging is called for, it must be carried out at the signal level. In such a case eight direction cosines (for one set of polarizations $\{\mathbf{e}_\lambda\}$) appear [see Eq. (1.5)] that involves a set of as many as eight (spatially correlated) chromophores. Each direction cosine represents the projection of the unit vector of a given transition moment (on a chromophore) onto the unit vector of the polarization direction of the intervening field. However, in the absence of long-range order among the chromophores (in amorphous media), rotational averaging can be carried out separately on each chromophore. In the common bichromophore model where the polarization develops fully on just one chromophore, the averaging over the four direction cosines is equivalent to a rotationally averaged projection of a fourth-rank chromophore transition tensor onto the polarization vectors of the four intervening fields.

Given the appropriate statistical models for the fluctuations of the material Bohr frequencies [via $F^Q(t)$ in Eqs. (1.40) and (1.42)] and also for the phase-or amplitude noise of the radiation field [via the spectral correlation function $J_\lambda(t)$], Eq. (1.16) with Eq. (1.17) [or the multichromophore version of Eq. (1.37)] for the polarization correlator, can be used to calculate signals in arbitrary interferometric 4WM experiments. However, Eq. (1.16) with Eq. (1.37) applies to the subset of such experiments that are based on the bichromophoric model. We continue with a closer look at the role of field correlation in these spectroscopies.

II. PHASE OR AMPLITUDE TEMPORAL FIELD CORRELATION IN 4WM WITH INCOHERENT AND COHERENT EXCITATIONS

The field time correlator $\Gamma^{(3,3)}$ is analyzed in more detail for three-beam 4WM experiments with incoherent light (Sec. II A) and with short-pulsed coherent light (Sec. II B). Recall that "incoherent" in this context refers to experimentally relevant fields having a time-bandwidth product several orders of magnitude greater than the theoretical transform limit. For such fields, the slowly varying stochastic temporal part of the electric field operator, given by $\bar{\mathcal{E}}_\lambda(t)$ [where the space dependence of $\bar{\mathcal{E}}_\lambda(\mathbf{r}_{Q_\lambda},t)$ in Eq. (1.5) has been suppressed], can be factored into its slowly varying (dimensionless) amplitude $\bar{\eta}_\lambda(t)$ and a (dimensionless) function $\bar{\phi}_\lambda(t)$ representing random short-term phase fluctuations. In contrast, short-pulsed coherent input fields will be represented by $\bar{\mathcal{E}}_\lambda(t)\rightarrow\epsilon_\lambda(t)$, an envelope of the pulse. A diagrammatic view of field correlated 4WM is given in Sec. II C.

A. Incoherent long-pulsed excitation

Mathematical simplification is gained by taking the random phase and amplitude noise of the input radiation fields to be described by circular complex Gaussian statistics. We take the given field-time ordering indicated in Eq. (1.23), and as an example of near degeneracy, assign the phase-matching condition $\{\xi_\lambda\}=(+,-,+,-)$ to give $\Delta\mathbf{k}=-\mathbf{k}_1+\mathbf{k}_2-\mathbf{k}_3+\mathbf{k}_s$. This allows us to write the sixth-order temporal correlation function $\Gamma^{(3,3)}$ as

$$\begin{aligned}&\langle\bar{\mathcal{E}}_1^{+}(t_1-\tau)\bar{\mathcal{E}}_2^{-}(t_2)\bar{\mathcal{E}}_3^{+}(t_3)\bar{\mathcal{E}}_1^{-}(s_1-\tau)\bar{\mathcal{E}}_2^{+}(s_2)\bar{\mathcal{E}}_3^{-}(s_3)\rangle\\&\quad=\hat{\Pi}_{\{\text{field pairs}\}}\langle\bar{\mathcal{E}}_1^{+}(t_1-\tau)\bar{\mathcal{E}}_2^{-}(t_2)\rangle\\&\qquad\times\langle\bar{\mathcal{E}}_3^{+}(t_3)\bar{\mathcal{E}}_1^{-}(s_1-\tau)\rangle\\&\qquad\times\langle\bar{\mathcal{E}}_1^{+}(s_2)\bar{\mathcal{E}}_3^{-}(s_3)\rangle\ ,\end{aligned}\tag{2.1}$$

where the $\hat{\Pi}_{\{\text{field pairs}\}}$ operator generates the six different ways of arranging the fields as conjugate pairs. Here we have

$$\begin{aligned}&\hat{\Pi}_{\{\text{field pairs}\}}\langle\bar{\mathcal{E}}_1^{+}(t_1-\tau)\bar{\mathcal{E}}_2^{-}(t_2)\rangle\langle\bar{\mathcal{E}}_3^{+}(t_3)\bar{\mathcal{E}}_1^{-}(s_1-\tau)\rangle\langle\bar{\mathcal{E}}_2^{+}(s_2)\bar{\mathcal{E}}_3^{-}(s_3)\rangle\\&\quad=\langle\bar{\mathcal{E}}_1^{+}(t_1-\tau)\bar{\mathcal{E}}_2^{-}(t_2)\rangle\langle\bar{\mathcal{E}}_3^{+}(t_3)\bar{\mathcal{E}}_1^{-}(s_1-\tau)\rangle\langle\bar{\mathcal{E}}_2^{+}(s_2)\bar{\mathcal{E}}_3^{-}(s_3)\rangle\\&\qquad+\langle\bar{\mathcal{E}}_1^{+}(t_1-\tau)\bar{\mathcal{E}}_2^{-}(t_2)\rangle\langle\bar{\mathcal{E}}_3^{+}(t_3)\bar{\mathcal{E}}_3^{-}(s_3)\rangle\langle\bar{\mathcal{E}}_1^{-}(s_1-\tau)\bar{\mathcal{E}}_2^{+}(s_2)\rangle\\&\qquad+\langle\bar{\mathcal{E}}_1^{+}(t_1-\tau)\bar{\mathcal{E}}_3^{-}(s_3)\rangle\langle\bar{\mathcal{E}}_2^{-}(t_2)\bar{\mathcal{E}}_2^{+}(s_2)\rangle\langle\bar{\mathcal{E}}_3^{+}(t_3)\bar{\mathcal{E}}_1^{-}(s_1-\tau)\rangle\\&\qquad+\langle\bar{\mathcal{E}}_1^{+}(t_1-\tau)\bar{\mathcal{E}}_3^{-}(s_3)\rangle\langle\bar{\mathcal{E}}_2^{-}(t_2)\bar{\mathcal{E}}_3^{+}(t_3)\rangle\langle\bar{\mathcal{E}}_1^{-}(s_1-\tau)\bar{\mathcal{E}}_2^{+}(s_2)\rangle\\&\qquad+\langle\bar{\mathcal{E}}_1^{+}(t_1-\tau)\bar{\mathcal{E}}_1^{-}(s_1-\tau)\rangle\langle\bar{\mathcal{E}}_2^{-}(t_2)\bar{\mathcal{E}}_2^{+}(s_2)\rangle\langle\bar{\mathcal{E}}_3^{+}(t_3)\bar{\mathcal{E}}_3^{-}(s_3)\rangle\\&\qquad+\langle\bar{\mathcal{E}}_1^{+}(t_1-\tau)\bar{\mathcal{E}}_1^{-}(s_1-\tau)\rangle\langle\bar{\mathcal{E}}_2^{-}(t_2)\bar{\mathcal{E}}_3^{+}(t_3)\rangle\langle\bar{\mathcal{E}}_2^{+}(s_2)\bar{\mathcal{E}}_3^{-}(s_3)\rangle\ .\end{aligned}\tag{2.2}$$

Eberly and Wodkiewicz have pointed out how a clear distinction in the time scales governing fluctuations in the field amplitude, or the phase, validates the factorization of the field autocorrelation (and cross-correlation) function (and consequently their spectral densities) into their slow and fast moving parts.[60] Since the classical field function $\bar{\mathcal{E}}_\lambda^{\xi_\lambda}(t)$ can be expressed in terms of a slowly varying amplitude function $\bar{\eta}_\lambda^{\xi_\lambda}(t)$ and a rapidly fluctuating phase function $\bar{\phi}_\lambda^{\xi_\lambda}(t)$, each of the pair correlators in Eq. (2.2) can be written in factored form

$$\begin{aligned}&\langle\bar{\mathcal{E}}_\lambda^{\pm}(t_m-\tau)\bar{\mathcal{E}}_{\lambda'}^{\mp}(s_n)\rangle\\&\qquad=e_{\lambda,\lambda'}^{\pm,\mp}\left[\frac{t_m+s_n}{2}\right]f_{\lambda,\lambda'}^{\pm,\mp}(|t_m-s_n-\tau|)\ .\end{aligned}\tag{2.3}$$

Here the experimental delay time τ is taken to be a small fraction of the pulse width. If field λ acts on chromophore α at time t_m, and field λ' on chromophore β at time s_n, then the τ-independent intensity function for the long pulse, evaluated at the mean local time $(t_m+s_n)/2$, is

$$e_{\lambda,\lambda'}^{\pm,\mp}\left[\frac{t_m+s_n}{2}\right]=\left\langle\left|\eta_\lambda^{\pm}\left[\frac{t_m+s_n}{2}\right]\right|^2\right\rangle\ ,\tag{2.4}$$

and the correlation among the fast stationary stochastic degrees of freedom for the same case is given by

$$f_{\lambda,\lambda'}^{\pm,\mp}(|t_m-s_n-\tau|)=\langle\bar{\phi}_\lambda^{\pm}(|t_m-s_n-\tau|)\bar{\phi}_{\lambda'}^{\mp}(0)\rangle\ .\tag{2.5}$$

After cycle averaging, the high-frequency correlators vanish. Thus

$$f_{\lambda,\lambda'}^{\pm,\pm}(|t_m-s_n|)=0\ .\tag{2.6}$$

Next we examine the stochastic correlators $f_{i,j}^{\pm,\mp}$ expressed as Fourier transforms of their spectral densities. Thus

$$\begin{aligned}f_{\lambda,\lambda'}^{\pm,\mp}(|t_m-s_n|)=\int_{-\infty}^{\infty}d\omega_\lambda'\int_{-\infty}^{\infty}d\omega_{\lambda'}''J_{\lambda,\lambda'}(\omega_\lambda',-\omega_{\lambda'}'')\\\times e^{-i(\omega_\lambda' t_m-\omega_{\lambda'}''s_n)}\ ,\end{aligned}\tag{2.7}$$

where the spectral densities ($J_{\lambda,\lambda}=J_\lambda$) take the form [see Eq. (1.36)]

$$J_{\lambda,\lambda'}(\omega_\lambda',-\omega_{\lambda'}'')=\langle\tilde{\bar{\phi}}_\lambda^{\pm}(\omega_\lambda')\tilde{\bar{\phi}}_{\lambda'}^{\mp}(\omega_{\lambda'}'')\rangle\delta(\omega_\lambda'-\omega_{\lambda'}'')\ .\tag{2.8}$$

There has been much effort in modeling phase fluctuations in the electromagnetic field and their influence on nonlinear optical processes.[60–64] Recently, Kofman

et al. have developed a non-Markovian model describing phase noise in laser fields having an arbitrary degree of coherence.[65] Such a description recovers the commonly used noise models (e.g., phase-diffusion model, telegraph noise model, Burshtein model, etc.) in the appropriate limits.

It is instructive to consider the similarities in the treatments of phase noise in the excitation fields and in the stochastic origins of material line broadening. For instance, the often used two-time fluctuation correlation function of the molecular (atomic) Bohr frequencies,[65–67] originating in Brownian motion theory, has the follow form:

$$f(t)=\exp\left[-\frac{\delta^2}{\Lambda^2}(e^{-\Lambda t}-1+\Lambda t)\right], \tag{2.9}$$

where δ and Λ^{-1} are measures of the amplitude and correlation time of the frequency fluctuations, respectively. Such a functional form is recovered in the generalized jump model of Ref. 65 in the limit of small, highly correlated, phase jumps. Here the factor $(\delta/\Lambda)^2$ is replaced with $[B/(1-\gamma)]^2$, where B is the variance of the distribution of phase jumps and γ represents a correlation parameter.

Fields having inhomogeneous bandwidths are obtained in the slow modulation limit $(\delta/\Lambda \gg 1)$ where the spectral densities become Gaussian,

$$J(\omega)=(\sqrt{2\pi}\delta)^{-1}\exp\left[\frac{-\omega^2}{2\delta^2}\right]. \tag{2.10}$$

In the fast modulation limit $(\delta/\Lambda \ll 1)$ Lorentzian spectral densities are recovered:

$$J(\omega)=\frac{1}{\pi}\frac{\Gamma}{\omega^2+\Gamma^2} \tag{2.11}$$

where

$$\Gamma=\frac{\delta^2}{\Lambda}. \tag{2.12}$$

Whereas the fast stochastic fluctuations of the field [represented by $J_\lambda(\omega)$] are directly responsible for generating the short time (τ) behavior of the signal, the slower degrees of freedom (defining the pulse envelope) will accumulate material responses on a much longer time scale. To account for the accumulation, the time local intensity factors $e^{\pm,\mp}_{\lambda,\lambda'}[(t_m+s_n)/2]$ are directly convolved with the material response function in the expression for the generalized susceptibility, Eqs. (1.37) and (1.38). The convolution of the material dynamics $(\langle \hat{R}^{(3)}_Q(t)\rangle_{\{Q\}}$, $Q=\alpha,\beta)$ over the time local intensities leads to an averaged steady state that reflects dynamical processes on a time scale as long as the pulse width itself (i.e., intensity correlation time) and no shorter than the coherence time τ_c of the incoherent light. A closely related point, previously discussed by Bai and Fayer,[68] concerns the discrepancy in optical dephasing times of complex condensed-phase systems, probed by long-time hole burning or by various short-time photon-echo spectroscopies.

In Sec. I it was emphasized how when all of the input fields are correlated, the time evolution of the third-order polarization amplitude may involve more than one chromophore (set $\{\alpha_\lambda\}$). Here we stay with the bichromophore model in which a single chromophore acquires full third-order polarization, and two-chromophore scattering unit leads to the phase-matched signal. The long-time averaging involving the local intensities [Eq. (2.4)] causes the individual chromophore third-order response operators $\hat{R}^{(3)}_\alpha(t)$ and $\hat{R}^{(3)\dagger}_\beta(t)$ to become linked, thus producing a bichromophore sixth-order spectral response function. From this end, the polarization correlator given in Eq. (1.37) can be rewritten here as

$$\begin{aligned}\mathcal{C}(t',s';\tau)=&\left[\prod_{\lambda=1}^{3}|E^0_\lambda|^2\right]\frac{\Xi(\Delta\mathbf{k})}{N_\alpha N_\alpha}\\
&\times\int_{-\infty}^{\infty}d\omega_1'\int_{-\infty}^{\infty}d\omega_2'\cdots\int_{-\infty}^{\infty}d\omega_3''\hat{\Pi}_{\{\text{field pairs}\}}J_{1,2}(\omega_1',\omega_2')J_{3,1}(\omega_3',\omega_1'')J_{2,3}(\omega_2'',\omega_3'')\\
&\times\psi^{(6)}_{S,1,2,3}((\omega_1-\omega_1'),-(\omega_2-\omega_2'),\ldots,-(\omega_3-\omega_3''))\\
&\times e^{i(\omega_1'-\omega_1'')\tau}\exp\left[-i\sum_{j=1}^{3}\xi_j[(\omega_j-\omega_j')t'-(\omega_j-\omega_j'')s']\right].\end{aligned} \tag{2.13}$$

The spectral material response function $\psi^{(6)}_{S,1,2,3}$, sixth order in the fields, is not a general sixth-order susceptibility, but is constructed from the product of third-order susceptibilities $\langle\hat{\chi}^{(3)}\hat{\chi}^{(3)\dagger}\rangle_R$ [see Eq. (1.37)]. Representing the accumulated steady state of the driven material system, this spectral material response function can be written with the help of Eq. (1.40) as

$$\begin{aligned}&\psi^{(6)}_{S,1,2,3}((\omega_1-\omega_1'),-(\omega_2-\omega_2'),\ldots,-(\omega_3-\omega_3''))\\
&=N_\alpha N_\beta\int_0^\infty d\tau_1\int_0^\infty d\tau_2\int_0^\infty d\tau_3\int_0^\infty d\sigma_1\int_0^\infty d\sigma_2\int_0^\infty d\sigma_3\hat{\Pi}^{\alpha}_{1,2,3}\hat{\Pi}^{\beta}_{1,2,3}\langle\hat{K}^{\alpha}(\tau_1,\tau_2,\tau_3)\hat{K}^{\beta\dagger}(\sigma_1,\sigma_2,\sigma_3)\rangle_R\\
&\times F^\alpha(\tau_1,\tau_2,\tau_3)F^\beta(\sigma_1,\sigma_2,\sigma_3)e^{+,-}_{1,2}\left[\frac{2t'-2\tau_1-\tau_2}{2}\right]\\
&\times e^{+,-}_{3,1}\left[\frac{t'-\tau_1-\tau_2-\tau_3+s'-\sigma_1}{2}\right]e^{+,-}_{2,3}\left[\frac{2s'-2\sigma_1-2\sigma_2-\sigma_3}{2}\right].\end{aligned} \tag{2.14}$$

The product $\hat{K}^{Q}F^{Q}$ ($Q=\alpha$ and β) is associated with the third-order response operator $\langle \hat{R}_{Q}^{(3)}(t)\rangle_{\{Q\}}$ and has been defined in Eqs. (1.41) and (1.42) for a given channel q identified with $\langle \hat{R}_{Q}^{(3)}(t)_{q}\rangle_{\{Q\}}$.

Where the short-time stochastic fluctuations of the radiation fields ($\tilde{\phi}_{\lambda}^{\pm}$) are responsible for its spectral width [through $J_{\lambda,\lambda'}(\omega_{\lambda},\omega_{\lambda'})$], the material stochastic dynamics (via $\tilde{H}_{MB}$), contained in the function $F^{Q}(t)$ ($Q=\alpha,\beta$) and convolved with the local time intensities in Eq. (2.14), bring out the spectral widths of the material resonances. Modeling of such material stochastic processes has been extensively discussed in the literature.[25,27,69] In general (Appendix A), the result of stochastic averaging over the material Bohr frequency fluctuations associated with qth channel [Eq. (1.42)] can be written as

$$F_{q}^{Q}(\tau_1,\tau_2,\tau_3)=\prod_{i}^{e}\exp\left[-\frac{\delta_i^2}{\Lambda_i}(\tau_1+\tau_3)-\frac{\delta_i^2}{\Lambda_i^2}[e^{-\Lambda_i\tau_1}+e^{-\Lambda_i\tau_3}-2+e^{-\Lambda_i\tau_2}(1-e^{-\Lambda_i\tau_1})(1-e^{-\Lambda_i\tau_3})]\right]$$
$$\times\prod_{j}^{v}\exp\left[-\frac{\delta_j^2}{\Lambda_j^2}(e^{-\Lambda_j\tau_2}+1-\Lambda_j\tau_2)\right], \tag{2.15}$$

where the product is over different statistically independent random processes, the ith being characterized by a rms amplitude δ_i and correlation time Λ_i^{-1}. The superscripts e and v on the product operator anticipate the Born-Oppenheimer approximation and stand for decoupled electronic and vibrational random processes, respectively.

A few general qualitative comments can be made concerning the integration in Eq. (2.14). The numerical modeling of accumulation effects important in long-pulse incoherent 4WM will be the focus of future work. The real-time material response characteristic of each time interval (τ_j or σ_j) will be averaged over an accumulation time determined by the local intensity functions. Whether a given random process is to be characterized in the slow-modulation limit [Eq. (2.10)], fast-modulation limit [Eq. (2.11)], or in between [Eq. (2.9)] depends on the ratio of the accumulation time (or the time scale of the experiment, $t_{\rm acc}$) to the correlation time of the bath, namely $\Lambda t_{\rm acc}$. Dynamical processes that are static relative to the field coherence time ($\Lambda\tau_c \ll 1$) may be motionally narrowed on the time scale of the intensity correlation ($\Lambda t_{\rm acc} \gg 1$). In such cases, line shapes that are measured with long-pulsed incoherent light may appear homogeneous in nature, having widths that reflect dynamics averaged over 3–4 decades. The same stochastic processes may lead to inhomogeneously broadened lines in measurements that use coherent short-pulsed light (where $\tau_c \approx t_{\rm acc}$) of comparable bandwidths. In such experiments any remaining homogeneous components would have to reflect only very short time dynamics.

The accumulated steady state is not only determined by the long-time averaging of independent stochastic processes associated with pure dephasing, but also reflects the averaged dynamics associated with the possible transfer of excitation to dark states (the inelastic contribution to the dephasing process). On a time scale characterized by a γ_{ij}^{-1} up to the temporal widths of the field envelopes, initially unexcited modes that are nevertheless coupled to the driven states can acquire excitation amplitude and thereby initiate new scattering pathways among the material states.

For long-pulsed incoherent excitation, the temporal pulse shape, contained in the local intensities, serves as a real-time filter in averaging the dynamical responses of the material. Suppose the distribution of relaxation rates in $F^{Q}(t)$ and the distribution of the inelastic rate constants γ_{ij}'s are both narrow compared to the field envelopes. In that case the field envelopes are constant over the time where $F^{\alpha}(t)$, $F^{\beta}(t)$, and $\langle \hat{K}^{\alpha}(t')\hat{K}^{\beta}(s')\rangle_{R}$ are nonvanishing in the integral in Eq. (2.14). For such material systems, the exciting fields are effectively continuous wave, and therefore their envelopes do not contribute to the dynamic polarization. Should the dynamical response of the system be characterized by a broad distribution of relaxation times, the slower ones would not significantly contribute to the material response in the leading part of the excitation pulse. However, if the excitation persists these slower processes are allowed to build up and influence that portion of the spectral line corresponding to their characteristic time scales. The interferograms then would show the decay of the steady-state material excitation. Such decays, in τ, potentially could be dramatically different, both in functionality and time scale, from those measured with short-pulsed excitation.

In general with incoherent excitation, the measured linewidth of the polarization correlator [Eq. (2.14)] corresponds to the six-dimensional Fourier transform of the product of the generalized spectral densities of the fields with the spectrum of the nonlinear response averaged on the time scale of the pulse width. Since the pulses are in constant temporal and spatial overlap, the τ dependence of the correlator is generated by delaying a given field(s) from any correlated conjugate field(s) and will be discussed further at the end of this section.

B. Coherent short-pulsed excitation

A formal transition to experiments that use coherent short pulses can be accomplished by allowing the temporal widths of the fields to narrow while maintaining a constant bandwidth defined by the spectral densities $J(\omega)$. While still maintaining a clear distinction between the time scales describing short- and long-time fluctuations ($\tilde{\phi}_{\lambda}$ and $\tilde{\eta}_{\lambda}$, respectively), the effect of narrowing the duration of the pulse is twofold. First, the reduced duration over which real-time averaging of the material dynamics occurs leads to a new steady state of the driven system. Second, for experimental delays exceeding the

pulse width, the interferograms acquire an asymmetry that reflects the distinction between pumping and probing steps in the scattering process. The necessary time ordering of the field envelopes when they are not cotemporal reduces the permutation symmetry of the operator $\hat{\Pi}$ appearing in Eqs. (1.38) and (2.14).

For the case of bandwidth-limited (coherent) excitation fields, the factorization of the sixth-order field correlation function, based on both complex Gaussian statistics and distinct stochastic time-scale arguments [Eqs. (2.1), and (2.3)], is no longer valid. Now, depending on the pulse shape, the coherence time (phase correlation time) is essentially equal to the width of the envelope (or the intensity correlation time). However, a different factorization approximation can be used based on the degree of coherence among the mixing fields. From the analysis in Ref. 54, full coherence at arbitrary orders leads to a general factorization condition. At second order, this corresponds to maximum visibility of the interference fringes where one can write

$$|\Gamma^{(1,1)}(t_i,s_j)|^2=\Gamma^{(1,1)}(t_i,t_i)\Gamma^{(1,1)}(s_j,s_j) . \tag{2.16}$$

Analogous to the notation in Eqs. (1.32) and (1.33), Eq. (2.16) refers to the pair correlators $\Gamma^{(1,1)}(t_i,s_j)=\langle\epsilon^{\pm}(t_i)\epsilon^{\mp}(s_j)\rangle$. Equation (2.16) can be used[54] to show pairwise correlation of the superposition field at two different times in terms of the average at one time t_0. To this end, one writes

$$\langle\epsilon^{\pm}(t_i)\epsilon^{\mp}(s_j)\rangle=\frac{\Gamma^{(1,1)}(t_i,t_0)\Gamma^{(1,1)}(t_0,s_j)}{[\Gamma^{(1,1)}(t_0,t_0)]^2}\langle\epsilon^{\pm}(t_0)\epsilon^{\mp}(t_0)\rangle$$

$$=C^{\pm}(t_i)C^{\mp}(s_j) . \tag{2.17}$$

Here the function $C^{+}(t_i)$ and $C^{-}(s_j)$ are given by

$$C^{+}(t_i)=\frac{\Gamma^{(1,1)}(t_i,t_0)}{[\Gamma^{(1,1)}(t_0,t_0)]^{1/2}} \tag{2.18}$$

and

$$C^{-}(s_j)=\frac{\Gamma^{(1,1)}(t_0,s_j)}{[\Gamma^{(1,1)}(t_0,t_0)]^{1/2}} . \tag{2.19}$$

In an identical manner, the full sixth-order temporal correlation function for the mixing process can be written as

$$\Gamma^{(3,3)}(t_1-\tau,t_2,t_3,s_1-\tau,s_2,s_3)$$
$$=\langle\epsilon^{+}(t_1-\tau)\epsilon^{+}(t_2)\cdots\epsilon^{-}(s_3)\rangle$$
$$=\gamma^{(3,3)}\prod_{i=1}^{3}C^{+}(t_i-\tau\delta_{i1})\prod_{j=1}^{3}C^{-}(s_j-\tau\delta_{j1}) \tag{2.20}$$

where the normalized degree of coherence $\gamma^{(3,3)}$ follows as

$$\gamma^{(3,3)}=\frac{\Gamma^{(3,3)}(t_0,t_0,\ldots,t_0)}{[\Gamma^{(1,1)}(t_0,t_0)]^3} . \tag{2.21}$$

Again the $\pm$ superscript on the superposition field $\epsilon^{\pm}(t)$ denotes the complex conjugate set of fields defined through the chosen phase matching condition $\{\xi_\lambda\}$. t_o is an arbitrary time point and therefore can be placed anywhere during the temporal evolution of the polarization amplitudes of chromophore α (t space) or chromophore β (s space). By assuming full sixth-order coherence, $\gamma^{(3,3)}$ can be set equal to unity and the correlation function can be expressed as a sum of products of the normalized pair correlators $C^{+}(t_i),C^{-}(s_j)$. Full coherence at arbitrary orders of correlation can be realized, for example, by fields in a coherent state. (In contrast, incoherent, or in some sense chaotic fields, can only exhibit full coherence at first order where $\gamma^{(1,1)}=1$, but $\gamma^{(n,n)}\neq 1$ for $n>1$.)

The field $\epsilon^{\pm}(t)$, in Eq. (2.20), represents a linear combination of fields whose active Fourier components are determined through the phase-matching condition. Therefore we write

$$\epsilon^{\pm}(t_j)=\sum_{\lambda=1}^{3}\epsilon_\lambda^{\pm\xi_\lambda}(t_j) . \tag{2.22}$$

The above superposition field is inserted into the $C^{\pm}(t_i)$ functions [Eqs. (2.18) and (2.19) using the definition of $\Gamma^{(1,1)}$]. Only those relevant terms giving three different fields along with their conjugates are considered. The six-field correlator $\Gamma^{(3,3)}$ [Eq. (2.20)] now gives a sum of products of pair correlators associated with a given ordering of the three fields on one chromophore α and a given time ordering of the three conjugate fields on chromophore β. We have

$$\Gamma^{(3,3)}(t_1-\tau,t_2,\ldots,s_3)=\langle\epsilon_1^{+}(t_1-\tau)\epsilon_2^{-}(t_2)\epsilon_3^{+}(t_3)\epsilon_1^{-}(s_1-\tau)\epsilon_2^{+}(s_2)\epsilon_3^{-}(s_3)\rangle$$
$$=\hat{\Pi}_{1,2,3}(t_o)\left[\prod_{i=1}^{3}C_{\lambda_i}^{+}(t_i+\tau\delta_{i1})\prod_{j=1}^{3}C_{\lambda_j}^{-}(s_j+\tau\delta_{j1})\right] . \tag{2.23}$$

The operator $\hat{\Pi}_{1,2,3}(t_o)$ permutes the three fields and conjugate fields at t_o among the $C_{\lambda_i}^{\pm}(t_i)$ functions (λ_i being the field associated with the time variable t_i). Two general types of pair correlators are reached after considering all permutations. The first type is one where a given field is correlated with its self-conjugate and includes intensity cross correlation. It is given by the product of $C_{\lambda_i}^{\pm}$ functions such as

$$C_\lambda^{-}(s_j)C_\lambda^{+}(t_i)=\frac{\langle\epsilon_\lambda^{-}(s_j)\epsilon_{\lambda'}^{+}(t_0)\rangle\langle\epsilon_{\lambda'}^{-}(t_0)\epsilon_\lambda^{+}(t_i)\rangle}{\langle\epsilon_{\lambda'}^{-}(t_0)\epsilon_{\lambda'}^{+}(t_0)\rangle} . \tag{2.24}$$

A second type of pair correlator represents cross correlation between two different, yet phase correlated, fields given by

$$C_{\lambda}^{-}(s_j)C_{\lambda''}^{+}(t_i)=\frac{\langle \epsilon_{\lambda}^{-}(s_j)\epsilon_{\lambda'}^{+}(t_0)\rangle\langle \epsilon_{\lambda'}^{-}(t_0)\epsilon_{\lambda''}^{+}(t_i)\rangle}{\langle \epsilon_{\lambda'}^{-}(t_0)\epsilon_{\lambda'}^{+}(t_0)\rangle} . \tag{2.25}$$

Correlators of the type given in Eqs. (2.24) and (2.25), and found in Eq. (2.23), are convolved with the material response through Eq. (1.26) (in its bichromophore version). Just as in the case involving incoherent excitation, nonlinear parametric mixing with correlated bandwidth limited fields can lead to correlation on a single chromophore (α or β) or across two chromophores (α and β). In fact, extensive correlation among the fields would require a return to the multichromophore picture ($\{\alpha_\lambda\},\{\beta_\lambda\}$) developed in Sec. I.

In addition to the 4WM transients generated by delaying mutually coherent conjugate fields, an additional τ dependence is introduced into the optical mixing because of the brief duration of the pulse envelopes. In general, a pumping step, represented by a τ independent field intervention, followed by an uncorrelated (or unconjugated) τ-dependent probing field, will produce signal transients that reflect material relaxation. If the material response is sufficiently fast, a direct intensity cross correlation of the uncoupled fields will be measured as given by Eq. (2.24) with $\lambda=\lambda'$. The τ dependence would reflect the reduced overlap between the $\lambda=1$ correlator of Eq. (2.24) with the analogous correlator for either the $\lambda=2$ or 3 fields. When all input fields are fully uncorrelated the τ dependence is solely derived from correlation of the type in Eq. (2.24) with $\lambda=\lambda'$. Such signals, not sensitive to the phase coherence among the driving fields, would not be seen in analogous measurements with long-pulsed incoherent light where these correlated fields always overlap in time because the τ parameter in the experiment normally scans on the scale of the coherence time of the light, not the time scale of the pulse duration. Furthermore, signal transients derived from the intensity cross correlation (an amplitude level envelope correlator), independent of the phase of the driving fields, do not directly depend on field induced interchromophore correlation, but originate at the polarization level. Such signals can be interpreted as a superposition of classical third-order polarization waves.

C. A diagrammatic view of the field-induced two-chromophore correlation in nonlinear mixing

The signal generated in 4WM processes (or general nonlinear mixing) using either long-pulse incoherent excitation or short-pulsed coherent excitation can be based on the phase-sensitive field correlator [Eq. (2.3)], on a field intensity correlator, or both. For the measurements involving incoherent exciting fields considered here, the phase correlators are solely responsible for the transient responses (in τ), and the local intensity correlators generate the constant background signal as well as define the accumulation time of the material dynamics. On the other hand, the use of coherent short-pulsed fields can lead to signal transients based on both field phase correlation and field intensity correlation. Both types of correlators will generate τ dependence on the same time scales (depending on material response time or "memory"). Experiments with incoherent light offer the chance to isolate signal responses that are phase sensitive to the exciting fields (though averaged in real time). Of primary interest in the remaining discussion will be such phase-sensitive responses based on the pair correlators of long-pulsed incoherent fields as well as coherent short-pulsed fields and both capable of inducing interesting interchromophore interferences.

Mutually coherent fields may have their intervention on the same chromophore or on separate chromophores, depending on the phase matching requirements of the detected signal (set by the choice of $\{\xi_\lambda\}$). Qualitatively, this can be understood by considering the Feynman diagrams in Fig. 2 (for the bichromophore model). Here the two time lines ending in t' and s' represent a given temporal evolution of the density operators for the α and β

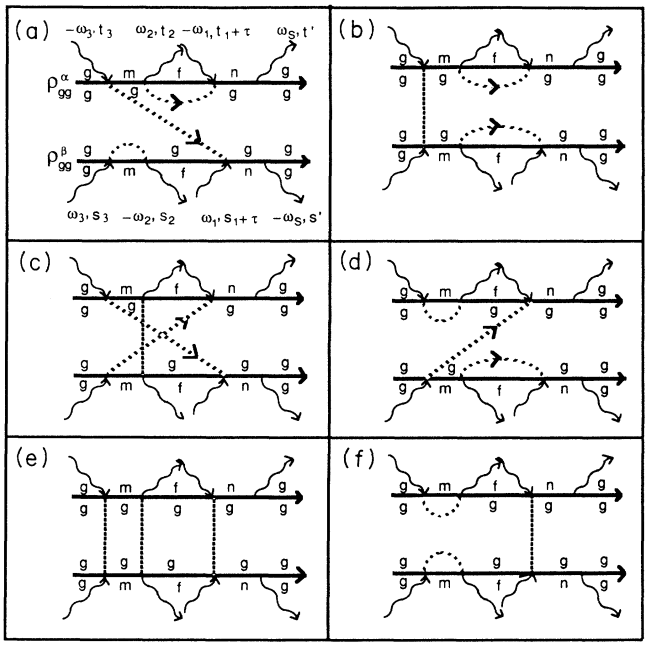

FIG. 2. Two-chromophore dual Feynman diagrams representing the optical mixing at eighth order in the field-matter interaction. Each of the two horizontal lines represents the time evolution of the density operator on a single chromophore, α (top line) and β (bottom line). A wavy arrow (field operator) touching a vertex point at the top side of a line represents a ket side field-matter intervention and one touching the bottom side of a line denotes a bra side intervention. Time increases from left to right, ending with the generation of $\dot{a}$ field quantum in the signal mode S at times t' and s' for the α and β chromophore evolution, respectively. Each of the six diagrams represents a unique combination of three field pair correlators, represented by the dashed lines, all for the same time ordering of the fields. The fields are labeled in (a) only. Every time ordering generates a new set of six such correlation diagrams. The dashed lines containing arrow heads indicate a source of direct dependence on the experimental delay parameter τ (see text).

chromophores, respectively. The incoming (outgoing) wavy arrows represent a positive (negative) frequency field intervention resulting in a promotion (demotion) of a ket amplitude shown at the top of the lines. Likewise, the promotion (demotion) of a bra amplitude component, represented by the vertex points on the bottom of the lines, results from an incoming (outgoing) arrows denoting a negative (positive) frequency intervention. The diagrams are for the rotating-wave terms only. The assumed central limit nature of the field statistics for incoherent excitation, or the assumed full coherence for bandwidth limited fields, permits factorization of the sixth-order field correlation function and results in six different products of pair correlators for the case of correlation among all of the driving fields [Eqs. (2.1) and (2.20)]. Such possible first-order coherences are schematically represented by the dashed lines connecting intervention points. The arrows on these lines serve to indicate the sign of the τ-dependent phase obtained in the Fourier transformation of the pair correlators. Of the six different sets of mutual coherence functions [Figs. 2(a)–2(f)], four of them [Figs. 2(a)–2(d)] are phase sensitive to delaying field $\tilde{\epsilon}_1^{\pm}(t-\tau)$, by time τ, and thus are responsible for the signal transients observed in the interferogram. In general, these phase-sensitive transients (sub-pulse-width transients for nonbandwidth limited fields) can be generated by mutually delaying any field, or combination of fields, from a given correlated field, or set of fields.

Further distinctions can be made among the τ-dependent field correlators [e.g., Fig. 2(a)] based on whether correlation is introduced at two points within one time line (single chromophore) or across the two time lines (dual chromophore). A physical interpretation of such mixing processes can be given in terms of quantum-mechanical interferences between coherent radiation-material oscillators (see Sec. IV).

Coherent oscillators are generated by allowing the phase structure of the driving fields to be imprinted in the material in the form of a radiation-chromophore superposition state. The contrast of this imprint will degrade due to the dephasing of the joint radiation-matter coherence, which oscillates at the detuning of the field carrier frequencies from the (near-resonant) chromophore Bohr frequencies. The coupling of such an oscillator to a mutually coherent probe field will occur as long as phase memory of the excitation step is retained. For example, this process is represented by the curved, dashed line connecting intervention points ω_2,t_2 and $-\omega_1,t_1+\tau$ in Fig. 2(a). In the same diagram, the two-chromophore field correlators denoted by the dashed line connecting the $-\omega_3,t_3$ and $\omega_1,s_1+\tau$ interventions, represent the interference between the mutually coherent superpositions involving the off-diagonal material density-matrix components ρ_{mg}^{α} and ρ_{gn}^{β}. A generalized coherence time characteristic of such an interference can be defined in terms of the dephasing times of the near-resonant material transitions, as well as the reciprocal bandwidths of the driving fields. In Sec. III, this point will be further discussed analytically in the context of particular 4WM applications.

Each of the six products of pair correlators, given in Eqs. (2.1) and (2.20) and illustrated in Fig. 2, contains at least one term independent of τ. In general, the effect of such τ-independent phase correlation is to introduce additional line-broadening mechanisms, or to mix the different resonances reached during the evolution of the third-order polarizations. In certain applications (see Sec. III), bandwidth control of the spectral densities, defined in terms of these τ-independent correlators, will serve to filter certain mixing channels to produce characteristically new features in the 4WM interferogram and signal spectrum.

In Sec. III, the previously generalized topics will be given analytic expression for certain 4WM mixing processes. An attempt is made to classify the various transient responses that can be seen under different conditions of excitation.

III. FIELD CORRELATED COHERENT RAMAN 4WM ANALYTIC RESULTS

A class of three-color 4WM processes known as the coherent Raman spectroscopies will be considered analytically in this section. Later, in Sec. IV, the results will be modeled. We begin with some general observations.

A. CARS and CSRS contrasted: some general remarks

By changing the wave vector and frequency labels $\mathbf{k}_3,\omega_3$ to $\mathbf{k}_2',\omega_2$ in Fig. 1, the anti-Stokes (CARS) signal component can be represented by the wave vectors $\mathbf{k}_C$, $\mathbf{k}_D$, and $\mathbf{k}_E$ for $\omega_1<\omega_2$, while the corresponding Stokes (CSRS) vectors are those labeled $\mathbf{k}_H$ and $\mathbf{k}_I$. Conversely, for $\omega_1>\omega_2$ the CSRS signal vectors are identified by $\mathbf{k}_C$, $\mathbf{k}_D$, and $\mathbf{k}_E$, where the CARS signal vectors are those labeled $\mathbf{k}_H$ and $\mathbf{k}_I$. As a probe of Raman-active vibrational dynamics, the three-beam geometry, generating the fourth wave in the $\mathbf{k}_C=\mathbf{k}_2'+\mathbf{k}_2-\mathbf{k}_1$ direction, is often used. Here one of the degenerate fields, for instance, $\mathbf{k}_2',\omega_2$, is delayed relative to the other, $\mathbf{k}_2,\omega_2$, which simultaneously mixes with the nondegenerate $-\mathbf{k}_1,-\omega_1$ field. The resulting signal frequency $\omega_S=2\omega_2-\omega_1$ is up-converted (down-converted) relative to the input fundamentals for the CARS (CSRS) process.

The diagrammatic representation discussed by Lee and Albrecht[70] is used to express some of the important rotating-wave terms that contribute to the evolution of the single-chromophore density matrix for a two-level electronically nonresonant case (Fig. 3) and for a four-level electronically resonant case (Fig. 4) in coherent Raman mixing. Here the energy levels connected by a solid (dotted) arrow represent a ket (bra) amplitude transition. For example, the fully resonant CARS process that is illustrated in Fig. 4(d) can be described as an initial bra-side intervention from the field-matter coupling Hamiltonian $\tilde{V}_2^{-}(t_3)$ to give the radiation-matter superposition state generated by the density operator

$$\hat{\rho}_{g,n_2;n_2-1,n}=|g,n_1,n_2,n_2',0_S\rangle\langle 0_S,n_2',n_2-1,n_1,n| \ . \tag{3.1}$$

The input radiation modes λ are denoted by the occupa-

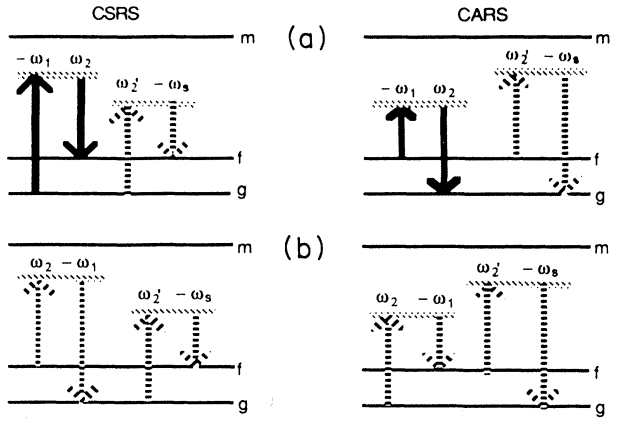

FIG. 3. Energy-level diagrams showing the Raman resonance in electronically nonresonant CSRS and CARS. The solid and dashed arrows represent a ket and bra side transition between the connected levels, respectively. Here, time increases from left to right. (See text for further discussion.)

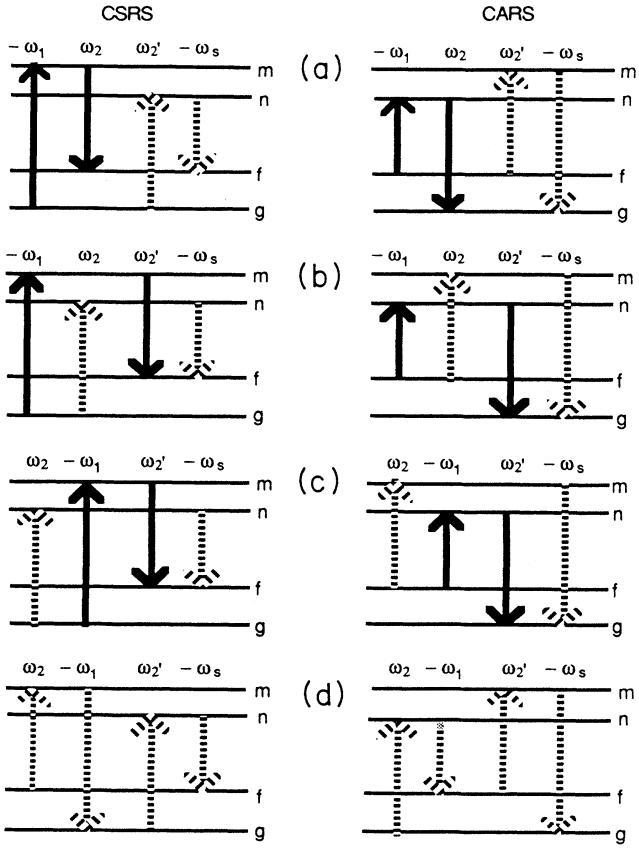

FIG. 4. Energy-level diagrams for fully resonant CSRS and CARS. The solid and dashed arrows represent a ket and bra side transition between the connected levels, respectively. Here time increases from left to right. (See text for further discussion.)

tion number n_λ, which for realistic fields, ought to represent a linear combination of number states for each mode (e.g., a coherent state). This coherence, oscillating at a carrier frequency given by the detuning $\omega_{ng}-\omega_2$, acquires a spectral width determined by the convolution of the ω_2 field spectral density with the ω_{ng} resonant line. Evolving under the assumed "dark" propagator for a time period $\tau_3=t_2-t_3$, the chromophore is then driven to the new radiation-matter superposition by

$$\hat{\rho}_{g,n_1,n_2;n_2-1,n_1+1,f} = |g,n_1,n_2,n_2',0_S\rangle\langle 0_S,n_2',n_2-1,n_1+1f| \ . \tag{3.2}$$

In the usual application of this technique, the Raman mode coherence is probed by delaying the $\omega_2'[\tilde{V}_2^{-\prime}(t_1+\tau)]$ intervention, which creates the output polarization given in terms of the off-diagonal state by

$$\hat{\rho}_{g,n_1,n_2,n_2';n_2'-1,n_2-1,n_1+1,m} = |g,n_1,n_2,n_2',0_S\rangle\langle 0_S,n_2'-1,n_2-1,n_1+1,m| \ . \tag{3.3}$$

Here the superposition oscillates at a radiation-matter frequency beat called a detuning, $\omega_{mg}-\omega_2'-\omega_2+\omega_1$, and possesses a phase characteristic of the driving fields. An excitation of the signal mode S occurs due to the collapse of the third-order polarization [i.e., an intervention from the vacuum blackbody field $\tilde{V}_S^{+}(t')$], leaving the material unexcited, but the light fields in altered superposition states,

$$\hat{\rho}_{n_1,n_2,n_2',0_S;1_S,n_2'-1,n_2-1,n_1+1} = |g,n_1,n_2,n_2',0_S\rangle\langle 1_S,n_2'-1,n_2-1,n_1+1,g| \ . \tag{3.4}$$

As indicated by the correlation diagrams of Fig. 2, the fields are brought into quadrature by allowing the adjoint set of interaction operators to intervene on the partner chromophore required to achieve directionality in the emission. This leads to the final redistribution of energy among the active modes of the radiation field $(n_1,n_2,n_2',0_S\rightarrow n_1+1,n_2-1,n_2'-1,1_S)$. In order to conserve momentum and energy in parametric (phase-matched) scattering, it is commonly accepted that there is no net energy exchanged between the chromophore and radiation. In other words, energy is conserved separately in the radiation and material subspaces. This is the case in the above example of resonant CARS, as well as for resonant degenerate 4WM and nonresonant parametric scattering in general (e.g., optical parametric oscillation).

An interesting situation arises when considering CSRS. Figures 3(b) and 4(d) show scattering terms where the material is left in the same initial state after the four-field intervention sequence. However, now the relevant initial state is thermally unpopulated whenever $|\omega_1-\omega_2| > k_BT/\hbar$. On the other hand, CSRS, initiated from the

ground state, leaves the chromophore in a different final state [Figs. 4(a)–4(c), or Fig. 3(a)], suggesting a net light-matter exchange of energy. Characteristic of these terms (usually referred to as nonparametric contributions) is that the off-diagonal state reached at third order in the field-matter interaction is a superposition between two initially unpopulated energy levels. Four-color frequency domain 4WM experiments have shown the importance of such terms for measuring homogeneous linewidths within an inhomogeneously broadened line.[71–74]

The remaining diagrams in Figs. 3 and 4 are included to demonstrate the complete symmetry between (fully resonant, or not) CSRS and CARS, provided level f is initially populated. In what follows, we take $\hbar\omega_{fg} > k_B T$ in order to consider only scattering that is initiated from the ground state of our chromophore.

The analytic signal limit of Eq. (1.37) is explored next for CSRS with incoherent light fields. This limit can be obtained in the usual manner by assuming a fast-modulation limit for the stochastic perturbations of the material Bohr frequencies [like Eq. (A11)] as well as an exponential temporal correlation among the driving fields. Furthermore, the nondegenerate fields will be taken to be statistically independent. Correlation between the nondegenerate fields, $\pm\omega_2$ (or $\pm\omega_{2'}$) and $\mp\omega_1$, in CARS spectroscopy has been investigated by Li, Radzewicz, and Raymer.[75]

Here the six-field correlation function in Eq. (2.1), for the generic time ordering, can be written as

$$\begin{aligned}\langle \tilde{\phi}_{\bar{2}}(t_1-\tau)\tilde{\phi}_{\bar{2}}(t_2)\tilde{\phi}_{1}^{+}(t_3)\tilde{\phi}_{2}^{+}(s_1-\tau)\tilde{\phi}_{\bar{2}}^{+}(s_2)\tilde{\phi}_{\bar{1}}(s_3)\rangle \\ = \{ f_{2',\bar{2}'}^{-,+}(|t_1-s_1|) f_{2,\bar{2}}^{-,t}(|t_2-s_2|) \\ + f_{2',\bar{2}}^{-,t}(|t_1-s_2-\tau|) f_{2,\bar{2}'}^{-,+}(|t_2-s_1+\tau|)\} \\ \times f_{1,\bar{1}}^{+,-}(|t_3-s_3|) \, . \end{aligned} \tag{3.5}$$

The modeling of possible accumulation effects of the material response on the time scale characterized by the local intensities $e_{\lambda,\lambda'}^{\pm,\mp}(t)$ will not be developed here. Instead, these are taken to be constants over the time scale of the interferometric experiment. We consider explicitly only the short-time stochastic degrees of freedom of the fields. As discussed in Sec. II such field coherence draws correlation among the evolution of the separate chromophore scattering amplitudes. In this CSRS spectroscopy, the phase-matched selected field components, acting on one chromophore, are such that the τ dependence arises only from dual-chromophore pair correlators. This is illustrated in Fig. 5 where the t' and s' time lines each stand for a particular amplitude level scattering channel, the same one represented in Figs. 3 and 4. The first term on the right-hand side (rhs) of Eq. (3.5) represents a product of self-correlation between beams 2 and 2'. Under the present assumption of stationarity, this term is independent of τ and contributes to the constant background signal. Built upon this dc signal is the τ dependence generated by mixed dual-chromophore correlators (beam 2 with 2') such as those found in the second term of Eq. (3.5). Since correlation only between degenerate fields is being considered, the nondegenerate ω_1 field serves as a constant source of polarization at frequency ω_1 to which the 2 and 2' fields may couple. The corresponding pair

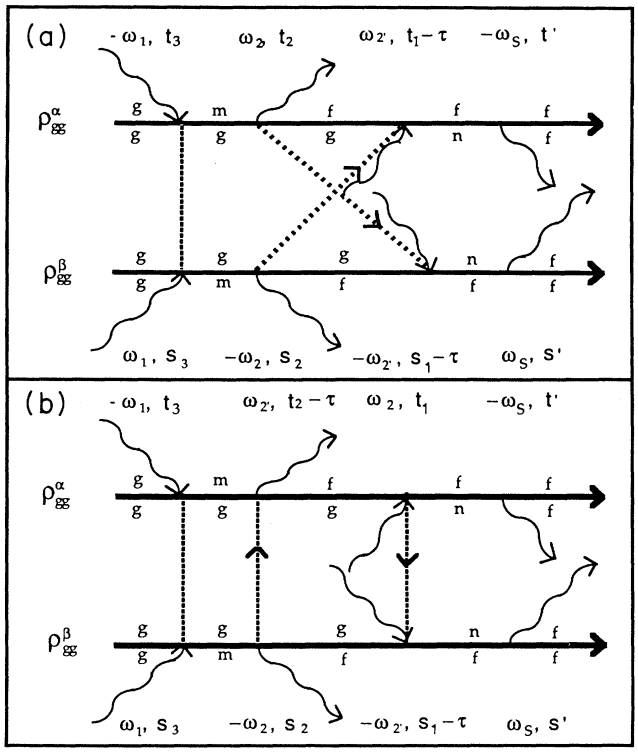

FIG. 5. The dual Feynman diagrams of Fig. 2 applied to the CSRS process: (a) the field correlation as given in Eq. (3.5); (b) the field correlation after permuting the 2 and 2' interventions on chromophore α. The corresponding energy-level diagram is that of Fig. 4(a) (for CSRS).

correlator $f_{1,\bar{1}}^{+,-}(t)$ (solid lines in Fig. 5), when Fourier transformed $[J_1(\omega_1)]$, will act as a spectral filter in much the same way as the signal filter $J_D(\omega_S')$.

In this ω_1,ω_2 decoupled limit, the τ sensitivity in incoherent CSRS (and CARS) has its origin in the four-field correlation function involving the 2 and 2' fields and their conjugates. This field coherence is identical to that probed in noncollinear autocorrelation via second-harmonic generation (SHG). For both measurements, theoretical predictions give a peak ($\tau=0$) to background ($\tau \gg \tau_c$) ratio of 2:1. A comparative study of noncollinear SHG and nonresonant three-beam CSRS or CARS signals can serve as a diagnostic for incoherent light and the validity of its being uncorrelated with field ω_1. A contrast ratio that is consistent in both measurements will test the central limit assumption for the field statistics. Any discrepancy between the two signals would test the assumption of independent statistics for the nondegenerate field used in the CSRS (CARS) experiments. If present, this residual coherence between the fields of different color could be probed more directly by measuring the fast coherent transient to be found in a nonresonant two-beam CSRS (CARS) experiment.

With the above approximations leading to the field correlator given in Eq. (3.5), the filtered signal [Eq. (1.16)] [with the polarization correlator for Eq. (2.13) with Eq. (2.14)], in the presence of constant accumulation, can be rewritten here as

$$I(\omega_S;\tau)=\left[\prod_{\lambda=1}^{3}|E_\lambda^0|^2\right]\frac{\Xi(\Delta\mathbf{k})}{N_\alpha N_\beta}\int_{-\infty}^{\infty}d\omega_S'\int_{-\infty}^{\infty}d\omega_1'\int_{-\infty}^{\infty}d\omega_2'\int_{-\infty}^{\infty}d\omega_{2'}'J_D(\omega_S')J_1(\omega_1')J_2(\omega_2')J_{2'}(\omega_{2'}')$$
$$\times\delta(\omega_2+\omega_{2'}-\omega_S-\omega_1-(\omega_S'+\omega_1'+\omega_2'+\omega_{2'}'))$$
$$\times(|\chi^{(3)}_{S,2',2,1}((\omega_S+\omega_S');(\omega_1+\omega_1'),-(\omega_2-\omega_2'),(\omega_{2'}-\omega_{2'}'))|^2$$
$$+\{[e^{-i(\omega_2'-\omega_{2'}')\tau}\chi^{(3)*}_{S,2',2,1}((\omega_S+\omega_S');(\omega_1+\omega_1'),-(\omega_2-\omega_{2'}'),-(\omega_{2'}-\omega_2'))$$
$$\times\chi^{(3)}_{S,2',2,1}((\omega_S+\omega_S');(\omega_1+\omega_1'),-(\omega_2-\omega_2'),-(\omega_{2'}-\omega_{2'}'))]+\text{c.c.}\})\ . \tag{3.6}$$

It is assumed that the quantum-mechanical trace over the susceptibility operators in Eq. (1.37) [Eq. (2.14)] has been carried out. In Sec. IV we present an interpretation of the scattering in terms of projectors of the quantum-field operators, but neglect their contributions here. Originating from the self-correlators, the first term in Eq. (3.6) represents the constant background signal. Of direct experimental interest is the τ-dependent second term derived from mixed 2,2′ correlation.

B. Analytic results for electronically nonresonant coherent Raman scattering

1. *Phase fluctuations in the fast-modulation limit for the broadband fields 2 and 2′ and monochromatic fields 1 and S*

We first treat the simple case of electronically nonresonant CSRS where a vibrational resonance is driven at second order. This resonance can be viewed at the amplitude level [e.g., Fig. 3(a)] nas a near-resonant stimulated Stokes Raman process on the ket side (fields $-\omega_1$ and ω_2) followed by a spontaneous Stokes Raman step on the bra side (field $\omega_{2'}$ and the signal field $-\omega_S$). In considering all resonant possibilities, the fields ω_2 and $\omega_{2'}$ are allowed to exchange roles and the stimulating fields $-\omega_1$ and ω_2 or $\omega_{2'}$ are permuted as well.

To anticipate the presence of more than one Raman active line within the bandwidth of an experiment, a "binary" system is considered in which the spatially separated system of two chromophores, essential to coherent scattering, may involve identical Bohr frequencies on each chromophore or different Bohr frequencies on each chromophore. Such a system can be modeled by a sample consisting of chemically identical molecules having two Raman frequencies within the experimental spectral range. It can also be modeled by a binary mixture of chemically distinct molecules each having one Raman frequency within the spectral range. In either case, the bichromophore scattering unit can involve "like" Raman frequencies or "unlike" Raman frequencies. To achieve such generality the sample is taken as a mixture of two chemically distinct chromophores α and β, each having two levels with relevant fundamental Bohr frequencies ω_{fg}^α and ω_{fg}^β, linewidths Γ_{fg}^α and Γ_{fg}^β, and numbers N_α and N_β. Until now the α and β indices have identified the two spatially distinct chromophores of the bichromophore model. In this binary system scattering arises from two spatially distinct chromophores which may be like or unlike. We now take a double index to stand for the bichromophore model, but use α,α (or β,β) for the like bichromophore and α,β (or β,α) for the unlike bichromophore.

The integrations in Eq. (3.6) are performed initially under the assumption of δ-function spectral densities for the ω_1 and ω_S fields [$J_D(\omega_S')=\delta(\omega_S')$ and $J_1(\omega_1')=\delta(\omega_1')$] corresponding to zero spectral widths: $\Gamma_S=\Gamma_1=0$. It turns out that the signal intensity then can be written as a sum of the three contributions,

$$I^{\alpha\beta}(\tau)=I^{\alpha\beta}_{\Gamma^{\alpha\beta}_{fg+fg}}(\tau)+I^{\alpha\beta}_{\Gamma_{2+2}}(\tau)+I_c^{\alpha\beta}\ , \tag{3.7}$$

where $I^{\alpha\beta}_{\Gamma_{2+2}}$ decays in τ with the time constant $(2\Gamma_2)^{-1}$, a measure of the field coherence time. $I^{\alpha\beta}_{\Gamma^{\alpha\beta}_{fg+fg}}$ decays in τ with the reciprocal material dephasing rate constants $(2\Gamma^\alpha_{fg})^{-1}$ and $(2\Gamma^\beta_{fg})^{-1}$, where $\Gamma^\alpha_{fg}=\gamma^\alpha_{fg}+\Gamma'^\alpha_{fg}$ ($\Gamma'_{fg}=\delta^2_{fg}/\Lambda_{fg}$) and similarly for Γ^β_{fg}. Finally, $I_c^{\alpha\beta}$ is the constant background signal. It is equal to the sum of the first two terms evaluated at $\tau=0$.

For the term damped by the material dynamics, we obtain

$$I^{\alpha\beta}_{\Gamma^{\alpha\beta}_{fg+fg}}\propto 2\Gamma_2^2\{y_\alpha^2F(\alpha,\alpha)+y_\beta^2F(\beta,\beta)+y_\alpha y_\beta[F(\alpha,\beta)+F(\beta,\alpha)]\}\ , \tag{3.8}$$

where

$$y_\alpha=N_\alpha\sum_{ij}\frac{\mu^\alpha_{jf}\mu^\alpha_{gj}\mu^\alpha_{fi}\mu^\alpha_{ig}}{(\omega^\alpha_{ig}-\omega_1)(\omega^\alpha_{fj}+\omega_1-\omega_{2'})}\ , \tag{3.9}$$

and similarly for y_β,

$$F(\alpha,\beta)=\frac{e^{-\Gamma^{\alpha\alpha}_{fg+fg}|\tau|}}{[(\Delta_1^\alpha)^2+(\Gamma^\alpha_{fg+2})^2][(\Delta_1^\alpha)^2+(\Gamma^\alpha_{fg-2})^2][(\Delta_S^\alpha)^2+(\Gamma^\alpha_{fg+2})^2][(\Delta_S^\alpha)^2+(\Gamma^\alpha_{fg-2})^2]}$$
$$\times\left[\left[\frac{\mathrm{Re}[A(\Delta,\Gamma)]\Delta^{\alpha\beta}+\mathrm{Im}[A(\Delta,\Gamma)]\Gamma^{\beta\alpha}_{fg-fg}}{[(\Delta^{\alpha\beta})^2+(\Gamma^{\alpha\beta}_{fg-fg})^2]}+\frac{\mathrm{Re}[A(\Delta,\Gamma)]\Delta^{\beta\alpha}_{fg-fg}+\mathrm{Im}[A(\Delta,\Gamma)]\Gamma^{\alpha\beta}_{fg+fg}}{[(\Delta^{\beta\alpha}_{fg-fg})^2+(\Gamma^{\alpha\beta}_{fg+fg})^2]}\right]\sin[\Delta^\alpha|\tau|]\right.$$

$$+\left[\frac{Re[A(\Delta,\Gamma)]\Gamma^{\beta\alpha}_{fg-fg}+\mathrm{Im}[A(\Delta,\Gamma)]\Delta^{\alpha\beta}}{[(\Delta^{\alpha\beta})^2+(\Gamma^{\alpha\beta}_{fg-fg})^2]}+\frac{\mathrm{Re}[A(\Delta,\Gamma)]\Gamma^{\alpha\beta}_{fg+fg}+\mathrm{Im}[A(\Delta,\Gamma)]\Delta^{\beta\alpha}_{fg-fg}}{[(\Delta^{\beta\alpha}_{fg-fg})^2+(\Gamma^{\alpha\beta}_{fg+fg})^2]}\right]\cos[\Delta^{\alpha}\tau]\Bigg]. \tag{3.10}$$

for Q (or Q')$=\alpha,\beta$, we have $\Delta^{Q}_{1}=\omega^{Q}_{fg}+\omega_2-\omega_1$, the detuning on the stimulated Raman process; and $\Delta^{Q}_{S}=\omega^{Q}_{fg}+\omega_S-\omega_2$, the detuning on the spontaneous Raman process. Their sum combination is $\Delta^{QQ'}=\Delta^{Q}_{1}+\Delta^{Q'}_{S}=\omega^{Q}_{fg}+\omega^{Q'}_{fg}+\omega_S-\omega_1$, from which $\Delta^{QQ}=\Delta^{Q}=2\omega^{Q}_{fg}+\omega_S-\omega_1$. To condense the notation, the various detunings and linewidth parameters will be written as

$$\Delta^{QQ'}_{ij\pm kl\pm 2\pm 1}=\omega^{Q}_{ij}\pm\omega^{Q'}_{kl}\pm\omega_2\pm\omega_1,\quad \Gamma^{QQ'}_{ij\pm kl\pm 2\pm 1}=\Gamma^{Q}_{ij}\pm\Gamma^{Q'}_{kl}\pm\Gamma_2\pm\Gamma_1\ , \tag{3.11}$$

unless otherwise specified. The ordering in the chromophore superscript level is to match the ordering of the chromophore-based state pairs indicated by a double subscript. The single subscripts 1, 2, or S identify, as before, the field whose property (frequency, width parameter, spectral density) is so labeled.

Interchange of α,β in $F(\alpha,\beta)$ gives $F(\beta,\alpha)$, and $\alpha=\beta$ produces the like chromophore functions $F(\alpha,\alpha)$ and $F(\beta,\beta)$:

$$F(\alpha,\alpha)=\frac{e^{-\Gamma^{\alpha\alpha}_{fg+fg}|\tau|}}{[(\Delta^{\alpha}_{1})^2+(\Gamma^{\alpha}_{fg+2})^2][(\Delta^{\alpha}_{1})^2+(\Gamma^{\alpha}_{fg-2})^2][(\Delta^{\alpha}_{S})^2+(\Gamma^{\alpha}_{fg+2})^2][(\Delta^{\alpha}_{S})^2+(\Gamma^{\alpha}_{fg-2})^2]}$$
$$\times\left[\left[\frac{\mathrm{Re}[A(\Delta,\Gamma)]}{\Delta^{\alpha}}+\frac{\mathrm{Im}[A(\Delta,\Gamma)]}{2\Gamma^{\alpha}_{fg}}\right]\sin[\Delta^{\alpha}|\tau|]+\left[\frac{\mathrm{Im}[A(\Delta,\Gamma)]}{\Delta^{\alpha}}+\frac{\mathrm{Re}[A(\Delta,\Gamma)]}{2\Gamma^{\alpha}_{fg}}\right]\cos[\Delta^{\alpha}\tau]\right], \tag{3.12}$$

and similarly for $F(\beta,\beta)$. In both Eqs. (3.10) and (3.12) the complex function $A(\Delta,\Gamma)$ is written as

$$\mathrm{Re}[A(\Delta,\Gamma)]=[(\Delta^{\alpha}_{1})^2-\Gamma^{\alpha}_{fg+2}\Gamma^{\alpha}_{fg-2}][(\Delta^{\alpha}_{S})^2-\Gamma^{\alpha}_{fg+2}\Gamma^{\alpha}_{fg-2}]-4\Delta^{\alpha}_{S}\Delta^{\alpha}_{1}(\Gamma^{\alpha}_{fg})^2 \tag{3.13}$$

and

$$\mathrm{Im}[A(\Delta,\Gamma)]=\Delta^{\alpha}\Gamma^{\alpha}_{fg}(\Delta^{\alpha}_{S}\Delta^{\alpha}_{1}-\Gamma^{\alpha}_{fg+2}\Gamma^{\alpha}_{fg-2})\ . \tag{3.14}$$

The second term on the rhs of Eq. (3.7) represents the fast transient response of the fourth-wave signal. Just as in the material damped term, this component has contributions from like chromophore pair ($Q=Q'$), as well as cross terms between unlike chromophores ($Q\neq Q'$). It can be expressed as

$$I^{\alpha\beta}_{\Gamma_{2+2}}\propto\Gamma_2\{y^2_{\alpha}G(\alpha,\alpha)+y^2_{\beta}G(\beta,\beta)+y_{\alpha}y_{\beta}[G(\alpha,\beta)+G(\beta,\alpha)]\}\ , \tag{3.15}$$

where

$$G(\alpha,\beta)=\frac{e^{-\Gamma_{2+2}|\tau|}}{(\Delta_R)^2[(\Delta_R)^2+(\Gamma_{2+2})^2]}\left[\left[\frac{\mathrm{Re}[B(\Delta,\Gamma)_1]\cos(\Delta_R\tau)+\mathrm{Im}[B(\Delta,\Gamma)_1]\sin(\Delta_R|\tau|)}{[(\Delta^{\alpha}_{S})^2+(\Gamma^{\alpha}_{fg-2})^2][(\Delta^{\beta}_{1})^2+(\Gamma^{\beta}_{fg-2})^2]}\right]\right.$$
$$+\left[\frac{\mathrm{Re}[B(\Delta,\Gamma)_2]\cos(\Delta_R\tau)+\mathrm{Im}[B(\Delta,\Gamma)_2]\sin(\Delta_R|\tau|)}{[(\Delta^{\alpha}_{S})^2+(\Gamma^{\alpha}_{fg+2})^2][(\Delta^{\beta}_{1})^2+(\Gamma^{\beta}_{fg+2})^2]}\right]$$
$$+\left[\frac{\mathrm{Re}[B(\Delta,\Gamma)_3]\cos(\Delta_R\tau)+\mathrm{Im}[B(\Delta,\Gamma)_3]\sin(\Delta_R|\tau|)}{[(\Delta^{\alpha}_{1})^2+(\Gamma^{\alpha}_{fg-2})^2][(\Delta^{\beta}_{1})^2+(\Gamma^{\beta}_{fg+2})^2]}\right]$$
$$\left.+\left[\frac{\mathrm{Re}[B(\Delta,\Gamma)_4]\cos(\Delta_R\tau)+\mathrm{Im}[B(\Delta,\Gamma)_4]\sin(\Delta_R|\tau|)}{[(\Delta^{\alpha}_{S})^2+(\Gamma^{\alpha}_{fg-2})^2][(\Delta^{\beta}_{S})^2+(\Gamma^{\beta}_{fg+2})^2]}\right]\right], \tag{3.16}$$

from which $G(\beta,\alpha)$, $G(\alpha,\alpha)$, and $G(\beta,\beta)$ can be obtained. The τ dependence of this signal component oscillates at a frequency given by the detuning of the radiation fields, $\Delta_R=2\omega_2-\omega_S-\omega_1$, and is damped by the spectral width of the broadband fields. The multiplicative factors on the sines and cosines consist of algebraic expressions involving the detunings and line widths. For example,

$$\mathrm{Re}[B(\Delta,\Gamma)_1]=\Delta^2_R(\Delta^{\alpha}_{S}\Delta^{\beta}_{1}+\Gamma^{\alpha}_{fg-2}\Gamma^{\beta}_{fg-2})-2\Delta_R\Gamma_2(\Delta^{\beta}_{1}\Gamma^{\alpha}_{fg-2}-\Delta^{\alpha}_{S}\Gamma^{\beta}_{fg-2}) \tag{3.17}$$

and

$$\mathrm{Im}[B(\Delta,\Gamma)_1]=2\Delta_R\Gamma_2(\Delta^{\alpha}_{S}\Delta^{\beta}_{1}+\Gamma^{\alpha}_{fg-2}\Gamma^{\beta}_{fg-2})+\Delta^2_R(\Delta^{\beta}_{1}\Gamma^{\alpha}_{fg-2}-\Delta^{\alpha}_{S}\Gamma^{\beta}_{fg-2})\ . \tag{3.18}$$

Given Eq. (3.17) and (3.18), we can define $B(\Delta,\Gamma)_1 \equiv B(\Delta_S^\alpha, \Delta_1^\beta, \Gamma_{fg-2}^\alpha, \Gamma_{fg-2}^\beta)$ from which the terms $B(\Delta,\Gamma)_2 = B(\Delta_S^\alpha, \Delta_1^\beta, \Gamma_{fg+2}^\alpha, \Gamma_{fg+2}^\beta)$, $B(\Delta,\Gamma)_3 = B(\Delta_1^\alpha, \Delta_1^\beta, \Gamma_{fg-2}^\alpha, \Gamma_{fg+2}^\beta)$, and $B(\Delta,\Gamma)_4 = B(\Delta_S^\alpha, \Delta_S^\beta, \Gamma_{fg-2}^\alpha, \Gamma_{fg+2}^\beta)$ are obtained.

Though these equations involve field-mediated coherences across distant chromophores, it is striking that no beating is seen between two different Raman frequencies. Such beating might have been expected from the $\alpha \neq \beta$ signal component, yet for it, only a superposition of two detuning oscillations is found, one based on a Raman frequency from α, the other on a Raman frequency from β. Each is damped by twice the dephasing rate constant of its Raman mode. On the other hand, the denominators of these terms (that dictate their spectral line shapes) do recognize a joint two-chromophore (α,α; β,β; or α,β) resonance, not to be seen at the amplitude level of the susceptibility. The rigorous absence of interchromophore Raman beats is relieved as soon as a nonzero spectral width is assigned either to the nondegenerate field or to the detector response (or both). This becomes apparent in Secs. III B 2 and III B 3 that follow.

2. *Phase fluctuations in the fast-modulation limit for all intervening fields*

Next, the effect on interferograms and spectra is examined when the spectrum of the nondegenerate field and that of the signal field is made Lorentzian with nonzero Γ_1 and Γ_S, respectively. Upon integrating Eq. (3.6), the signal proves to be a sum of seven contributions,

$$I^{\alpha\beta}(\tau) = I^{\alpha\beta}_{\Gamma_{fg+fg+1+S}}(\tau) + I^{\alpha\beta}_{\Gamma_{fg+2+1}}(\tau) + I^{\alpha\beta}_{\Gamma_{fg+2+S}}(\tau) + I^{\alpha\beta}_{\Gamma_{fg+fg}}(\tau) + I^{\alpha\beta}_{\Gamma_{2+2+1+S}}(\tau) + I^{\alpha\beta}_{\Gamma_{2+2}}(\tau) + I_c^{\alpha\beta} . \tag{3.19}$$

We discuss each in turn. The first term is similar in form to the first term in Eq. (3.7). However, nonzero Γ_1 and Γ_S introduces additional broadening to the existing resonances found in Eq. (3.10). $I^{\alpha\beta}_{\Gamma_{fg+fg+1+S}}(\tau)$ can replace $I^{\alpha\beta}_{\Gamma_{fg+fg}}(\tau)$ on the left-hand side of Eq. (3.8) and the unlike chromophore component [$F(\alpha,\beta)$ in Eq. (3.10)] can be written as

$$F(\alpha,\beta) = \frac{e^{-\Gamma^{\alpha\alpha}_{fg+fg+1+S}|\tau|}}{[(\Delta_1^\alpha)^2+(\Gamma^\alpha_{fg+2+1})^2][(\Delta_1^\alpha)^2+(\Gamma^\alpha_{fg-2+1})^2][(\Delta_S^\alpha)^2+(\Gamma^\alpha_{fg+2+S})^2][(\Delta_S^\alpha)^2+(\Gamma^\alpha_{fg-2+S})^2]} \times \left[\left[\frac{\mathrm{Re}[A(\Delta,\Gamma)]\Delta^{\alpha\beta} + \mathrm{Im}[A(\Delta,\Gamma)]\Gamma^{\beta\alpha}_{fg-fg+1+S}}{[(\Delta^{\alpha\beta})^2+(\Gamma^{\alpha\beta}_{fg-fg+1+S})^2]} + \frac{\mathrm{Re}[A(\Delta,\Gamma)]\Delta^{\beta\alpha}_{fg-fg} + \mathrm{Im}[A(\Delta,\Gamma)]\Gamma^{\alpha\beta}_{fg+fg}}{[(\Delta^{\beta\alpha}_{fg-fg})^2+(\Gamma^{\alpha\beta}_{fg+fg})^2]} \right] \sin(\Delta^\alpha|\tau|) + \left[\frac{\mathrm{Re}[A(\Delta,\Gamma)]\Gamma^{\beta\alpha}_{fg-fg+1+S} + \mathrm{Im}[A(\Delta,\Gamma)]\Delta^{\alpha\beta}}{[(\Delta^{\alpha\beta})^2+(\Gamma^{\alpha\beta}_{fg-fg+1+S})^2]} + \frac{\mathrm{Re}[A(\Delta,\Gamma)]\Gamma^{\alpha\beta}_{fg+fg} + \mathrm{Im}[A(\Delta,\Gamma)]\Delta^{\beta\alpha}_{fg-fg}}{[(\Delta^{\beta\alpha}_{fg-fg})^2+(\Gamma^{\alpha\beta}_{fg+fg})^2]} \right] \cos(\Delta^\alpha\tau) \right] . \tag{3.20}$$

Here the exponentially decaying envelope is damped by $\Gamma^{\alpha\alpha}_{fg+fg+1+S}$, now containing contributions from two nonzero spectral widths in addition to the purely material component $2\Gamma_{fg}$. Thus in the limit where Γ_1 and Γ_S are nonzero, but still only a small fraction of the Raman linewidth (Γ_{fg}), these detuning oscillations continue to damp essentially with the dephasing time of the driven material mode. However, as the bandwidth of field 1, and/or that of the signal field increases, such transients rapidly attenuate with τ and becomes unobservable, for instance, in the limit of white detection.

In Eq. (3.20), the real and imaginary parts of the complex function $A(\Delta,\Gamma)$ [Eqs. (3.13) and (3.14)] are now written as

$$\mathrm{Re}[A(\Delta,\Gamma)] = [(\Delta_1^\alpha)^2 - \Gamma^\alpha_{fg+2+1}\Gamma^\alpha_{fg-2+1}] \times [(\Delta_S^\alpha)^2 - \Gamma^\alpha_{fg+2+S}\Gamma^\alpha_{fg-2+S}] - 4\Delta_S^\alpha\Delta_1^\alpha\Gamma^\alpha_{fg+1}\Gamma^\alpha_{fg+S} \tag{3.21}$$

and

$$\mathrm{Im}[A(\Delta,\Gamma)] = \Delta_1^\alpha\Gamma^\alpha_{fg+1}[(\Delta_S^\alpha)^2 - \Gamma^\alpha_{fg+2+S}\Gamma^\alpha_{fg-2+S}] + \Delta_S^\alpha\Gamma^\alpha_{fg+S}[(\Delta_1^\alpha)^2 - \Gamma^\alpha_{fg+2+1}\Gamma^\alpha_{fg-2+1}] . \tag{3.22}$$

New transient responses appear in the interferogram as a result of the nonzero spectral width of the nondegenerate input field and of the detector field. The second and third terms on the rhs of Eq. (3.19) represent detuning oscillations from the stimulated and spontaneous Raman steps in the scattering process, respectively. For oscillations on the stimulated Raman detuning (Δ_1^α) one has

$$I^{\alpha\beta}_{\Gamma_{fg+2+1}}(\tau) \propto 2\Gamma_2\Gamma_S\{y_\alpha^2 K(\alpha,\alpha) + y_\beta^2 K(\beta,\beta) + y_\alpha y_\beta[K(\alpha,\beta)+K(\beta,\alpha)]\} , \tag{3.23}$$

where

$$K(\alpha,\beta)=\frac{e^{-\Gamma^{\alpha}_{fg+2+1}|\tau|}}{[(\Delta^{\alpha}_{S})^2+(\Gamma^{\alpha}_{fg-2+S})^2][(\Delta^{\alpha}_{S})^2+(\Gamma^{\alpha}_{fg-2-S})^2][(\Delta^{\alpha}_{1})^2+(\Gamma^{\alpha}_{fg+2+1})^2][(\Delta^{\alpha}_{1})^2+(\Gamma^{\alpha}_{fg-2+1})^2]}$$
$$\times\left[\left\{\frac{\mathrm{Re}[C(\Delta,\Gamma)]\Delta^{\beta}_{1}+\mathrm{Im}[C(\Delta,\Gamma)]\Gamma^{\beta}_{fg-2-1}}{[(\Delta^{\beta}_{1})^2+(\Gamma^{\beta}_{fg-2-1})^2]}+\frac{\mathrm{Re}[C(\Delta,\Gamma)]\Delta^{\beta\alpha}_{fg-fg}+\mathrm{Im}[C(\Delta,\Gamma)]\Gamma^{\alpha\beta}_{fg+fg}}{[(\Delta^{\beta\alpha}_{fg-fg})^2+(\Gamma^{\alpha\beta}_{fg+fg})^2]}\right\}\sin[\Delta^{\alpha}_{1}|\tau|]\right.$$
$$\left.+\left\{\frac{\mathrm{Re}[C(\Delta,\Gamma)]\Gamma^{\beta}_{fg-2-1}-\mathrm{Im}[C(\Delta,\Gamma)]\Delta^{\beta}_{1}}{[(\Delta^{\beta}_{1})^2+(\Gamma^{\beta}_{fg-2-1})^2]}+\frac{\mathrm{Re}[C(\Delta,\Gamma)]\Gamma^{\alpha\beta}_{fg+fg}-\mathrm{Im}[C(\Delta,\Gamma)]\Delta^{\beta\alpha}_{fg-fg}}{[(\Delta^{\beta\alpha}_{fg-fg})^2+(\Gamma^{\alpha\beta}_{fg+fg})^2]}\right\}\cos[\Delta^{\alpha}_{1}\tau]\right]. \tag{3.24}$$

Important to the phase of this detuning oscillation is the relative weighting of the sine and cosine functions through $C(\Delta,\Gamma)$ whose real and imaginary parts are given by

$$\mathrm{Re}[C(\Delta,\Gamma)]=[(\Delta^{\alpha}_{S})^2-\Gamma^{\alpha}_{fg-2+S}\Gamma^{\alpha}_{fg-2-S}]\times[(\Delta^{\alpha}_{1})^2-\Gamma^{\alpha}_{fg+2+1}\Gamma^{\alpha}_{fg-2+1}]-4\Delta^{\alpha}_{S}\Delta^{\alpha}_{1}\Gamma^{\alpha}_{fg-2}\Gamma^{\alpha}_{fg+1} \tag{3.25}$$

and

$$\mathrm{Im}[C(\Delta,\Gamma)]=2\{\Delta^{\alpha}_{1}\Gamma^{\alpha}_{fg+1}[(\Delta^{\alpha}_{S})^2-\Gamma^{\alpha}_{fg-2+S}\Gamma^{\alpha}_{fg-2-S}]+\Delta^{\alpha}_{S}\Gamma^{\alpha}_{fg-2}[(\Delta^{\alpha}_{1})^2-\Gamma^{\alpha}_{fg+2+1}\Gamma^{\alpha}_{fg-2+1}]\}. \tag{3.26}$$

The third term on the rhs of Eq. (3.19) represents an oscillation at the spontaneous Raman detuning frequency Δ_S. It turns out that this component can be obtained from Eqs. (3.23)–(3.26) upon interchanging the variables Δ_S and Δ_1 and the parameters Γ_S and Γ_1. Thus we can write

$$I^{\alpha\beta}_{\Gamma_{fg+2+S}}(\tau)=\hat{T}(\Delta^{Q}_{S}\leftrightarrow\Delta^{Q}_{1},\Gamma^{Q}_{S}\leftrightarrow\Gamma^{Q}_{1})I^{\alpha\beta}_{\Gamma_{fg+2+1}}(\tau), \tag{3.27}$$

where $\hat{T}$ represents the indicated variable or parameter interchange. Damping of both of these spontaneous and stimulated Raman detuning oscillations is dominated by Γ_2 of the fields 2 (2′), and, therefore, cannot persist for time delays greater than the coherence time of the broadband light.

New transients oscillating at beat frequencies of the material, and damped only by material dephasing times, are represented by the fourth term in Eq. (3.19). For the α,β mixture, this component can be written as

$$I^{\alpha\beta}_{fg+fg}(\tau)\propto 2\Gamma_2(y^2_{\alpha}e^{-2\Gamma^{\alpha}_{fg}|\tau|}\{\Gamma_2\Gamma_1J_1(\alpha,\alpha)+\Gamma_2\Gamma_SJ_2(\alpha,\alpha)+\Gamma_S\Gamma_1[J_3(\alpha,\alpha)+J_4(\alpha,\alpha)]\}$$
$$+y^2_{\beta}e^{-2\Gamma^{\beta}_{fg}|\tau|}\{\Gamma_2\Gamma_1J_1(\beta,\beta)+\Gamma_2\Gamma_SJ_2(\beta,\beta)+\Gamma_S\Gamma_1[J_3(\beta,\beta)+J_4(\beta,\beta)]\}$$
$$+y_{\alpha}y_{\beta}e^{-\Gamma^{\alpha\beta}_{fg+fg}|\tau|}\{\Gamma_2\Gamma_1[J_1(\alpha,\beta)+J_1(\beta,\alpha)]+\Gamma_2\Gamma_5[J_2(\alpha,\beta)+J_2(\beta,\alpha)]$$
$$+\Gamma_S\Gamma_1[J_3(\alpha,\beta)+J_4(\alpha,\beta)+J_3(\beta,\alpha)+J_4(\beta\alpha)]\}), \tag{3.28}$$

where, for instance,

$$J_1(\alpha,\beta)=\frac{L_1(\Delta,\Gamma)}{[(\Delta^{\alpha}_{S})^2+(\Gamma^{\alpha}_{fg+2-S})^2][(\Delta^{\alpha}_{S})^2+(\Gamma^{\alpha}_{fg-2-S})^2][(\Delta^{\beta}_{S})^2+(\Gamma^{\beta}_{fg+2+S})^2][(\Delta^{\beta}_{S})^2+(\Gamma^{\beta}_{fg-2+S})^2]}$$
$$\times(\{\mathrm{Re}[D_1(\Delta,\Gamma)]\mathrm{Re}[E_1(\Delta,\Gamma)]-\mathrm{Im}[D_1(\Delta,\Gamma)]\mathrm{Im}[E_1(\Delta\Gamma)]\}\cos(\Delta^{\alpha\beta}_{fg-fg}\tau)$$
$$-\{\mathrm{Re}[D_1(\Delta,\Gamma)]\mathrm{Im}[E_1(\Delta,\Gamma)]+\mathrm{Im}[D_1(\Delta,\Gamma)]\mathrm{Re}[E_1(\Delta,\Gamma)]\}\sin(\Delta^{\alpha\beta}_{fg-fg}|\tau|)). \tag{3.29}$$

Oscillations are now seen at the difference between the material Bohr frequencies where $\Delta^{\alpha\beta}_{fg-fg}=\omega^{\alpha}_{fg}-\omega^{\beta}_{fg}$. The remaining terms in Eq. (3.29) are defined as follows:

$$\mathrm{Re}[D_1(\Delta,\Gamma)]=[(\Delta^{\alpha}_{S})^2-\Gamma^{\alpha}_{fg+2-S}\Gamma^{\alpha}_{fg-2-S}][(\Delta^{\beta}_{S})^2-\Gamma^{\beta}_{fg+2+S}\Gamma^{\beta}_{fg-2+S}]+4\Delta^{\alpha}_{S}\Delta^{\beta}_{S}\Gamma^{\alpha}_{fg-S}\Gamma^{\beta}_{fg+S}, \tag{3.30}$$

$$\mathrm{Im}[D_1(\Delta,\Gamma)]=2\Delta^{\beta}_{S}\Gamma^{\beta}_{fg+S}[(\Delta^{\alpha}_{S})^2-\Gamma^{\alpha}_{fg+2-S}\Gamma^{\alpha}_{fg-2-S}]-2\Delta^{\alpha}_{S}\Gamma^{\alpha}_{fg-S}[(\Delta^{\beta}_{S})^2-\Gamma^{\beta}_{fg+2+S}\Gamma^{\beta}_{fg-2+S}], \tag{3.31}$$

$$\mathrm{Re}[E_1(\Delta,\Gamma)]=(\Delta^{\alpha\beta})^2-\Gamma^{\beta\alpha}_{fg-fg+1+S}\Gamma^{\beta\alpha}_{fg-fg-1+S}, \tag{3.32}$$

$$\mathrm{Im}[E_1(\Delta,\Gamma)]=2\Delta^{\alpha\beta}\Gamma^{\beta\alpha}_{fg-fg+S}, \tag{3.33}$$

$$L_1(\Delta,\Gamma)=\frac{1}{[(\Delta^{\alpha\beta})^2+(\Gamma^{\beta\alpha}_{fg-fg+1+S})^2][(\Delta^{\alpha\beta})^2+(\Gamma^{\beta\alpha}_{fg-fg-1+S})^2]}. \tag{3.34}$$

$J_2(\alpha,\beta)$ can be obtained from $J_1(\alpha,\beta)$ by interchanging $\Delta_S \rightarrow \Delta_1$ and $\Gamma_S \rightarrow \Gamma_1$. The expressions for $J_3(\alpha,\beta)$ and $J_4(\alpha,\beta)$ are similar in form, but contain resonances different from those in Eqs. (3.30)–(3.34). For $J_3(\alpha,\beta)$ we can write

$$J_3(\alpha,\beta)=\frac{L_2(\Delta,\Gamma)}{[(\Delta_S^\beta)^2+(\Gamma_{fg-2+S}^\beta)^2][(\Delta_S^\beta)^2+(\Gamma_{fg-2-S}^\beta)^2][(\Delta_1^\alpha)^2+(\Gamma_{fg-2-1}^\alpha)^2][(\Delta_1^\alpha)^2+(\Gamma_{fg-2+1}^\alpha)^2]}$$
$$\times(\{\mathrm{Re}[D_2(\Delta,\Gamma)]\mathrm{Re}[E_2(\Delta,\Gamma)]+\mathrm{Im}[D_2(\Delta,\Gamma)]\mathrm{Im}[E_2(\Delta,\Gamma)]\}\cos(\Delta_{fg-fg}^{\alpha\beta}\tau)$$
$$+\{\mathrm{Re}[D_2(\Delta,\Gamma)]\mathrm{Im}[E_2(\Delta,\Gamma)]-\mathrm{Im}[D_2(\Delta,\Gamma)]\mathrm{Re}[E_2(\Delta,\Gamma)]\}\sin(\Delta_{fg-fg}^{\alpha\beta}|\tau|)) \ , \tag{3.35}$$

where

$$\mathrm{Re}[D_2(\Delta,\Gamma)]=[(\Delta_1^\alpha)^2-\Gamma_{fg-2-1}^\alpha\Gamma_{fg-2+1}^\alpha][(\Delta_S^\beta)^2-\Gamma_{fg-2+S}^\beta\Gamma_{fg-2-S}^\beta]+4\Delta_1^\alpha\Delta_S^\beta\Gamma_{fg-2}^\alpha\Gamma_{fg-2}^\beta \ , \tag{3.36}$$

$$\mathrm{Im}[D_2(\Delta,\Gamma)]=2\Delta_S^\beta\Gamma_{fg-2}^\beta[(\Delta_1^\alpha)^2-\Gamma_{fg-2-1}^\alpha\Gamma_{fg-2+1}^\alpha]-2\Delta_1^\alpha\Gamma_{fg-2}^\alpha[(\Delta_S^\beta)^2-\Gamma_{fg-2+S}^\beta\Gamma_{fg-2-S}^\beta] \ , \tag{3.37}$$

$$\mathrm{Re}[E_2(\Delta,\Gamma)]=(\Delta_{fg-fg}^{\alpha\beta})^2-\Gamma_{fg-fg-2-2}^{\alpha\beta}\Gamma_{fg+fg}^{\alpha\beta} \ , \tag{3.38}$$

$$\mathrm{Im}[E_2(\Delta,\Gamma)]=2\Delta_{fg-fg}^{\alpha\beta}\Gamma_{fg+fg-2}^{\alpha\beta} \ , \tag{3.39}$$

and

$$L_2(\Delta,\Gamma)=\frac{1}{[(\Delta_{fg-fg}^{\alpha\beta})^2+(\Gamma_{fg+fg-2-2}^{\alpha\beta})^2][(\Delta_{fg-fg}^{\alpha\beta})^2+(\Gamma_{fg+fg}^{\alpha\beta})^2]} \ . \tag{3.40}$$

$J_4(\alpha,\beta)$ can be obtained by substituting $\Gamma_{fg+2\pm S}^Q$ and $\Gamma_{fg+2\pm1}^Q$ for $\Gamma_{fg-2\pm S}^Q$ and $\Gamma_{fg-2\pm1}^Q$ respectively, as well as interchanging the detuning parameters Δ_1 and Δ_s in Eqs. (3.35)–(3.40). Again, an interchange of α and β gives $J_i(\beta,\alpha)$, while $\alpha=\beta$ gives $J_i(\alpha,\alpha)$ and $J_i(\beta,\beta)$. The latter terms, representing like chromophore pairs, are at zero-frequency difference beats and do not oscillate with τ. They only decay exponentially with a rate constant given by twice the reciprocal dephasing time of the chromophore ρ_{fg} superposition state for α or for β.

The fifth and sixth terms in Eq. (3.19) decay with a rate constant given by $\Gamma_{2+2+1+S}$ and Γ_{2+2}. These fourth-wave signal components represent the coherent peak, or the purely light-related signal transient. The coherent peak contribution given by $I_{\Gamma_{2+2+1+S}}^{\alpha\beta}$ is the nonzero Γ_1,Γ_S analog of the signal component given by Eq. (3.15). Both like and unlike chromophore contributions to this signal oscillate in τ at the four-field detuning frequency Δ_R. A zero-frequency transient represented by the signal term $I_{\Gamma_{2+2}}^{\alpha\beta}$ decays with the rate constant Γ_{2+2}. A large number of terms is required to fully represent these components. These are given in Appendix B [Eqs. (B1)–(B10)].

Finally, the last term in Eq. (3.19) represents the τ-independent background signal which can be determined from the equation $I_c^{\alpha\beta}=I^{\alpha\beta}(\tau=0)/2$, assuming statistical independence of the ω_1 and ω_2 ($\omega_{2'}$) fields. Next we compare these results with those obtained for the case where the light field statistics are in the slow-modulation limit of Eq. (2.9).

3. *Field statistics in the slow-modulation limit*

Consider phase perturbations of the driving fields that are large in amplitude, but infrequent, resulting in a static distribution of excitation frequencies. Here the spectral densities are Gaussians of variable width. (A Gaussian for the signal field is nonstochastic reflecting, instead, a proposed spectral filter function.) Substituting Eq. (2.10), for all four spectral densities, into Eq. (3.6), one finds that the signal can be written as a sum of three contributions:

$$I^{\alpha\beta}(\tau)=I_{\mathrm{I}}^{\alpha\beta}(\tau)+I_{\mathrm{II}}^{\alpha\beta}(\tau)+I_{\mathrm{III}}^{\alpha\beta} \ . \tag{3.41}$$

Most of the oscillatory transients obtained in Eq. (3.19) are recovered, though now in different functional form.

Purely material quantum beats, represented by Eqs. (3.28)–(3.40) in the motionally narrowed regime of the field phase fluctuations, are described in the Gaussian limit by the first term in Eq. (3.41). In terms of its like and unlike chromophore contributions this component can be written as

$$I_{\mathrm{I}}^{\alpha\beta}(\tau)\propto\left[\frac{\pi}{B+C}\right]^{1/2}\{y_\alpha^2\mathcal{J}_{\mathrm{I}}(\alpha,\alpha)+y_\beta^2\mathcal{J}_{\mathrm{I}}(\beta,\beta)$$
$$+y_\alpha y_\beta[\mathcal{J}_{\mathrm{I}}(\alpha,\beta)+\mathcal{J}_{\mathrm{I}}(\beta,\alpha)]\} \ , \tag{3.42}$$

where

$$\mathcal{J}_{\mathrm{I}}(\alpha,\beta)=\left\{\exp\left[-\Delta_R^2[16\delta_2^4(B+C)]^{-1}\left[1+\frac{\delta_2^2(\delta_1^2+\delta_S^2)}{\delta_1^2\delta_S^2}\right]\right]\exp[-(2\delta_2^2)^{-1}(\Delta_1^\alpha\Delta_1^\beta+\Gamma_{fg}^\alpha\Gamma_{fg}^\beta)]\right.$$
$$\left.\times\exp\{-B\Delta_R\Delta^{\alpha\beta}[2\delta_2^2(B+C)]^{-1}\}\exp\{-BC(B+C)^{-1}[(\Delta^{\alpha\beta})^2-(\Gamma_{fg-fg}^{\alpha\beta})^2]\}\right\}$$
$$\times e^{-\Gamma_{fg+fg}^{\alpha\beta}|\tau|}\cos[\Delta_{fg-fg}^{\alpha\beta}\tau+\phi_{\mathrm{I}}(\Delta,\Gamma)] \ . \tag{3.43}$$

Coherently prepared, closely spaced Raman modes beat at the difference frequency with a phase given by

$$\phi_I(\Delta,\Gamma)=(2\Delta_2^2)^{-1}[\Delta_1^\alpha\Gamma_{fg}^\beta-\Delta_1^\beta\Gamma_{fg}^\alpha+\Delta_R\Gamma_{fg-fg}^{\alpha\beta}B(B+C)^{-1}]+2B\Delta^{\alpha\beta}\Gamma_{fg-fg}^{\alpha\beta}[B(B+C)^{-1}-1] \tag{3.44}$$

and attenuate with the sum of the dephasing rate constants of the superposed modes. The parameters B and C in Eqs. (3.42)–(3.44) are defined as

$$B=\frac{\delta_2^2+\delta_1^2}{4\delta_2^2\delta_1^2},\quad C=\frac{\delta_2^2+\delta_S^2}{4\delta_2^2\delta_S^2},$$

respectively. Contributions to this signal component from like chromophores, $\alpha=\beta$, give a zero-frequency transient damped by twice its dephasing rate.

The radiation-matter transient behavior described by the first three terms of Eq. (3.19) is contained in the second term of Eq. (3.41). Here we have

$$I_{II}^{\alpha\beta}(\tau)\propto 2\frac{\delta_2^2\delta_1\delta_S}{[(\delta_2^2+\delta_1^2)(\delta_2^2+\delta_S^2)]^{1/2}}\{y_\alpha^2\mathcal{J}_{II}(\alpha,\alpha)+y_\beta^2\mathcal{J}_{II}(\beta,\beta)+y_\alpha y_\beta[\mathcal{J}_{II}(\alpha,\beta)+\mathcal{J}_{II}(\beta,\alpha)]\}\ , \tag{3.45}$$

where

$$\begin{aligned}\mathcal{J}_{II}(\alpha,\beta)=&\left[\frac{\exp\left[\frac{-1}{2\delta_2^2}\left[\frac{\Delta_R^2}{2}+\Delta_1^\alpha\Delta_S^\alpha-(\Gamma_{fg}^\alpha)^2\right]\right]\exp\left[\frac{1}{16\delta_2^4}\left[\frac{[(\Delta_1^\alpha)^2-(\Gamma_{fg}^\alpha)^2]}{B}+\frac{[(\Delta_S^\alpha)^2-(\Gamma_{fg}^\alpha)^2]}{C}\right]\right]}{[(\Delta_{fg-fg}^{\alpha\beta})^2+(\Gamma_{fg+fg}^{\alpha\beta})^2]}\right]\\&\times\exp\left[-\frac{-\tau^2}{4}\left[\frac{B+C}{BC}\right]\right]\exp\left[-\Gamma_{fg}^\alpha|\tau|\left[2-\frac{B+C}{4\delta_2^2BC}\right]\right]\\&\times\{\Gamma_{fg+fg}^{\alpha\beta}\cos[\bar{\Delta}^\alpha\tau+\phi_{II}(\Delta,\Gamma)]-\Delta_{fg-fg}^{\alpha\beta}\sin[\bar{\Delta}^\alpha|\tau|+\phi_{II}(\Delta,\Gamma)]\}\ .\end{aligned} \tag{3.46}$$

This signal component shows oscillations at a frequency

$$\bar{\Delta}^\alpha=\Delta^\alpha-(4\delta_2^2)^{-1}\left[\frac{\Delta_1^\alpha}{B}+\frac{\Delta_S^\alpha}{C}\right] \tag{3.47}$$

and phase

$$\begin{aligned}\phi_{II}(\Delta,\Gamma)=&-\Gamma_{fg}^\alpha(2\delta_2^2)^{-1}\{\Delta_1^\alpha[1-(4B\delta_2^2)^{-1}]\\&+\Delta_S^\alpha[1-(4C\delta_2^2)^{-1}]\}\ .\end{aligned} \tag{3.48}$$

When the nondegenerate field and the signal field are spectrally narrow compared to the broadband fields (i.e., $\delta_1,\delta_S\ll\delta_2$), Eq. (3.46) oscillates with a frequency and phase of $\bar{\Delta}^Q\approx\Delta^Q$ and $\phi_{II}(\Delta,\Gamma)\approx-\Delta^Q\Gamma_{fg}^Q(2\delta_2^2)^{-1}$.

Although a more detailed discussion will be given in Sec. IV, noted here is the presence of new ultranarrow spectral features found in Eqs. (3.28) [i.e., $L_1(\Delta,\Gamma)$ in Eq. (3.34)] and (B1), for the case of Lorentzian spectral densities, and in Eq. (3.43) (fourth exponential terms on the rhs) when Gaussian spectral densities are convolved into the theory. In both cases, like chromophore term ($\alpha=\beta$) show spectral resonances that track with the detuning resonance $\Delta^\alpha=0$ and possess widths given by $\Gamma_1+\Gamma_S$ ($\delta_1+\delta_S$ for the Gaussian case), which are entirely independent of the Raman linewidth in the assumed Markovian limit of material line broadening. For Lorentzian spectral densities for the fields, an additional sharp resonance appears at a detuning given by $\Delta_R=0$ that is independent of the material Bohr frequencies. These new resonances do not appear in the amplitude level susceptibility, but arise from an interference between different susceptibility-level resonances (here referring to the spontaneous and stimulated Raman branches) on the paired chromophores of the bichromophore scattering unit.

Zinth, Nuss, and Kaiser[76] have recently reported submaterial linewidth narrowing phenomena in CARS spectra when a Raman-active mode is excited with short-pulsed driving fields and probed with a delayed long pulse. For Gaussian pulses, spectral features whose width is determined by the bandwidth of the probe field can be obtained under certain excitation conditions. These conditions require probe delays greater than its pulse width, which in turn must be greater than the dephasing time of the driven vibration. Such narrow resonances are therefore necessarily strongly quenched by the material dephasing and are exposed only through logarithmic plots. These narrow spectral features appear in the anti-Stokes spectrum upon tuning the Stokes field and the laser field difference frequency through a Raman vibrational resonance ($\Delta_1=0$). They are entirely derived at the level of the third-order polarization, unlike the narrow resonance phenomena presented here. The ultranarrow resonances reported in the present work are derived from interference between the time development of the polarization amplitude on the different chromophores required to generate the phase-matched signal. Most importantly, the sharp resonances at $\Delta^Q=0$, as well as the analogous resonances in the excited electronic state (to be discussed later), appear at all τ delays less than the

nanosecond pulse width. They are best seen at $\tau=0$, but are quenched at most only by a factor of 2 for any τ less than the pulse width of the incoherent light.

Always present in the signal are contributions from fully nonresonant scattering amplitudes arising from the 24 different mixing channels in the (unsaturated, three-color limit) CSRS (CARS) third-order susceptibility. Most of these amplitude components are inherently nonresonant due to the particular intervention sequence. Each field intervention involves a sum over states, which for those scattering amplitudes able to reach material resonances, leads to both nonresonant and resonant contributions. The nonresonant components can greatly outnumber the resonant channels and therefore potentially overwhelm the resonance enhancement. When two such nonresonant amplitudes (involving conjugate fields) pair to form a signal component, the τ dependence is given only by the coherence properties of the fields. Here only the purely light related transients discussed in this section are obtained. Stronger signal channels, though less numerous, involve the quadrature pairing of resonant scattering channels with nonresonant scattering channels. If the τ dependence were generated directly at the level of the CSRS (CARS) polarization [for example, by the field envelope (or intensity) correlation of a short pulse], then such signal components would decay in τ with the coherence time of the light fields. With incoherent light, or, in general, with a phase-sensitive amplitude correlation of the fields, the τ dependence arising from these resonant-nonresonant cross pairs contains a contribution from terms oscillating at the detuning frequencies Δ^Q (damped by $\Gamma^Q_{fg+fg+1+S}$), just as in the resonant-resonant channels treated at length above. Here Q is the chromophore involved in the resonant polarization channel. Naturally, not seen in the mixed channel are the new spectral features that require resonant contributions from both chromophores.

In Sec. IV, both the interferograms and the signal spectrum generated by these analytic results will be modeled and discussed for both single- and two-component systems. Oscillatory and spectral phenomena appear in CARS that are fully analogous to those found here for CSRS. In CARS, the material oscillations, as Γ_1,Γ_S approach zero [via Eq. (3.20)], tune with the frequency $\Delta^Q=2\omega_{fg}+\omega_1-\omega_S$. The additional transient features obtained by introducing nonzero Γ_1,Γ_S also appear in the CARS process.

C. Analytic results for electronically resonant coherent Raman 4WM

When vibronic levels are brought into near resonance with the ω_1 and ω_2 fundamentals, three fully resonant terms appear in the CSRS process. The corresponding scattering diagrams are shown in Figs. 4(a), 4(b), and 4(c). The latter two contain vibrational coherences in the excited electronic state, generated at second order. At the signal level of the bichromophore model, these three mixing channels (A, B, and C) on chromophore α join their respective conjugate mixing channels (A^*, B^*, and C^*) on chromophore β, to create a total of nine different components in the phase-matched signal. Three of these are the exact conjugate scattering amplitudes (the diagonal terms) and the remaining six are the cross terms. Each cross term must be summed with its conjugate partner to represent a real signal component. After integrating over the four spectral densities [Eq. (3.6)], each of these signal terms produces a set of oscillatory and zero-frequency transients. The τ-dependent interferograms generated in electronically nonresonant CSRS (Sec. III B) represent only a subset of the total possible signal components obtained with electronically resonant mixing. Such signal components require a contribution from a ground-electronic-state Raman amplitude (A and/or A^*). Although identical in both their oscillation frequencies and effective dephasing rates, the electronically resonant versions of these signals differ in their spectral line shape, or resonance structure, depending on whether they involve an excited-state vibrational resonance, a Raman amplitude in an excited electronic state (B or C), or a resonance drawn from a vibronic transition.

It is impractical to give the full analytic solution to the problem in this manuscript. Only the strong signal terms in the limit $\Gamma_1,\Gamma_S \ll \Gamma_M$ (where Γ_M is a representative material linewidth) are presented in their entirety. The omitted "weak" components are identified only by their characteristic oscillation frequencies and their damping constants.

When both Γ_1 and Γ_S are nonzero, but small compared to the Γ_M's and any active Bohr frequency differences, the major contributions to the electronically resonant signals are similar to those described by the first term on the rhs of Eq. (3.19). With the notation of Eq. (3.8) and with Lorentzian spectral densities for all fields, one obtains

$$\begin{aligned} I^{\alpha\beta}_{\Gamma_{fg+fg+1+S}} \propto 2\Gamma_2^2\{ & y_\alpha^2[F_{AA^*}(\alpha,\alpha)+F_{AB^*}(\alpha,\alpha)+F_{BA^*}(\alpha,\alpha)]+y_\beta^2[F_{AA^*}(\beta,\beta)+F_{AB^*}(\beta,\beta)+F_{BA^*}(\beta,\beta)] \\ & +y_\alpha y_\beta[F_{AA^*}(\alpha,\beta)+F_{AB^*}(\alpha,\beta)+F_{BA^*}(\alpha,\beta)+F_{AA^*}(\beta,\alpha)+F_{AB^*}(\beta,\alpha)+F_{BA^*}(\beta,\alpha)] \\ & +\mathcal{T}(B\rightarrow C)\}\ , \end{aligned} \tag{3.49}$$

where $\mathcal{T}(B\rightarrow C)$ represents preceding terms with B replaced by C and where now

$$y_\alpha = N_\alpha \mu^\alpha_{nf}\mu^\alpha_{gn}\mu^\alpha_{fm}\mu^\alpha_{mg}\ . \tag{3.50}$$

The ground-electronic-state Raman process occurring on mixed chromophores generates the term

$$F_{AA^*}(\alpha,\beta)=L^I_{AA^*}(\Delta,\Gamma)L^2_{AA^*}(\Delta,\Gamma)e^{-\Gamma^{\alpha\alpha}_{fg+fg+1+S}|\tau|}$$
$$\times\left[\left[\frac{\mathrm{Re}[A_{AA^*}(\Delta,\Gamma)]\Delta^{\alpha\beta}+\mathrm{Im}[A_{AA^*}(\Delta,\Gamma)]\Gamma^{\beta\alpha}_{fg-fg-1-S}}{[(\Delta^{\alpha\beta})^2+(\Gamma^{\alpha\beta}_{fg-fg+1+S})^2]}\right.\right.$$
$$\left.+\frac{\mathrm{Re}[A_{AA^*}(\Delta,\Gamma)]\Delta^{\beta\alpha}_{fg-fg}+\mathrm{Im}[A_{AA^*}(\Delta,\Gamma)]\Gamma^{\alpha\beta}_{fg+fg}}{[(\Delta^{\beta\alpha}_{fg-fg})^2+(\Gamma^{\alpha\beta}_{fg+fg})^2]}\right]\sin(\Delta^\alpha|\tau|)$$
$$+\left[\frac{\mathrm{Re}[A_{AA^*}(\Delta,\Gamma)]\Gamma^{\beta\alpha}_{fg-fg-1-S}+\mathrm{Im}[A_{AA^*}(\Delta,\Gamma)]\Delta^{\alpha\beta}}{[(\Delta^{\alpha\beta})^2+(\Gamma^{\alpha\beta}_{fg-fg+1+S})^2]}\right.$$
$$\left.\left.+\frac{\mathrm{Re}[A_{AA^*}(\Delta,\Gamma)]\Gamma^{\alpha\beta}_{fg+fg}+\mathrm{Im}[A_{AA^*}(\Delta,\Gamma)]\Delta^{\beta\alpha}_{fg-fg}}{[(\Delta^{\beta\alpha}_{fg-fg})^2+(\Gamma^{\alpha\beta}_{fg+fg})^2]}\right]\cos(\Delta^\alpha\tau)\right], \tag{3.51}$$

where Δ^α and $\Delta^{\alpha\beta}$ have been previously defined (Sec. III B). Here the common resonant denominators are given as

$$L^1_{AA^*}(\Delta,\Gamma)=\frac{1}{[(\Delta^\alpha_1)^2+(\Gamma^\alpha_{fg+2+1})^2][(\Delta^\alpha_1)^2+(\Gamma^\alpha_{fg-2+1})^2][(\Delta^\alpha_S)^2+(\Gamma^\alpha_{fg+2+S})^2][(\Delta^\alpha_S)^2+(\Gamma^\alpha_{fg-2+S})^2]}, \tag{3.52}$$

$$L^2_{AA^*}(\Delta,\Gamma)=\frac{1}{[(\Delta^\alpha_{nf-S})^2+(\Gamma^\alpha_{nf+S})^2][(\Delta^\beta_{nf-S})^2+(\Gamma^\beta_{nf-S})^2][(\Delta^\alpha_{mg-1})^2+(\Gamma^\alpha_{mg+1})^2][(\Delta^\beta_{mg-1})^2+(\Gamma^\beta_{mg-1})^2]}, \tag{3.53}$$

and the expressions for the complex functions $A_{AA'}(\Delta,\Gamma)$ are given, using Eqs. (3.21) and (3.22), by

$$\mathrm{Re}[A_{AA^*}(\Delta,\Gamma)]=\mathrm{Re}[A(\Delta,\Gamma)][(\Delta^\alpha_{nf-S}\Delta^\beta_{nf-S}+\Gamma^\alpha_{nf+S}\Gamma^\beta_{nf-S})(\Delta^\alpha_{mg-1}\Delta^\beta_{mg-1}+\Gamma^\alpha_{mg+1}\Gamma^\beta_{mg-1})$$
$$-(\Delta^\alpha_{mg-1}\Gamma^\beta_{mg-1}-\Delta^\beta_{mg-1}\Gamma^\alpha_{mg+1})(\Delta^\beta_{nf-S}\Gamma^\alpha_{nf+S}-\Delta^\alpha_{nf-S}\Gamma^\beta_{nf-S})]$$
$$+2\,\mathrm{Im}[A(\Delta,\Gamma)][(\Delta^\alpha_{nf-S}\Delta^\beta_{nf-S}+\Gamma^\alpha_{nf+S}\Gamma^\beta_{nf-S})(\Delta^\alpha_{mg-1}\Gamma^\beta_{mg-1}-\Delta^\beta_{mg-1}\Gamma^\alpha_{mg+1})$$
$$+(\Delta^\alpha_{mg-1}\Delta^\beta_{mg-1}+\Gamma^\alpha_{mg+1}\Gamma^\beta_{mg-1})(\Delta^\beta_{nf-S}\Gamma^\alpha_{nf+S}-\Delta^\alpha_{nf-S}\Gamma^\beta_{nf-S})] \tag{3.54}$$

and

$$\mathrm{Im}[A_{AA^*}(\Delta,\Gamma)]=2\,\mathrm{Im}[A(\Delta,\Gamma)][(\Delta^\alpha_{nf-S}\Delta^\beta_{nf-S}+\Gamma^\alpha_{nf+S}\Gamma^\beta_{nf-S})(\Delta^\alpha_{mg-1}\Delta^\beta_{mg-1}+\Gamma^\alpha_{mg+1}\Gamma^\beta_{mg-1})$$
$$-(\Delta^\alpha_{mg-1}\Gamma^\beta_{mg-1}-\Delta^\beta_{mg-1}\Gamma^\alpha_{mg+1})(\Delta^\beta_{nf-S}\Gamma^\alpha_{nf+S}-\Delta^\alpha_{nf-S}\Gamma^\beta_{nf-S})]$$
$$-\mathrm{Re}[A(\Delta,\Gamma)][(\Delta^\alpha_{nf-S}\Delta^\beta_{nf-S}+\Gamma^\alpha_{nf+S}\Gamma^\beta_{nf-S})(\Delta^\alpha_{mg-1}\Gamma^\beta_{mg-1}-\Delta^\beta_{mg-1}\Gamma^\alpha_{mg+1})$$
$$+(\Delta^\alpha_{mg-1}\Delta^\beta_{mg-1}+\Gamma^\alpha_{mg+1}\Gamma^\beta_{mg-1})(\Delta^\beta_{nf-S}\Gamma^\alpha_{nf+S}-\Delta^\alpha_{nf-S}\Gamma^\beta_{nf-S})]. \tag{3.55}$$

The new detuning parameters found in Eq. (3.53) represent the near-resonant vibronic transitions $\Delta^Q_{nf-S}=\omega^Q_{nf}-\omega_S$ and $\Delta^Q_{mg-1}=\omega^Q_{mf}-\omega_1$.

A detuning beat, similar to Δ^Q in Eq. (3.52), originates in the excited state when the difference frequency $\omega_1-\omega_2$ is in near-resonance with, for instance, a vibration in an excited electronic state. Such terms require in their construction at least one amplitude component involving the diagrams of Fig. 4(b) or 4(c) and can be expressed as

$$I^{\alpha\beta}_{\Gamma_{mn+mn+1+S}}\approx 2\Gamma_2^2\{y^2_\alpha[F'_{BB^*}(\alpha,\alpha)+F'_{AB^*}(\alpha,\alpha)+F'_{BA^*}(\alpha,\alpha)]$$
$$+y^2_\beta[F'_{BB^*}(\beta,\beta)+F'_{AB^*}(\beta,\beta)+F'_{BA^*}(\beta,\beta)]+y_\alpha y_\beta[F'_{BB^*}(\alpha,\beta)+F'_{AB^*}(\alpha,\beta)$$
$$+F'_{BA'}(\alpha,\beta)+F'_{BB^*}(\beta,\alpha)+F'_{AB^*}(\beta,\alpha)+F'_{BA^*}(\beta,\alpha)]+\mathcal{T}(B\rightarrow C)\}, \tag{3.56}$$

where, for example,

$$F'_{BB^*}(\alpha,\beta)=L^1_{BB^*}(\Delta,\Gamma)L^2_{BB^*}(\Delta,\Gamma)e^{-\Gamma^{\alpha\alpha}_{mn+mm+1+S}|\tau|}$$
$$\times\left[\left[\frac{\mathrm{Re}[A_{BB^*}(\Delta,\Gamma)]\Delta'^{\alpha\beta}+\mathrm{Im}[A_{BB^*}(\Delta,\Gamma)]\Gamma^{\beta\alpha}_{mn-mn-1-S}}{[(\Delta'^{\alpha\beta})^2+(\Gamma^{\alpha\beta}_{mn-mn+1+S})^2]}\right.\right.$$
$$\left.+\frac{\mathrm{Re}[A_{BB^*}(\Delta,\Gamma)]\Delta^{\beta\alpha}_{mn-nm}+\mathrm{Im}[A_{BB^*}(\Delta,\Gamma)]\Gamma^{\alpha\beta}_{nm+mn}}{[(\Delta^{\beta\alpha}_{mn-mn})^2+(\Gamma^{\alpha\beta}_{mn+mn})^2]}\right]\sin(\Delta'^{\alpha}|\tau|)$$
$$+\left[\frac{\mathrm{Re}[A_{BB^*}(\Delta,\Gamma)]\Gamma^{\beta\alpha}_{mn-mn-1-S}+\mathrm{Im}[A_{BB^*}(\Delta,\Gamma)]\Delta'^{\alpha\beta}}{[(\Delta'^{\alpha\beta})^2+(\Gamma^{\alpha\beta}_{nm-mn+1+S})^2]}\right.$$
$$\left.+\frac{\mathrm{Re}[A_{BB^*}(\Delta,\Gamma)]\Gamma^{\alpha\beta}_{mn+mn}+\mathrm{Im}[A_{BB^*}(\Delta,\Gamma)]\Delta^{\beta\alpha}_{mn-mn}}{[(\Delta^{\beta\alpha}_{mn-mn})^2+(\Gamma^{\alpha\beta}_{mn+mn})^2]}\right]\cos(\Delta'^{\alpha}\tau)\Bigg]\ . \tag{3.57}$$

Here $L^2_{BB^*}(\Delta,\Gamma)=L^2_{AA^*}(\Delta,\Gamma)$ and

$$L^1_{BB^*}(\Delta,\Gamma)=\frac{1}{[(\Delta'^{\alpha}_1)^2+(\Gamma^{\alpha}_{mn+2+1})^2][(\Delta'^{\alpha}_1)^2+(\Gamma^{\alpha}_{mn-2+1})^2][(\Delta'^{\alpha}_S)^2+(\Gamma^{\alpha}_{mn+2+S})^2][(\Delta'^{\alpha}_s)^2+(\Gamma^{\alpha}_{mn-2+S})^2]}\ . \tag{3.58}$$

The primes on the detuning parameters denote the excited-electronic-state version of the detuning with $\Delta'^{Q}_1=\omega^Q_{mn}+\omega_2-\omega_1$, $\Delta'^{Q}_S=\omega^Q_{mn}+\omega_S-\omega_2$, $\Delta'^{Q}=\Delta'^{Q}_1+\Delta'^{Q}_S$, and $\Delta'^{QQ'}=\Delta'^{Q}_1+\Delta'^{Q'}_S$.

A permutation of the stimulated Raman driving fields results in the diagram shown in Fig. 4(c). This scattering channel, when squared with its identical conjugate, or crossed with the conjugate channels of Fig. 4(a) or 4(b), also generates detuning beats at the frequencies Δ^Q and Δ'^Q, but involves different energy denominators at the ω_1 and ω_S transitions. These expressions are presented in Appendix B, Eqs. (B11)–(B20).

Cross terms (A-B) between ground- and excited-state Raman channels are responsible for the ground-state Raman signal components $F_{AB^*}(Q,Q')+F_{BA^*}(Q,Q')$ in Eq. (3.49) and excited-state Raman component in $F'_{AB^*}(Q,Q')+F'_{BA^*}(Q,Q')$ in Eq. (3.56). When mixed chromophores (a binary system) are considered, the $F_{AB^*}(Q,Q')+F_{BA^*}(Q,Q')$ component can be equated to $F_{AA^*}(\alpha,\beta)$ Eq. (3.51) by writing ω^β_{mn} instead of ω^β_{fg}, and Γ^β_{mn} instead of Γ^β_{fg}. This parameter exchange results in a new resonance with a detuning $\omega^\alpha_{fg}+\omega^\beta_{mn}+\omega_S-\omega_1$ and a damping $\Gamma^{\alpha\beta}_{fg-mn+1+S}$. Also a different field-independent Lorentzian is found with a resonant frequency $\Delta^{\beta\alpha}_{mn-fg}$ and width $\Gamma^{\alpha\beta}_{fg+mn}$. Similarly, $F'_{AB^*}(Q,Q')+F'_{BA^*}(Q,Q')$ can be obtained from $F'_{BB^*}(\alpha,\beta)$ by replacing both ω^β_{mn} with ω^β_{fg} and Γ^β_{mn} with Γ^β_{fg} in Eq. (3.57).

Cross terms of the A-B type show the identical τ dependence as their respective diagonal components (i.e., AA^*, and BB^*). However, additional resonances are seen in the cross amplitude terms that corresponding to a mixing between ground- and excited-electronic-state Raman modes. The diagonal terms, instead, show a mixing between two ground-state Raman modes or between two excited-state Raman modes. In both cases, the two material Bohr frequencies involved in mixed resonances are from different chromophores.

A third signal feature appearing with electronically resonant scattering originates from channel C [Fig. 4(c)]. Unlike all previous signal components, the material dependent part (i.e., resonant frequency and dephasing rate) of this transient is vibronic in nature. Its contribution to the fourth-wave signal is given by

$$I^{\alpha\beta}_{\Gamma_{ng+ng+1+S}}\approx 2\Gamma^2_2\{y^2_\alpha[F''_{CC^*}(\alpha,\alpha)+F''_{AC^*}(\alpha,\alpha)+F''_{CA^*}(\alpha,\alpha)]+y^2_\beta[F''_{CC^*}(\beta,\beta)+F''_{AC^*}(\beta,\beta)+F''_{CA^*}(\beta,\beta)]$$
$$+y_\alpha y_b[F''_{CC^*}(\alpha,\beta)+F''_{AC^*}(\alpha,\beta)+F''_{CA^*}(\alpha,\beta)+F''_{CC^*}(\beta,\alpha)+F''_{AC^*}(\beta,\alpha)+F''_{CA^*}(\beta,\alpha)]$$
$$+\mathcal{J}(A\rightarrow B)\}\ , \tag{3.59}$$

where for the diagonal CC^* component

$$F''_{CC^*}(\alpha,\beta)=L^3_{CC^*}(\Delta,\Gamma)L^4_{CC^*}(\Delta,\Gamma)e^{-\Gamma^{\alpha\alpha}_{ng+ng+1+S}|\tau|}$$
$$\times\left\{\left[\mathrm{Re}[\zeta_1(\Delta,\Gamma)]\left[\frac{\mathrm{Im}[\zeta_2(\Delta,\Gamma)]}{|\zeta_2(\Delta,\Gamma)|^2}+\frac{\mathrm{Im}[\zeta_3(\Delta,\Gamma)]}{|\zeta_3(\Delta,\Gamma)|^2}\right]\right.\right.$$
$$\left.+\mathrm{Im}[\zeta_1(\Delta,\Gamma)]\left[\frac{\mathrm{Re}[\zeta_2(\Delta,\Gamma)]}{|\zeta_2(\Delta,\Gamma)|^2}+\frac{\mathrm{Re}[\eta_3(\Delta,\Gamma)]}{|\zeta_3(\Delta,\Gamma)|^2}\right]\right]\cos(\Delta''^{\alpha}\tau)$$
$$+\left[\mathrm{Re}[\zeta_1(\Delta,\Gamma)]\left[\frac{\mathrm{Re}[\zeta_2(\Delta,\Gamma)]}{|\zeta_2(\Delta,\Gamma)|^2}+\frac{\mathrm{Re}[\zeta_3(\Delta,\Gamma)]}{|\zeta_3(\Delta,\Gamma)|^2}\right]\right.$$
$$\left.\left.-\mathrm{Im}[\zeta_1(\Delta,\Gamma)]\left[\frac{\mathrm{Im}[\zeta_2(\Delta,\Gamma)]}{|\zeta_2(\Delta,\Gamma)|^2}+\frac{\mathrm{Im}[\zeta_3(\Delta,\Gamma)]}{|\zeta_3(\Delta,\Gamma)|^2}\right]\right]\sin(\Delta''^{\alpha}|\tau|)\right\}. \tag{3.60}$$

Here oscillatory behavior at a frequency $\Delta''^{\alpha}=2\omega^{\alpha}_{ng}-\omega_S-\omega_1$ is damped by twice the dephasing rate of the ρ^{α}_{ng} vibronic coherence (for $\Gamma^{\alpha}_{ng}\gg\Gamma_1$ and Γ_S). The two common energy denominators are combinations of single-chromophore vibronic resonances and are written as

$$L^3_{CC^*}(\Delta,\Gamma)$$
$$=\frac{1}{[(\Delta^{\alpha}_{ng-2})^2+(\Gamma^{\alpha}_{ng-2})^2][(\Delta^{\alpha}_{ng-2})^2+(\Gamma^{\alpha}_{ng+2})^2][(\Delta^{\alpha}_{ng+2-1-S})^2+(\Gamma^{\alpha}_{ng+2+1+S})^2][(\Delta^{\alpha}_{ng+2-1-S})^2+(\Gamma^{\alpha}_{ng-2+1+S})^2]} \tag{3.61}$$

and

$$L^4_{CC^*}(\Delta,\Gamma)=\frac{1}{[(\Delta^{\beta}_{nf-S})^2+(\Gamma^{\beta}_{nf-S})^2][(\Delta^{\alpha}_{nf-S})^2+(\Gamma^{\alpha}_{nf+S})^2][(\Delta^{\alpha}_{mg-1})^2+(\Gamma^{\alpha}_{mn-ng-1})^2]}. \tag{3.62}$$

The expression for the complex function ζ_1 is written as

$$\zeta_1(\Delta,\Gamma)=(\{[(\Delta^{\alpha}_{ng-2})^2-\Gamma^{\alpha}_{ng-2}\Gamma^{\alpha}_{ng+2}][(\Delta^{\alpha}_{ng+2-S-1})^2-\Gamma^{\alpha}_{ng-2+S+1}\Gamma^{\alpha}_{ng+2+S+1}]$$
$$-4\Delta^{\alpha}_{ng-2}\Delta^{\alpha}_{ng+2-S-1}\Gamma^{\alpha}_{ng+S+1}\Gamma^{\alpha}_{ng}\}$$
$$-i\{\Delta^{\alpha}_{ng-2}\Gamma^{\alpha}_{ng}[(\Delta^{\alpha}_{ng+2-S-1})^2-\Gamma^{\alpha}_{ng-2+S+1}\Gamma^{\alpha}_{ng+2+S+1}]$$
$$+\Delta^{\alpha}_{ng+2-S-1}\Gamma^{\alpha}_{ng+S+1}[(\Delta^{\alpha}_{ng-2})^2-\Gamma^{\alpha}_{ng-2}\Gamma^{\alpha}_{ng+2}]\})$$
$$\times\{[(\Delta^{\alpha}_{nf-S}\Delta^{\beta}_{nf-S}+\Gamma^{\beta}_{ng-S}\Gamma^{\alpha}_{ng+S})\Delta^{\alpha}_{mg-1}-(\Gamma^{\beta}_{nf-S}\Delta^{\alpha}_{nf-S}-\Delta^{\beta}_{ng-S}\Gamma^{\alpha}_{ng+S})\Gamma^{\alpha\alpha}_{mn-ng-1}]$$
$$+i[\Gamma^{\alpha\alpha}_{mn-ng-1}(\Delta^{\beta}_{nf-S}\Delta^{\alpha}_{nf-S}+\Gamma^{\beta}_{ng-S}\Gamma^{\alpha}_{ng+S})-\Delta^{\alpha}_{mg-1}(\Gamma^{\beta}_{nf-S}\Delta^{\alpha}_{nf-S}-\Delta^{\beta}_{ng-S}\Gamma^{\alpha}_{ng+S})]\}. \tag{3.63}$$

This signal component shows enhancement from mixed two-chromophore resonances given by the functions ζ_2 and ζ_3, in Eq. (3.60),

$$\zeta_2(\Delta,\Gamma)=(\Delta^{\beta\alpha}_{mn-ng+S}-i\Gamma^{\beta\alpha}_{mn-ng-S})$$
$$\times(\Delta^{\beta\alpha}_{ng+ng-1-S}+i\Gamma^{\beta\alpha}_{ng-ng-1-S}), \tag{3.64}$$
$$\zeta_3(\Delta,\Gamma)=(\Delta^{\beta\alpha}_{ng-ng}-i\Gamma^{\beta\alpha}_{ng+ng})$$
$$\times(\Delta^{\beta\alpha}_{mn+ng-1}+i\Gamma^{\beta\alpha}_{ng+ng+1}). \tag{3.65}$$

Similar vibronic detuning oscillations also arise from the A-C cross terms $F''_{AC^*}(Q,Q')+F''_{CA^*}(Q,Q')$ as well as from the B-C cross terms $F''_{BC^*}(Q,Q')+F''_{CB^*}(Q,Q')$. The latter component can be converted to the diagonal CC^* component [Eq. (3.58)] by replacing $\Delta^{\beta\alpha}_{ng+ng-1-S}$ and $\Delta^{\beta\alpha}_{ng-ng}$ by the detuning Δ^{β}_{mg-1}, and $\Gamma^{\beta\alpha}_{ng-ng-1-S}$ and $\Gamma^{\beta\alpha}_{ng+ng}$ by Γ^{β}_{mg-1}. The substitution of ω^{β}_{fg} for ω^{β}_{mn} and Γ^{β}_{fg} for Γ^{β}_{mn} in the resulting equation generates the A-C cross term.

The τ dependence of Eqs. (3.49), (3.56), and (3.59) reflects single-chromophore dynamics even though the resonant enhancement draws on mixed chromophore resonances. Just as for the electronically nonresonant mixing (Sec. III B), other transient features, reflecting both radiation-matter detuning beats and purely material quantum beats, appear in the interferograms. As before, their magnitudes are sensitive to the spectral widths of fields 1 and S, among other parameters (e.g., material linewidths and detunings).

In order to complete the discussion of this complex mixing process, the remaining contributions to the τ dependence of the signal, along with all of those signal components already discussed in Sec. III, are organized in Tables I–III. Table I refers to "material only" responses. There the oscillation frequencies and effective dephasing rate constants are listed for those signal transients which beat at various combinations of material

TABLE I. Different signal transients showing material quantum beats listed in terms of their oscillation frequency and effective dephasing constants. The different oscillations reflect beating between (a) ground electronic state, (b) excited electronic state, (c) mixed ground excited state Raman modes, as well as (d) vibronic state beating and (e) mixed vibrational-vibronic trilevel beats. All of the above oscillatory transients involve two chromophores.

Scattering channel	Material Bohr frequency beats: Oscillation frequency	Oscillation type	Effective dephasing constant
AA^*	$\omega_{fg}^{Q}-\omega_{fg}^{Q'}$	(a)	$\Gamma_{fg}^{Q}+\Gamma_{fg}^{Q'}$
BB^* and CC^*	$\omega_{mn}^{Q}-\omega_{mn}^{Q'}$	(b)	$\Gamma_{mn}^{Q}+\Gamma_{mn}^{Q'}$
AB^*+BA^*, AC^*+CA^*	$\omega_{fg}^{Q}-\omega_{mn}^{Q'}$	(c)	$\Gamma_{fg}^{Q}+\Gamma_{mn}^{Q'}$
AA^*, AB^*+BA^*, AC^*+CA^*	$2\omega_{fg}^{Q}-\omega_{mg}^{Q'}+\omega_{nf}^{Q'}$	(e)	$2\Gamma_{fg}^{Q}+\Gamma_{mg}^{Q'}+\Gamma_{nf}^{Q'}$
BB^*, BA^*+AB^*, CC^*, CA^*+AC^*	$2\omega_{mn}^{Q}-\omega_{mg}^{Q'}+\omega_{nf}^{Q'}$	(e)	$2\Gamma_{mn}^{Q}+\Gamma_{mg}^{Q'}+\Gamma_{nf}^{Q'}$
CC^*	$\omega_{ng}^{Q}-\omega_{ng}^{Q'}$	(d)	$\Gamma_{ng}^{Q}+\Gamma_{ng}^{Q'}$
CC^*, CB^*+BC^*, CA^*+AC^*	$-2\omega_{ng}^{Q}+\omega_{mg}^{Q'}+\omega_{nf}^{Q'}$	(e)	$2\Gamma_{ng}^{Q}+\Gamma_{mg}^{Q'}+\Gamma_{nf}^{Q'}$
CC^*, CB^*+BC^*	$\omega_{ng}^{Q}-\omega_{mn}^{Q'}-\omega_{nf}^{Q'}$	(e)	$\Gamma_{ng}^{Q}+\Gamma_{mn}^{Q'}+\Gamma_{nf}^{Q'}$
	$\omega_{ng}^{Q}+\omega_{mn}^{Q'}-\omega_{mg}^{Q'}$	(e)	$\Gamma_{ng}^{Q}+\Gamma_{mn}^{Q'}+\Gamma_{mg}^{Q'}$
CA^*+AC^*	$\omega_{ng}^{Q}-\omega_{fg}^{Q'}-\omega_{nf}^{Q'}$	(e)	$\Gamma_{ng}^{Q}+\Gamma_{fg}^{Q'}+\Gamma_{nf}^{Q'}$
	$\omega_{ng}^{Q}+\omega_{fg}^{Q'}-\omega_{mg}^{Q'}$	(e)	$\Gamma_{ng}^{Q}+\Gamma_{fg}^{Q'}+\Gamma_{mg}^{Q'}$

Bohr frequencies and attenuate at a rate that depends purely on the rate of material coherence loss. Radiation-matter oscillations and their dephasing rate constants appear in Tables II and III. Those listed in Table II are independent of the broadband fields 2 and 2′. Table III lists components (including contributions from zero frequency and pure radiation detuning components) that are sensitive to the properties of these twin fields. The components in Table III labeled as "coherent peak" contributions define the short-time response ($\tau \approx \tau_c$), or the effective temporal resolution of the measurement. In each table, the first column, labeled "channel," indicates the combination of mixing channel (Fig. 4) required to generate the corresponding signal transient. Contributions from unlike chromophores are identified by the Q (α or β) and Q' (β or α) superscripts. For like chromophore signal terms, we have $Q=Q'$.

The information in all three tables only pertains to the τ dependence of the interferograms. It does not indicate the relative strengths of the various signal components, nor does it contain spectral information. While different combinations of scattering amplitudes may lead to the same transient response, the line shapes, particularly those reflecting combination resonances between chromophores, turn out to be unique to the signal level mixing channels.

Of the many types of oscillatory behavior listed in Tables I and II, two show interesting quantum interfer-

TABLE II. Different Γ_2-independent detuning transients generated in fully resonant CSRS listed in terms of their oscillation frequencies and effective dephasing constants. The nature of the material resonance involved in the detuning is (a) vibrational, (b), vibronic, (c) bichromophore (Q,Q') mixed vibrational-vibronic, or (d) bichromophore mixed vibronic.

Scattering channel	Detuning oscillations (Γ_2) independent) oscillation frequency	Resonance type	Effective dephasing constant
AA^*, AB^*+BA^*, AC^*+CA^*	Δ^{Q}	(a)	$2\Gamma_{fg}^{Q}+\Gamma_1+\Gamma_s$
	$2\omega_{fg}^{Q}+\omega_{nf}^{Q'}-\omega_1$	(c)	$2\Gamma_{fg}^{Q}+\Gamma_{nf}^{Q'}+\Gamma_1$
	$2\omega_{fg}^{Q}-\omega_{mg}^{Q'}+\omega_s$	(c)	$2\Gamma_{fg}^{Q}+\Gamma_{mg}^{Q'}+\Gamma_s$
BB^*, BA^*+AB^*	Δ'^{Q}	(a)	$2\Gamma_{mn}^{Q}+\Gamma_1+\Gamma_s$
CC^*, CA^*+AC^*,	$2\omega_{mn}^{Q}+\omega_{nf}^{Q'}-\omega_1$	(c)	$2\Gamma_{mn}^{Q}+\Gamma_{nf}^{Q'}+\Gamma_1$
	$2\omega_{mn}^{Q}-\omega_{mg}^{Q'}+\omega_s$	(c)	$2\Gamma_{mg}^{Q}+\Gamma_{mn}^{Q'}+\Gamma_s$
CC^*, CA^*+AC^*	Δ''^{Q}	(b)	$2\Gamma_{ng}^{Q}+\Gamma_1+\Gamma_s$
CB^*+BC^*	$-2\omega_{ng}^{Q}+\omega_{mg}^{Q'}+\omega_s$	(d)	$2\Gamma_{ng}^{Q}+\Gamma_{mg}^{Q'}+\Gamma_s$
	$-2\omega_{ng}^{Q}+\omega_{nf}^{Q'}+\omega_1$	(d)	$2\Gamma_{ng}^{Q}+\Gamma_{nf}^{Q'}+\Gamma_1$

TABLE III. Fast-time (Γ_2-dependent) signal transients listed in terms of their oscillation frequencies and effective dephasing constants.

Coherent peak components (Γ_2 dependent)		
Scattering channel	Oscillation frequency	Effective dephasing constant
AA^*, AB^*+BA^*	Δ_1^Q	$\Gamma_{fg}^Q+\Gamma_2+\Gamma_1$
AC^*+CA^*	Δ_S^Q	$\Gamma_{fg}^Q+\Gamma_2+\Gamma_S$
	$\omega_{fg}^Q+\omega_{nf}^{Q'}-\omega_2$	$\Gamma_{fg}^Q+\Gamma_{nf}^{Q'}+\Gamma_2$
	$\omega_{fg}^Q-\omega_{mg}^{Q'}+\omega_2$	$\Gamma_{fg}^Q+\Gamma_{mg}^{Q'}+\Gamma_2$
BB^*, BA^*+AB^*	$\Delta_1'^Q$	$\Gamma_{mn}^Q+\Gamma_2+\Gamma_1$
CC^*, CA^*+AC^*	$\Delta_S'^Q$	$\Gamma_{mn}^Q+\Gamma_2+\Gamma_1$
BC^*+CB^*	$\omega_{mn}^Q+\omega_{nf}^{Q'}-\omega_2$	$\Gamma_{mn}^Q+\Gamma_{nf}^{Q'}+\Gamma_2$
	$\omega_{mn}^Q-\omega_{mg}^{Q'}+\omega_2$	$\Gamma_{mn}^Q+\Gamma_{mg}^{Q'}+\Gamma_2$
CC^*, CA^*+AC^* CB^*+BC^*	$\omega_{ng}^Q-\omega_2$	$\Gamma_{ng}^Q+\Gamma_2$
All six independent components	Δ_R	$2\Gamma_2+\Gamma_S+\Gamma_1$
	$-2\omega_2+\omega_{mg}^Q+\omega_{nf}^{Q'}$	$2\Gamma_2+\Gamma_{mg}^Q+\Gamma_{nf}^{Q'}$
	$-2\omega_2+\omega_{mg}^Q+\omega_S$	$2\Gamma_2+\Gamma_{mg}^Q+\Gamma_S$
	$-2\omega_2+\omega_{nf}^Q+\omega_1$	$2\Gamma_2+\Gamma_{nf}^Q+\Gamma_1$
	0	$2\Gamma_2$

ence effects between a vibrational and a vibronic coherence on different chromophores (either $Q=Q'$ or $Q\neq Q'$). In one case (Table II), this vibronic-vibrational beating involves either the ω_1 or ω_S modes of the superposition field (a detuning oscillation) or another vibronic mode of the chromophore (purely material quantum beats). These latter transients are controlled by material parameters, with an attenuation given by the combination of different vibrational and vibronic dephasing rate constants. Also seen is beating between two modes that are both either vibrational or vibronic in nature. When like chromophore contributions are considered, such oscillations, having zero difference beats, cannot appear. In their place, smoothly decaying transients appear that reflect pure material coherence loss of the driven vibrational or vibronic state.

IV. DISCUSSION AND RESULTS

The analytical development in Sec. III is now examined in some detail. Model calculations are presented and an interpretation of the new light-matter oscillations is given in terms of "base" radiation-matter oscillators. Experimental details, with relevant data, will be given in the following paper (II).

A. Modeling

Guided by experiments on benzene, we initially consider the case of electronically nonresonant CSRS in a one-component sample, where the Raman-active mode is given a Bohr frequency of $\bar{\nu}_{fg}=991$ cm^{-1} [$\bar{\nu}_{fg}=\omega_{fg}(2\pi c)^{-1}$] and a width [half width at half maximum (HWHM)] of $\bar{\Gamma}_{fg}=1.2$ cm^{-1} [$\bar{\Gamma}_{fg}=\Gamma_{fg}(2\pi c)^{-1}$].

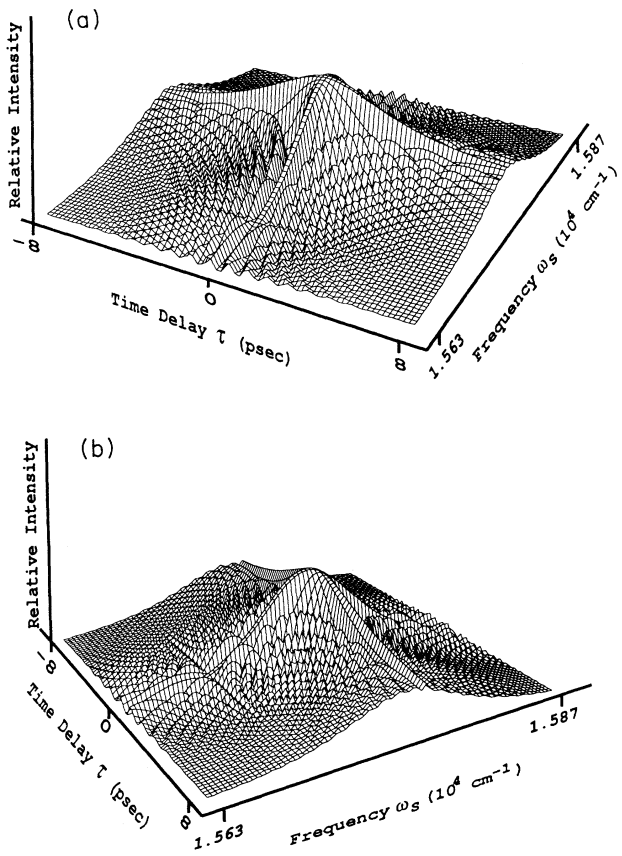

FIG. 6. Electronically nonresonant transient CSRS spectra for exponentially damped pair correlation between the broadband fields 2 and 2′ (coherences time=100 fs and $\bar{\nu}_2=16\,750$ cm^{-1}). There is one Raman-active mode. The parameters are $\bar{\nu}_{fg}=991.0$ cm^{-1} and $\bar{\Gamma}_{fg}=1.2$ cm^{-1}. (a) $\bar{\nu}_1=17\,741$ cm^{-1}, $J_1(\omega_1')=\delta(\omega_1')$, and $J_D(\omega_S')=\delta(\omega_S')$; (b) $\bar{\nu}_1=17\,753$ cm^{-1}; $J_1(\omega_1')=\delta(\omega_1')$, and $J_D(\omega_S')=\delta(\omega_S')$.

The twin broadband excitation fields are taken to have a carrier frequency ($\omega_2=\omega_{2'}$) of $\bar{\nu}_2=\bar{\nu}_{2'}=16\,750$ cm^{-1} and $\bar{\Gamma}_2=53$ cm^{-1} (a coherence time of 100 fs). In Fig. 6, the fourth-wave signal according to Eq. (3.7) is plotted as a function of the interferometric delay τ and the signal frequency $\bar{\nu}_S$ for two different narrow-band excitation frequencies. For zero detuning on the stimulated Raman branch $\Delta_1=0$ (or $\bar{\nu}_1=16\,741$ cm^{-1}), the plot in Fig. 6(a) is found. The center of the broad spectral feature, defined by the resonant condition on the spontaneous Raman branch $\Delta_S=0$, is also the point of zero oscillation in the interferogram (τ axis). Here the interferometric signal profile is seen to be a smoothly decaying exponential, damped by twice the Raman dephasing rate constant. As $\bar{\nu}_S$ is tuned away from the spectral peak, either to the blue or to the red, these oscillations, which track with the detuning Δ^Q, decrease in period. Upon tuning the narrow-band input field to $\bar{\nu}_1=18\,753$ cm^{-1}, the signal frequency at which the detuning oscillations vanish shifts

12.3 cm^{-1} to the blue of the spectral peak [Fig. 6(b)].

The purely light damped component found in Eq. (3.7) is a small contribution to the total signal intensity. In general, time domain measurements that use excitation fields having a spectral width large compared to that of the driven line ($\Gamma_2, \Gamma_1, \Gamma_S \gg \Gamma_M$) lead to a material damped signal that is much attenuated compared to the purely light related transient (the coherent peak). In such cases, logarithmic plots are commonly used to expose the relatively weak material response that remains. In the present case where $\Gamma_1, \Gamma_S \ll \Gamma_M$ (in fact, zero in this modeling), the material damped term dominates the signal, and interestingly, its contribution increases with the ratio $\Gamma_2/2\Gamma_{fg}$ in the limit that $\Gamma_2 \gg \Gamma_{fg}$.

However, upon assigning nonzero values to Γ_1 and Γ_S (but still less than Γ_M) qualitatively new features appear in both the interferogram as well as in the signal spectrum. A plot of Eq. (3.19) is shown in Fig. 7 for the same parameters used to generate the plot of Fig. 6(b), except now $\bar{\Gamma}_1 = 0.40$ cm^{-1} and $\bar{\Gamma}_S = 0.25$ cm^{-1}. Modulations similar to those seen in Fig. 6(b) are observed in the interferograms. However, in the spectrum of the signal two entirely new sharp resonant features appear at frequencies $\bar{\nu}_S = 15\,747$ and $15\,771$ cm^{-1}. These represent the zero detuning points of the resonances defined in terms of the difference combination of the stimulated Raman and spontaneous Raman branches $\Delta_R = \Delta_1^Q - \Delta_S^Q = 0$ and the corresponding sum combination $\Delta^Q = \Delta_1^Q + \Delta_S^Q = 0$. (It is important to note that these resonances, constructed from the two Raman branches, involve identical modes on spatially distinct chromophores.) The width of each of these new spectral lines is just the sum of the widths of the nondegenerate field and of the signal field ($\Gamma_S + \Gamma_1$) which, experimentally, can be made less than Raman linewidth. The emergence of the purely-light-related coherent peak in the interferograms is seen in the spectral region around the narrow resonance at $\Delta_R = 0$ [Fig. 7(b)].

Upon going from the motionally narrowed limit (Lorentzian) to the static limit (Gaussian) of the field phase fluctuations for fields $\lambda = 1, 2, 2'$ and a Gaussian detector spectral response function for $\lambda = S$, the purely-light-dependent narrow resonance at $\Delta_R = 0$ disappears. Still, the feature at $\Delta^Q = 0$ remains, provided that the material dephasing remains in the fast-modulation limit. The line shape is now an overall narrow Gaussian profile [full width that half maximum (FWHM) of $4\sqrt{\ln 2}(\delta_1 + \delta_S)$], again having no reference to the material dephasing rate constants. This is illustrated in Fig. 8(a) where a plot of Eq. (3.41) is shown using $\bar{\delta}_2 = 51$ cm^{-1}, $\bar{\delta}_1 = 0.24$ cm^{-1}, $\bar{\delta}_S = 0.15$ cm^{-1}, and otherwise the same set of frequencies as used in Fig. 7. The removal of the purely-light-related sharp resonance at $\Delta_R = 0$ for Gaussian spectral densities can be understood by regarding the broadband fields to consist of a static distribution of frequencies, that are inhomogeneously broadened. Just as for the two-chromophore narrow resonance at $\Delta^Q = 0$, the two ω_2 contributions in the $\Delta_R = 0$ resonance arise from the intervention of degenerate fields $\pm\omega_2$ and $\mp\omega_{2'}$, on separate chromophores. Now each statistically independent frequency in the inhomogeneous spectrum of field 2, say, will act conjugately with every statistically independent frequency of conjugate field 2'. This leads to a distribution in the $\Delta_R = 0$ condition. A broad spectrum of the overlapping, narrow, resonances will merge with the broad spontaneous Raman spectral feature and will thereby not be seen. An experimental CSRS spectrum of neat deuterated benzene (C_6D_6) showing the narrow material sensitive resonance at $\Delta^Q = 0$ is reported in paper II.

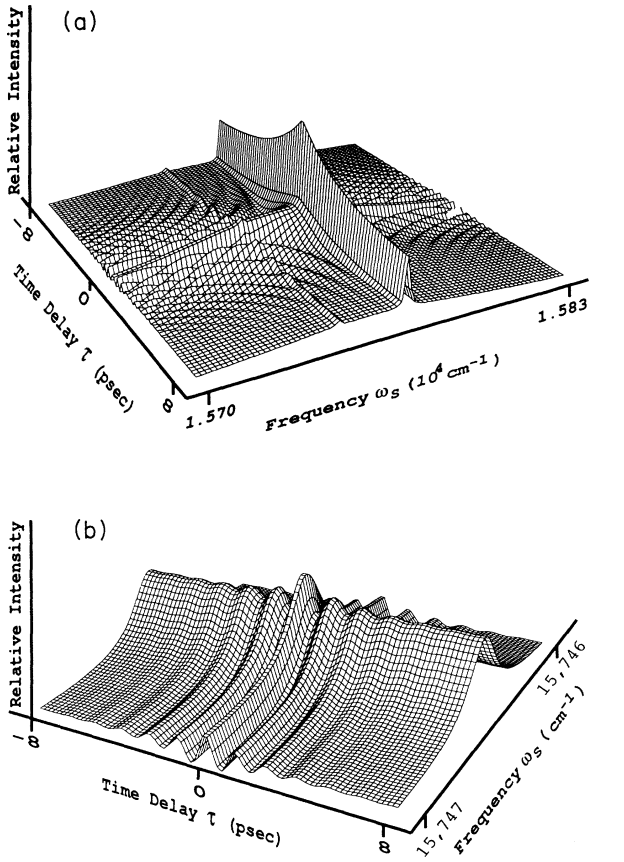

FIG. 7. Electronically nonresonant transient CSRS spectra for exponentially damped pair correlation between the broadband fields 2 and 2' (coherences time is 100 fs and $\bar{\nu}_2 = 16\,750$ cm^{-1}). There is one Raman-active mode. The parameters are $\bar{\nu}_{fg} = 991.0$ cm^{-1}, $\bar{\Gamma}_{fg} = 1.2$ cm^{-1}, $\bar{\nu} = 17\,753$ cm^{-1}, Lorentzian $J_1(\omega_1')$ and $J_D(\omega_S')$ with $\bar{\Gamma}_1 = 0.24$ cm^{-1} and $\bar{\Gamma}_S = 0.15$ cm^{-1} HWHM, respectively. (a) $\Delta\bar{\nu}_S = 15\,700$–$15\,830$ cm^{-1}; (b) $\Delta\bar{\nu}_S = 15\,746$–$15\,747$ cm^{-1}.

The signal structure, seen in Figs. 7(a) and 8(a), is lost whenever Γ_1 and/or $\Gamma_S \approx \Gamma_2$, that is, the bandwidth of the nondegenerate field and/or the signal field is comparable to the spectral width of the twin ω_2, ω_2' fields. For example, if only the bandwidth of the nondegenerate field is increased to $\bar{\delta}_1 = 50$ cm^{-1}, the interferogram in Fig. 8(a) changes to that in Fig. 8(b). Now only a coarse $\bar{\nu}_S$ dependence remains in the spectrum and the interferograms show a rapidly decaying detuning beat (Δ^Q) superimposed upon a spontaneous Raman detuning beat (Δ_S^Q). Both the Δ^Q oscillation and the Δ_S^Q oscillation are rapidly

attenuated due to their dependence on δ_1 and δ_2, respectively. These oscillatory transients give way to a purely-material-dependent decay at twice the dephasing rate constant of the driven vibration [Eq. (3.42) for the $\alpha=\beta$ component term] which is weak compared to the signal at $\tau=0$. For Lorentzian spectral densities with the same HWHM as the Gaussian spectral densities used in Fig. 8(b), except now $\Gamma_S=5.0\ \text{cm}^{-1}$, the plot in Fig. 8(c) is obtained revealing the same characteristic signal transients seen in previous experimental and theoretical work,[42] where a coherent peak gives way to a much attenuated and featureless transient that reflects vibrational dephasing.

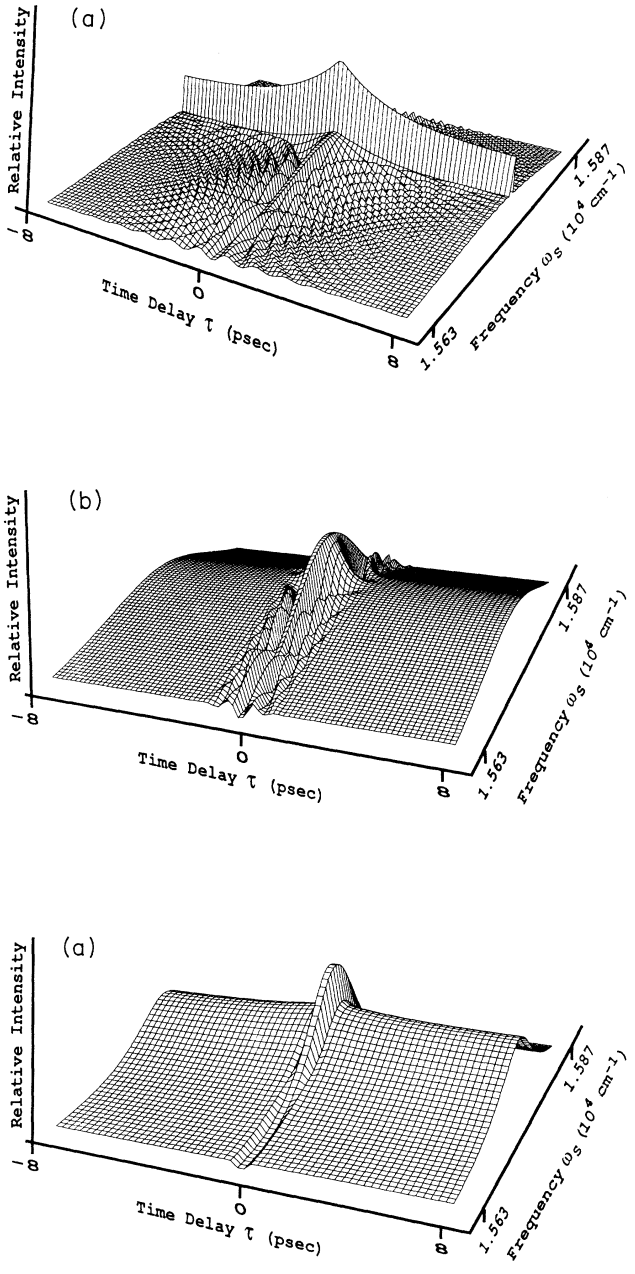

FIG. 8. Electronically nonresonant transient CSRS spectra for (a) and (b) Gaussian pair correlation and (c) exponential pair correlation. One Raman-active mode is assumed at a frequency of 991.0 cm^{-1} and $\bar{\Gamma}_{fg}=1.2\ \text{cm}^{-1}$. The field parameters are $\bar{\nu}_2=16\,750\ \text{cm}^{-1}$, $\bar{\delta}_2=53\ \text{cm}^{-1}$; $\bar{\nu}_1=17\,753\ \text{cm}^{-1}$. (a) $\bar{\delta}_1=0.24\ \text{cm}^{-1}$, $\bar{\delta}_S=0.15\ \text{cm}^{-1}$; (b) $\bar{\delta}_1=50\ \text{cm}^{-1}$, (c) $\Gamma_1=50\ \text{cm}^{-1}$, $\Gamma_S=50\ \text{cm}^{-1}$, $\Gamma_S=5.0\ \text{cm}^{-1}$. In each case $\Delta\bar{\nu}_S=15\,630$–$15\,870\ \text{cm}^{-1}$.

The dependence of both the interferograms and the spectra on the bandwidth of the nondegenerate field is demonstrated in Fig. 9 for a two-component two-level system (or alternatively for a one-component trilevel system). The two Bohr frequencies (dephasing times) are 991 cm^{-1} (4.60 ps) and 970 cm^{-1} (5.30 ps). The two broadband twin fields are at $\bar{\nu}_2=\bar{\nu}_{2'}=16\,750\ \text{cm}^{-1}$ with $\bar{\delta}_2=51\ \text{cm}^{-1}$. Spectral filtering of the generated signal field is performed at a resolution of $\bar{\delta}_S=0.15\ \text{cm}^{-1}$ HWHM (centered at $\bar{\nu}_S=15\,805\ \text{cm}^{-1}$ for the τ scans). The nondegenerate field is set $\bar{\nu}_1=17\,720\ \text{cm}^{-1}$ with $\bar{\delta}_1=0.24\ \text{cm}^{-1}$ [Figs. 9(a) and 9(c)] or 48 cm^{-1} [Figs. 9(b) and 9(d)].

For $\bar{\delta}_1=0.24\ \text{cm}^{-1}$, the interferogram [from Eq. (3.41)] is given in Fig. 9(a). The ω_S spectrum at $\tau=0$ is given in Fig. 9(c). The interferograms reveal a superposition of two detuning beats, one at a period of 510 fs and the other at 1.43 ps, each damped by twice the dephasing rate constant (slightly modified by the nonzero δ_1 and δ_S) of the appropriate detuning Raman mode. In the spectrum [Fig. 9(c)], the three narrow features at frequencies $\bar{\nu}_S=15\,751$, 15 772, and 15 793 cm^{-1} are the resonances at $\Delta^Q=0$, $\Delta^{QQ'}=0$, and $\Delta^{Q'}=0$, respectively (where Q refers to the 991-cm^{-1} mode and Q' to the 970-cm^{-1} mode). While the widths of the $\Delta^Q=0$ and $\Delta^{Q'}=0$ peaks are rigorously independent of the homogeneous Raman linewidths (in the fast-modulation limit of the material Bohr frequencies), the width of the mixed resonance at $\Delta^{QQ'}=0$ (at $\bar{\nu}_S=15\,772\ \text{cm}^{-1}$) depends on the difference in the homogeneous linewidths of the two separate Raman modes. Such bichromophoric resonant features, generated from a field-induced mixing of chemically and spatially distinct material states, may show oscillatory behavior in the spectral domain arising from the phase term in Eq. (3.44). The frequency of this oscillation depends on the difference between the two homogeneous linewidths modified by functions of the bandwidth of the driving fields.

Upon increasing the bandwidth of the nondegenerate field to $\bar{\delta}_1=48\ \text{cm}^{-1}$ ($\Gamma_1\gg\Gamma_{fg}$) the interferogram in Fig. 9(b) is obtained. The detuning oscillations attenuate with τ at a faster rate, giving way to a much weaker, yet longer-lived, Bohr frequency difference beat. This latter, purely-material-related difference beat actually increases with increasing δ_1, though remains weak compared to the coherent peak. At $\bar{\delta}_1=48\ \text{cm}^{-1}$, the CSRS spectrum [Fig. 9(d)] is broad and featureless.

B. Interpretation

The physical origin of the beats in the fourth-wave interferograms and of the sharp bichromophore features in the spectra can be interpreted in terms of the interference

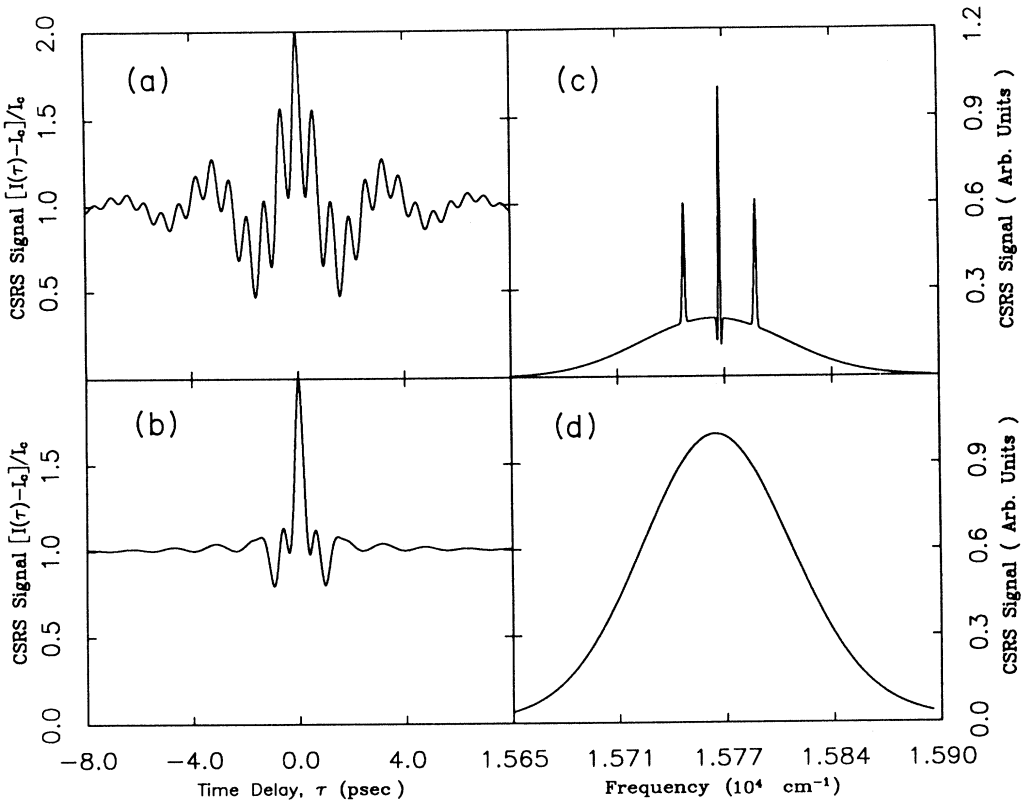

FIG. 9. CSRS (a) and (b) interferograms and (c) and (d) spectra for a two-component system with mode frequencies (dephasing times) of 991.0 cm^{-1} (4.6 ps) and 970.0 cm^{-1} (5.3 ps). Gaussian spectral densities are used for all fields. For $J_2(\omega_2')$, $\bar{\nu}_2=16\,750$ cm^{-1} and $\bar{\delta}_2=51$ cm^{-1}; $J_D(\omega_S')$, $\bar{\delta}_S=0.15$ cm^{-1} and $\bar{\nu}_S=15\,805$ cm^{-1} (for the τ scans); $J_1(\omega_1')$, $\bar{\nu}_1=17\,733$ cm^{-1} and $\bar{\delta}_1$ equals the following: (a) 0.24, (b) 48, (c) 0.24, and (d) 48 cm^{-1}.

between radiation and matter oscillators that are created by mutually coherent fields driving material superposition states that are located on spatially distinct chromophores. The interference of correlated fields in vacuum has its classical interpretation in terms of a superposition of phase-coherent waves. It can be viewed quantum mechanically as a field quantum exchange between the correlated radiation modes. Analogously, the interfering radiation-matter oscillators of our problem involve radiation-matter amplitude level quantum exchange.

Correlation among our radiation-matter oscillators is derived entirely from coherence among the interacting light waves, since the chromophores themselves are otherwise uncoupled. The spectroscopy of a conventional coupled chromophore problem leads to an "exciplex" description. Here, by analogy, we shall refer to radiation-bichromophoric "exciplexes." In fact, we find that a properly defined combination of these radiation-matter exciplexes, expressed in operator form, leads to each of the signal beats that are found analytically in Sec. III.

Though in the present problem full correlation is at sixth order in the incident fields, we have seen how such high-order interferences reduce to pairwise intensity level interferences (first-order coherences) as long as the central limit approximation [Eq. (2.1)] is used for the phase noise of incoherent fields, or coherent fields are used that retain full nth order coherence [$\gamma^{(n,n)}=1$, Eq. (2.21)]. Thus by way of demonstrating quantum exchange we first recall, briefly, the quantum description of the interference in a vacuum between two correlated fields as might be observed interferometrically.

To anticipate the use of such operator formalism in our 4WM application, the following field operator is defined by superposing fields 2 and 2′:

$$\hat{E}_I=(\hat{E}_2+\hat{E}_{2'})=\tfrac{1}{2}[(\hat{E}_{2'}^{+}+\hat{E}_{2}^{-})+(\hat{E}_{2}^{+}+\hat{E}_{2'}^{-})]\ . \tag{4.1}$$

Now let fields 2 and 2′ have unit magnitude ($E_\lambda^0=1$), carry noise, and 2′ be relatively delayed by τ from 2. We now write, as before $\hat{E}_\lambda^{+}(t)=\mathcal{E}_\lambda^{+}(t)\hat{a}_\lambda$ and $\hat{E}_\lambda^{-}(t)=\mathcal{E}_\lambda^{-}(t)\hat{a}_\lambda^{\dagger}$ [where $\mathcal{E}_\lambda^{\pm}(t)$ is the stochastic field function for field λ].

The superposition field can be represented by a density operator of the coupled 2 and 2′ modes, which for realistic fields should represent a statistical mixture of such states. However, to simplify the development we consider an amplitude stabilized field represented by the pure

state density operator of the superposition field given as

$$\begin{aligned}\hat{\rho}_I &= |n_I\rangle\langle n_I| \\ &= |\{n_2,n_{2'}\}\rangle\langle\{n_{2'},n_2\}| \\ &= \frac{1}{2^{n_I}(n_I!)}\sum_{n_2,n_{2'}}{}' \sqrt{n_2!}\sqrt{n_{2'}!}|n_2\rangle|n_{2'}\rangle \\ &\quad\otimes \sum_{m_2,m_{2'}}{}' \langle m_{2'}|\langle m_2|\sqrt{m_2!}\sqrt{m_{2'}!}\,.\end{aligned} \tag{4.2}$$

The prime on the sums denotes the constraint that the total mode quantum number $n_I=n_2+n_{2'}$ ($n_I=m_2+m_{2'}$), is conserved for each product state in the sum. Throughout what follows the state vectors for field 2 ($\{|n_2\rangle\}$ or $\{\langle n_2|\}$) are taken at time t. Those for field 2' ($\{|n_{2'}\rangle\}$ or $\{\langle n_{2'}|\}$) are taken at time $t+\tau$.

The intensity operator $\hat{I}(\tau)$ of the superposition field is usually given in terms of the measurement process, where for photoelectric detection, a normal ordering of field operators is used. Here, however, we want to consider the possible first-order coherence that gives rise to the signal in nonlinear 4WM when four of the six input fields are coupled. To this end, the intensity operator is written simply as the square of the field operator in Eq. (4.1). The intensity of the superposition field is then given as

$$\begin{aligned}\langle\hat{I}(\tau)\rangle &= \mathrm{Tr}[(\hat{E}_I)^2\hat{\rho}_I] \\ &= \frac{n_I}{2}[f_{2,2}^{-,+}(0)+f_{2',2'}^{-,+}(0)]+\frac{n_I+1}{2}[f_{2,2}^{+,-}(0)+f_{2',2'}^{+,-}(0)] \\ &\quad+\left[\frac{n_I}{2}f_{2',2}^{-,+}(|\tau|)+\frac{n_I+1}{2}f_{2,2'}^{+,-}(|\tau|)\right]\sum_{n_2,n_{2'}}{}'\langle n_2-1|\langle n_{2'}+1|n_I\rangle\langle n_I|n_{2'}\rangle|n_2\rangle \\ &\quad+\left[\frac{n_I}{2}f_{2,2'}^{-,+}(|\tau|)+\frac{n_I+1}{2}f_{2',2}^{+,-}(|\tau|)\right]\sum_{n_2,n_{2'}}{}'\langle n_2+1|\langle n_{2'}-1|n_I\rangle\langle n_I|n_{2'}\rangle|n_2\rangle\,.\end{aligned} \tag{4.3}$$

where the functions $f_{2',2}^{\pm,\mp}(|\tau|)$ are just the previously introduced $\bar{\epsilon}_{2'}^{\pm},\bar{\epsilon}_{2}^{\mp}$ pair correlators defined in terms of a classical average over field fluctuations [see Eq. (2.1)]. The first four terms on the rhs of Eq. (4.3) are diagonal in the $\lambda=2,2'$ basis and represent the average occupation number of the λ mode in the superposition field. Interference between the two correlated field modes, or quantum exchange between them, is represented by the off-diagonal matrix elements of $\hat{\rho}_I$ in Eq. (4.3) in the $\lambda=2,2'$ basis. In this picture, the coupling strength is defined in terms of the temporal pair correlation function $f_{2',2}^{\pm,\mp}(|\tau|)$. Thus the coupling is maximized at $\tau=0$ when the two fields are identically overlapped in time, as is always the case for the self-correlators $f_{2,2}^{\pm,\pm}(0)$ and $f_{2',2'}^{\pm,\pm}(0)$. On the other hand, for τ such that $f_{2',2}^{\pm,\mp}(|\tau|)\approx 0$, the radiation modes $\lambda=2,2'$ are no longer coupled and the interference has vanished. This interference coupling, inherent among correlated fields, is just the means for establishing a coupling between distinct chromophores that are excited by such radiation fields. Quantum exchange between radiation-chromophore oscillators can then occur.

For application to our nonlinear radiation-matter problem it is useful to rewrite Eq. (4.3) in terms of radiation exciplex operators. Thus the interferogram [Eq. (4.3)] can be expressed as a beating between off-diagonal states of the coupled 2 and 2' radiation modes. By introducing the identity operator $\hat{\mathbb{1}}=\sum_{n_I}|n_I\rangle\langle n_I|$ we can write

$$\langle\hat{I}(\tau)\rangle=\mathrm{Tr}\left[\sum_{n_I'}[\hat{\rho}^{+}(n_I',\tau)+\hat{\rho}^{-}(n_I',\tau)]\times[\hat{\rho}^{+}(n_I,\tau)+\hat{\rho}^{-}(n_I,\tau)]\right] \tag{4.4}$$

in which the operators $\hat{\rho}^{\pm}(n_I,\tau)$ represent the following linear combinations of states connected through quantum exchange. They are written as

$$\hat{\rho}^{+}(n_I,\tau)=[\bar{\epsilon}_2^{+}(t)|\{n_2-1,n_{2'}\}\rangle+\bar{\epsilon}_{2'}^{-}(t+\tau)|\{n_2,n_{2'}+1\}\rangle]\langle\{n_{2'},n_2\}| \tag{4.5}$$

and

$$\hat{\rho}^{-}(n_I,\tau)=[\bar{\epsilon}_2^{-}(t)|\{n_2+1,n_{2'}\}\rangle+\bar{\epsilon}_{2'}^{+}(t+\tau)|\{n_2,n_{2'}-1\}\rangle]\langle\{n_{2'},n_2\}|\,. \tag{4.6}$$

These operators project exciplexlike (τ-dependent) pure radiation states from an original ket $|\{n_{2'},n_2\}\rangle$. Thus $\hat{\rho}^{+}(n_I,\tau)$ creates the exciplex superposition between a radiation state where field 2 is diminished by one quantum and a second radiation state in which field 2' is raised by one quantum. [$\rho^{-}(n_I,\tau)$ projects the complementary exciplex superposition.]

In the presence of a resonant nonlinear medium, the in-

terference (or coupling) is mediated via field-correlated radiation-matter superposition states. In the bichromophore model for 4WM two otherwise uncoupled material modes, vibrational or vibronic, one each on two separate chromophores, will couple if driven by interfering fields. It is necessary that the two chromophores lie within the coherence volume V of the fields [defined by $\Phi(r_{\alpha,\beta})$ of, e.g., Eq. (1.30)]. The interchromophore coupling is generated by the radiation-matter operators $\hat{V}_2^-(t)\hat{V}_{2'}^+(s-\tau)$ and $\hat{V}_{2'}^-(t-\tau)\hat{V}_2^+(s)$ (in general, their commutators $[\hat{V}_2^-(t),[\hat{V}_{2'}^+(s-\tau),\cdot]]$ and $[\hat{V}_{2'}^-(t-\hat{\tau}),[\hat{V}_2^+(s),\cdot]]$) which bring about interchromophore coupling through their field dependence. In this picture, the coupling (or interference) between different single-chromophore-based coherences allows one to write a basis representation in terms of a linear combination of their projection operators. The particular linear combination of these single-chromophore radiation-matter coherences is dictated by the nature of the field-induced correlation in the scattering process. For electronically nonresonant CSRS there are four elementary radiation-chromophore (quadrupole) oscillators from which exciplexes are created by field correlation. These four oscillators correspond to the two kinds of two-field polarizations that appear on chromophore α and on chromophore β. One kind is the stimulated Raman polarization. On α, say, it is generated by $\hat{p}_{\rm st}(\alpha)=\hat{V}_1^+(t),\hat{V}_2^-(t)$, or by $\hat{p}_{\rm st}(\alpha,\tau)=\hat{V}_1^+(t)\hat{V}_{2'}^-(t-\tau)$. The second kind is the spontaneous Raman polarization. On β, say, it is generated by $\hat{p}_{\rm sp}^{\dagger}(\beta)=\hat{V}_2^+(s)\hat{V}_S^-(s)$, or by $\hat{p}_{\rm sp}^{\dagger}(\beta,\tau)=\hat{V}_{2'}^+(s-\tau)\hat{V}_S^-(s)$. Such stimulated Raman polarizations oscillate with the detuning frequencies Δ_1^α and Δ_1^β, and the two spontaneous Raman oscillators oscillate with their detuning frequencies Δ_S^α and Δ_S^β. These four elementary radiation-chromophore oscillators can be projected from the initial radiation-two-chromophore state $|g\rangle$ with their corresponding operators $(\hat{p}_{\rm st}(Q)$, $\hat{p}_{\rm sp}^{\dagger}(Q)$, $\hat{p}_{\rm st}(Q,\tau)$, and $\hat{p}_{\rm sp}{}^{\dagger}(Q,\tau)$ for $Q=\alpha,\beta)$. (To account for all scattering channels these operators should be considered in their tetradic form.) In their place we consider the corresponding four off-diagonal projectors. Written explicitly in terms of the time-dependent state vectors of the four fields (2′ shifted by τ) and the two chromophores Q and Q', these are

$$\begin{aligned}|\hat{p}_{\rm st}(Q)\rangle\langle g|=&\bar{\mathcal{E}}_1^+(t)|n_1-1\rangle\langle n_1|\\&\otimes\bar{\mathcal{E}}_2^-(t)|\{n_2+1,n_{2'}\}\rangle\langle\{n_{2'},n_2\}|\\&\otimes|0_S\rangle\langle 0_S|\otimes|f_Q\rangle\langle g_Q|\otimes|g_{Q'}\rangle\langle g_{Q'}|\ ,\end{aligned}\tag{4.7}$$

$$\begin{aligned}|\hat{p}_{\rm sp}^{\dagger}(Q)\rangle\langle g|=&|n_1\rangle\langle n_1|\\&\otimes\bar{\mathcal{E}}_2^+(t)|\{n_2-1,n_{2'}\}\rangle\langle\{n_{2'},n_2\}|\\&\otimes\bar{\mathcal{E}}_S^-(t)|1_S\rangle\langle 0_S|\\&\otimes|f_Q\rangle\langle g_Q|\otimes|g_{Q'}\rangle\langle g_{Q'}|\ ,\end{aligned}\tag{4.8}$$

$$\begin{aligned}|\hat{p}_{\rm st}(Q,\tau)\rangle\langle g|=&\bar{\mathcal{E}}_1^+(t)|n_1-1\rangle\langle n_1|\\&\otimes\bar{\mathcal{E}}_{2'}^-(t+\tau)|\{n_2,n_{2'}+1\}\rangle\langle\{n_{2'},n_2\}|\\&\otimes|0_S\rangle\langle 0_S|\otimes|f_Q\rangle\langle g_Q|\otimes|g_{Q'}\rangle\langle g_{Q'}|\ ,\end{aligned}\tag{4.9}$$

$$\begin{aligned}|\hat{p}_{\rm sp}^{\dagger}(Q,\tau)\rangle\langle g|=&|n_1\rangle\langle n_1|\\&\otimes\bar{\mathcal{E}}_{2'}^+(t+\tau)|\{n_2,n_{2'}-1\}\rangle\langle\{n_{2'},n_2\}|\\&\times\otimes\bar{\mathcal{E}}_S^-(t)|1_S\rangle\langle 0_S|\\&\otimes|f_Q\rangle\langle g_Q|\otimes|g_{Q'}\rangle\langle g_{Q'}|\ ,\end{aligned}\tag{4.10}$$

in which $Q\neq Q'$. Explicit mention of τ tells that field 2′, not 2, is involved in preparing a given oscillator. We next prepare the exciplex states that superpose these elementary oscillators, through 2,2′ correlation, thus exposing the τ dependence. The exciplexes built of 2,2 or 2′,2′ correlation show no τ dependence and are not considered here. Similar to the example of first-order coherence previously discussed, quadrature phase field operators for the 2 and 2′ modes, analogous to that given in Eq. (3.1), can be defined which project these radiation–two-chromophore exciplex superposition states.

There are two kinds of radiation-matter exciplexes based on the two types of field induced correlation. In one, exciplexes are built of like elementary oscillators [either both spontaneous Raman polarization or stimulated Raman polarization; Fig. 5(b)]. These are projected by the operators of the form $\hat{p}_{\rm st}(Q)\cdot+\cdot\hat{p}_{\rm st}{}^{\dagger}(Q',\tau)$ and $\hat{p}_{\rm sp}{}^{\dagger}(Q,\tau)\cdot+\cdot\hat{p}_{\rm sp}(Q')$ (and their adjoint operators). In a second kind, exciplexes are built of unlike oscillators [mixed stimulated Raman polarization, spontaneous Raman polarization; Fig. 5(a)]. These are projected by $\hat{p}_{\rm st}(Q)\cdot+\hat{p}_{\rm sp}{}^{\dagger}(Q',\tau)\cdot$ and $\hat{p}_{\rm st}(Q,\tau)\cdot+\hat{p}_{\rm sp}{}^{\dagger}(Q')\cdot$. For the unlike projectors we have

$$\hat{\Psi}_1^u(\tau_{Q'})=|\hat{p}_{\rm st}(Q)\rangle\langle g|+|\hat{p}_{\rm sp}^{\dagger}(Q';\tau)\rangle\langle g|\ ,\tag{4.11}$$

and

$$\hat{\Psi}_2^u(\tau_Q)=|\hat{p}_{\rm st}(Q;\tau)\rangle\langle g|+|\hat{p}_{\rm sp}^{\dagger}(Q')\rangle\langle g|\ ,\tag{4.12}$$

and for the like projectors

$$\hat{\Psi}_1^l(\tau_{Q'})=|\hat{p}_{\rm st}^{\dagger}(Q)\rangle\langle g|+|g\rangle\langle\hat{p}_{\rm st}^{\dagger}(Q';\tau)|\tag{4.13}$$

and

$$\hat{\Psi}_2^l(\tau_Q)=|\hat{p}_{\rm sp}^{\dagger}(Q;\tau)\rangle\langle g|+|g\rangle\langle\hat{p}_{\rm sp}(Q')|\ .\tag{4.14}$$

The state vector space of fields 2 and 2′ appear in the exciplex projector $\hat{\Psi}_1^u$ [Eq. (4.11)] exactly as they do in the quantum exchange (interference) projector $\hat{\rho}^-$ [Eq. (4.6)]; $\hat{\Psi}_2^u$ [Eq. (4.12)] is similarly related to $\hat{\rho}^+$ [Eq. (4.5)]. The projectors $\hat{\Psi}_1^l$ [Eq. (4.13)] and $\hat{\Psi}_2^l$ [Eq. (4.14)] involve mixed ket- and bra-side projection, but similarly involve quantum exchange between the interfering modes 2 and 2′.

That two radiation-bichromophore superposition projectors exist for like and unlike correlation is related to the fact that each broadband field can intervene equally in the stimulated Raman step or in the spontaneous Raman step. Therefore, to fully display correlation Fig. 5 must be supplemented by another in which the roles of the twin broadband fields are interchanged (let $\pm\omega_2 \leftrightarrow \pm\omega_{2'}$).

The operators in Eqs. (4.11)–(4.14) represent intermediate states in the mixing process. For the scattering channel shown in Fig. 5(a), the amplitude level radiation-bichromophore coherence is given by $\hat{\psi}_1^u(\tau_\beta)$ and $\hat{\psi}_2^{u\dagger}(\tau_\alpha)$. These project the superposition state generated by the interference of a stimulated Raman coherence on chromophore $\alpha(\rho_{fg}^\alpha)$ and a spontaneous Raman probing of a ρ_{gf}^β coherence on chromophore β. (They differ only in exchanged roles of 2 and 2′). Simultaneously (at the amplitude level) a stimulated Raman coherence ρ_{gf}^β driven on chromophore β with one of the conjugate fields is coupled to a spontaneous Raman probe of the ρ_{fg}^α coherence on chromophore α. At steady state these two concerted exciplex superpositions give rise to the bichromophore resonance at $\Delta^{\alpha\beta}=0$.

When ρ_{fg}^α and ρ_{gf}^β belong to the same homogeneous ensemble (α and β are chemically identical), their Bohr frequencies are stochastically modulated identically (in the fast-modulation limit). On the other hand, their natural fg polarization is π out of phase. This leads to an exact cancellation of their homogeneous widths. The resulting spectral line is also independent of the spectral density of the broadband fields (that cause the coupling) because the probing of ρ_{gf}^β (ρ_{fg}^α) by field, say 2′, is π out of phase from the action of field 2 in generating ρ_{fg}^α (ρ_{gf}^β).

The radiation-bichromophore exciplex states represented by the operators in Eqs. (4.13) and (4.14) correspond to the coupling channel shown in Fig. 5(b) (the like correlation). This superposition state gives rise to a resonance in the steady state at a frequency given by the difference between the Raman mode frequencies on chromophore α and β, independently of the driving field frequencies. The spectral width of this line is given by the sum of the homogeneous widths of the two Raman modes [Eqs. (3.10) and (3.46)]. (For identical modes this difference beat vanishes.)

In some sense, the narrow bichromophore spectral features (at $\Delta^{\alpha\beta}=0$) are phenomena similar to the extra resonances discussed by Prior *et al.*[77] This phenomenon, termed PIER4 (pressure-induced extra resonance in 4WM), is associated with pure-dephasing-induced relief of a destructive interference between different mixing channels contributing to the susceptibility. Each of these interfering amplitudes leads to the same intermediate off-diagonal state. Such cancellation within the third-order resonance structure is seen, for example, in the excited-state Raman contribution to the CSRS susceptibility. Their amplitudes [represented in Figs. 4(b) and 4(c)] reach the identical off-diagonal state (ρ_{mn}) at second order in the field-matter interaction. The "extra" resonance appears at the zero detuning of Δ_1' only if pure dephasing, induced by coupling of the excitation to the material bath, or to a fluctuating radiation field, contributes to the line broadening of the ρ_{mn} coherence. (A dressing of the chromophore states in a strong radiation field is also seen to remove this cancellation to expose the extra resonance.)

The new two-chromophore resonances examined in this paper show, in theory, behavior similar to such extra resonance phenomena. Here two kinds of exact cancellation are encountered. In one, all reference to the frequencies of the broadband fields 2 and 2′ vanishes identically at the bichromophore exciplex level because of their out-of-phase role on the two chromophores. This is the basis for the interference coupling. In the second, an exact cancellation of homogeneous linewidths (for identical resonances) takes place. However, the latter cancellation comes with zero amplitude when neither the incident nondegenerate field nor the signal field convey dephasing (that is, $\Gamma_1=\Gamma_S=0$). In that limit there is complete destructive interference between the two identical bichromophore exciplexes generated by $\hat{\Psi}_1^u$ and $\hat{\Psi}_2^{u\dagger}$. By introducing pure dephasing via nonzero Γ_1 and/or Γ_S, or by allowing the two coupled chromophores not to belong to the same homogeneous ensemble, the destructive interference is removed to expose these new sub-Raman linewidth resonant features. A sufficient increase of Γ_1 and/or Γ_S will ultimately break up the phase coherence of the stimulated Raman polarization amplitude and the spontaneous Raman polarization amplitude set up on different chromophores. This is the underlying premise for constructing the unlike exciplexes. The narrow resonances are then completely removed and the detuning oscillations are strongly attenuated.

Next we consider the τ dependence in the interferograms as revealed by the exciplex description. Modulations in the interferograms arise from the beating between the different radiation-bichromophore coherences, each undergoing a phase shift of τ. The resulting fourth-wave signal can be constructed from the base exciplex projectors given in Eqs. (4.11)–(4.14).

The signal, involving a quadrature combination of the four fields, can now be constructed by tracing over the proper algebraic combination of four exciplex operators:

$$I^{\alpha\beta}(\tau)=\langle \hat{\hat{\Psi}}_2^u(\tau_\beta)\hat{\hat{\Psi}}_1^{u\dagger}(\tau_\alpha)\hat{\hat{\Psi}}_2^{u\dagger}(\tau_\alpha)\hat{\hat{\Psi}}_1^u(\tau_\beta)+\text{H.a.}\rangle + \langle \hat{\hat{\Psi}}_4^1(\tau_\beta)\hat{\hat{\Psi}}_3^{1\dagger}(\tau_\alpha)\hat{\hat{\Psi}}_4^{1\dagger}(\tau_\alpha)\hat{\hat{\Psi}}_3^1(\tau_\beta)+\text{H.a.}\rangle \ . \tag{4.15}$$

The algebra is contained in the definition of the exciplex operator $\hat{\hat{\Psi}}_j^\dagger=[\hat{\Psi}_j^\dagger,\cdot]$, where $\hat{\Psi}_j^\dagger$ is one of the four exciplex projectors defined above.

The first term on the rhs of Eq. (4.15) involves only unlike exciplex projectors. Its τ dependence can be expressed in the

$$\{|\hat{p}_{\text{st}}(Q)\rangle,|\hat{p}_{\text{st}}(Q,\tau)\rangle,|\hat{p}_{\text{sp}}^\dagger(Q)\rangle,|\hat{p}_{\text{sp}}^\dagger(Q,\tau)\rangle,|g\rangle\}$$

basis as

$$\langle \hat{\hat{\Psi}}_2^{u}(\tau_\beta)\hat{\hat{\Psi}}_1^{u\dagger}(\tau_\alpha)\hat{\hat{\Psi}}_2^{u\dagger}(\tau_\alpha)\hat{\hat{\Psi}}_1^{u}(\tau_\beta)+\text{H.a.}\rangle$$
$$=2\{\langle \hat{p}_{st}^{\dagger}(\alpha;\tau)|\hat{p}_{st}(\alpha)\rangle+\langle \hat{p}_{sp}(\alpha)|\hat{p}_{sp}^{\dagger}(\alpha;\tau)\rangle+\langle \hat{p}_{st}^{\dagger}(\beta;\tau)|\hat{p}_{st}(\beta)\rangle+\langle \hat{p}_{sp}(\beta)|\hat{p}_{sp}^{\dagger}(\beta;\tau)\rangle+\text{c.c.}\}$$
$$+\{\langle \hat{p}_{st}^{\dagger}(\alpha;\tau)|\hat{p}_{st}(\alpha)\rangle\langle \hat{p}_{sp}(\alpha;\tau)|\hat{p}_{sp}^{\dagger}(\alpha)\rangle+\langle \hat{p}_{st}^{\dagger}(\beta)|\hat{p}_{st}(\beta;\tau)\rangle\langle \hat{p}_{sp}(\beta)|\hat{p}_{sp}^{\dagger}(\beta;\tau)\rangle+\text{c.c.}\}$$
$$+\{\langle \hat{p}_{st}^{\dagger}(\alpha;\tau)|\hat{p}_{st}(\alpha)\rangle\langle \hat{p}_{st}^{\dagger}(\beta)|\hat{p}_{st}(\beta;\tau)\rangle+\langle \hat{p}_{sp}(\alpha;\tau)|\hat{p}_{sp}^{\dagger}(\alpha)\rangle\langle \hat{p}_{sp}(\beta)|\hat{p}_{sp}^{\dagger}(\beta;\tau)\rangle+\text{c.c.}\}\ . \tag{4.16}$$

In Eq. (4.15), we note that since the chromophores are uncoupled $\langle \hat{p}_{st}^{\dagger}(Q)|\hat{p}_{st}(Q')\rangle=\langle \hat{p}_{sp}(Q)|\hat{p}_{sp}^{\dagger}(Q')\rangle=\delta_{Q,Q'}$ and $\langle \hat{p}_{st}(Q)|\hat{p}_{sp}^{\dagger}(Q')\rangle=0$ for all Q and Q' if only because of the orthogonality in the space of fields 1 and S. $\langle \hat{p}_{st}^{\dagger}(Q,\tau)|\hat{p}_{st}(Q)\rangle\neq 0$ and $\langle \hat{p}_{sp}(Q,\tau)|\hat{p}_{sp}^{\dagger}(Q)\rangle\neq 0$ due to the correlation between fields 2 and 2′. Detuning oscillations in τ at the frequencies Δ_1^Q (STR) and Δ_S^Q (SPR) are represented by the quantity contained within the first set of curly brackets on the rhs of Eq. (4.16). The analytic results identifying these oscillatory transients are given in Eqs. (3.23)–(3.26) for the spontaneous Raman polarization beat and in Eq. (3.27) for the stimulated Raman polarization beat. The second set of curly of brackets contains terms that represent beating between the stimulated Raman polarization and spontaneous Raman polarization branches on the same chromophore $[\pm\Delta_1^Q\pm\Delta_S^Q=\pm\Delta^Q$, see Eq. (3.20)]. Finally, the terms contained in the third set of curly brackets represent both the beating between the stimulated Raman polarization branch and the conjugate stimulated Raman polarization branch on different chromophores $(\pm\Delta_1^Q\mp\Delta_1^{Q'}=\pm\Delta_{fg-fg}^{QQ'})$, as well as the beating between the spontaneous Raman polarization and its self-conjugate branches $(\pm\Delta_S^Q\mp\Delta_S^{Q'}=\pm\Delta_{fg-fg}^{QQ'})$. Such Bohr frequency difference beats are represented analytically in Eqs. (3.28)–(3.40). The second signal component on the rhs of Eq. (4.15) involves only projection of like exciplexes. This term reproduces only the detuning oscillations contained in the first two sets of curly brackets on the rhs of Eq. (4.16). It does not exhibit Bohr frequency difference beats, in agreement with the analytic results (Sec. III B) where Bohr frequency difference beats [Eqs. (3.19) and (3.41)] occur only when the fields correlate spontaneous Raman polarization on one chromophore with stimulated Raman polarization on the other (that is, when unlike exciplexes are generated).

For electronically resonant mixing, new radiation-matter oscillators appear in addition to the four ground-state Raman oscillators set fourth in Eqs. (4.7)–(4.10). Oscillators involving excited-electronic-state Raman modes can be prepared, and others involving purely vibronic modes can be made as well. One therefore anticipates a variety of radiation-bichromophoric exciplexes generated by the 2,2′ field correlation. These may consist of a pair of Raman oscillators of the electronic ground state (as above), two Raman oscillators in the excited electronic state, or mixed excited-state–ground state Raman exciplexes as well as vibronic-Raman exciplexes. For example, the AB^*+BA^* scattering channel (Fig. 4) produces the two-chromophore exciplexes involving an excited-electronic-state mode, say on chromophore Q, and a ground-state mode on chromophore Q'. The excited-state two-field stimulated Raman polarization and spontaneous Raman polarization off-diagonal projectors corresponding, respectively, to the operator action of $\hat{V}_1^{+}\hat{V}_2^{-}$ and $\hat{V}_{2'}^{-}\hat{V}_S^{+}$ on chromophore Q, and can be written as

$$\hat{\Xi}_1^{u}(\tau_{Q'})=|\hat{V}_1^{+}(Q)\rangle\langle g|\cdot|g\rangle\langle \hat{V}_2^{-}(Q)|+|\hat{p}_{sp}^{\dagger}(Q';\tau)\rangle\langle g| \tag{4.17}$$

and

$$\hat{\Xi}_2^{u}(\tau_Q)=|g\rangle\langle \hat{p}_{st}^{\dagger}(Q')|+|\hat{V}_2^{-}(Q)\rangle\langle g|\cdot|g\rangle\langle \hat{V}_S^{+}(Q)|\ . \tag{4.18}$$

These are mixed Raman oscillator exciplexes. An excited- (ground-) electronic-state stimulated Raman polarization step on chromophore Q (Q') is coupled to a ground- (excited-) electronic-state spontaneous Raman polarization step on chromophore Q' (Q). In Eqs. (4.17) and (4.18), the excited-electronic-state stimulated Raman polarization operator is given by

$$|\hat{V}_1^{+}(Q)\rangle\langle g|\cdot|g\rangle\langle \hat{V}_2^{-}(Q)|$$
$$=(\tilde{\epsilon}_1^{+}(t)|n_1-1\rangle\langle n_1|\otimes|\{n_2,n_{2'}\}\rangle\langle\{n_{2'},n_2\}|\otimes|0_S\rangle\langle 0_S|\otimes|m_Q\rangle\langle g_Q|$$
$$\otimes|g_{Q'}\rangle\langle g_{Q'}|)\cdot(|n_1\rangle\langle n_1|\otimes|\{n_2,n_{2'}\}\rangle\langle\{n_{2'},n_2-1\}|\tilde{\epsilon}_2^{-}(t)\otimes|0_S\rangle\langle 0_S|\otimes|g_Q\rangle\langle n_Q|\otimes|g_{Q'}\rangle\langle g_{Q'}|) \tag{4.19}$$

and the corresponding excited-electronic-state spontaneous Raman polarization operator can be written as

$$|\hat{V}_2^{-}(Q;\tau)\rangle\langle g|\cdot|g\rangle\langle \hat{V}_S^{+}(Q)|$$
$$=(|n_1\rangle\langle n_1|\otimes\tilde{\epsilon}_{2'}^{-}(t+\tau)|\{n_2,n_{2'}+1\}\rangle\langle\{n_{2'},n_2\}|\otimes|0_S\rangle\langle 0_S|\otimes|f_Q\rangle\langle m_Q|$$
$$\otimes|g_{Q'}\rangle\langle g_{Q'}|)\cdot(|n_1\rangle\langle n_1|\otimes|\{n_2,n_{2'}\}\rangle\langle\{n_{2'},n_2\}|\otimes|0_S\rangle\langle 1_S|\tilde{\epsilon}_S^{+}(t)\otimes|n_Q\rangle\langle f_Q|\otimes|g_{Q'}\rangle\langle g_{Q'}|)\ . \tag{4.20}$$

The radiation-bichromophore exciplex represented in Eqs. (4.17) and (4.18) form a resonances at steady state with a detuning $\omega^{\alpha}_{mn}+\omega^{\beta}_{fg}+\omega_S-\omega_1$ and a width $\Gamma^{\alpha}_{mn}-\Gamma^{\beta}_{fg}+\Gamma_S+\Gamma_1$. Similarly, correlation between like processes (both being a stimulated Raman polarization or a spontaneous Raman polarization step, one in the electronic excited state) will give rise to the field-independent resonance with a frequency $\omega^{\alpha}_{mn}-\omega^{\beta}_{fg}$ and width $\Gamma^{\alpha}_{mn}+\Gamma^{\beta}_{fg}$.

The hybrid vibronic-Raman exciplexes appear when two base oscillators are coupled (one on each chromophore) which appear at different orders in the fully resonant polarization. Thus consider a vibronic coherence on α (ρ^{α}_{ng}) [Fig. 4(c)] oscillating at $\omega^{\alpha}_{ng}-\omega_2$ (if appearing at first order) or at $-\omega^{\alpha}_{ng}-\omega_2+\omega_S+\omega_1$ (if at fourth order), that is coupled to a Raman oscillator on β (ρ^{β}_{fg}, oscillating at Δ^{β}_1 or at $-\Delta^{\beta}_S$). Such exciplexes appear in the AC^*+CA^* channel (Fig. 4). They offer hybrid detuning resonant structure in steady state at $\omega^{\alpha}_{ng}-\omega^{\beta}_{fg}-\omega_S=0$ and $\omega^{\alpha}_{ng}+\omega^{\beta}_{fg}-\omega_1=0$, having corresponding linewidths $\Gamma^{\alpha}_{ng}-\Gamma^{\beta}_{fg}-\Gamma_S$ and $\Gamma^{\alpha}_{ng}+\Gamma^{\beta}_{fg}+\Gamma_1$.

Constructing the signal with the commutator algebra used in Eqs. (4.15) and (4.16), but now with the different electronically resonant exciplex operators, results in the various oscillatory transients listed in Tables I–III and obtained analytically through the theory in Sec. III.

Speaking more generally, a Rabi detuning oscillation, associated with one of four mutually coherent broadband fields and generated at any point in the evolution of the fourth-order scattering amplitudes, can couple to another Rabi detuning oscillator (possibly at a different order in the field interventions) containing one of the two remaining twin conjugate fields. In some sense, these two Rabi oscillators, associated with separate chromophores, become phase locked due to the cancellation (or destructive interference) of the broadband fields. Under the assumption of central limit statistics for the field fluctuations, each one of these phase-locked two-chromophore superposition states can be associated with a pair correlator given in Eq. (3.5). Two such bichromophore coherences contribute to each signal component due to the quadrature level fourth-order correlation of the broadband fields 2 and 2′, and therefore possess both a τ-dependent and a τ-independent phase. The latter bichromophore coherences arise from the self-correlators $f^{\pm,\mp}_{2,2}(t)$ and $f^{\pm,\mp}_{2',2'}(t)$ and as a result, have a τ dependence based on the intensity correlation of the fields. Thus these steady-state resonances are observed in the signal spectrum for all τ delays less than the pulse width.

When vibronic levels are brought into near resonance with the field fundamentals, steady-state vibronic coherences, ρ^{Q}_{mg} oscillating at $-\Delta^{Q}_{mg-1}$ and ρ^{Q}_{fn} oscillating at Δ^{Q}_{nf-S}, can become phase locked with Raman oscillators generated at second-order stimulated Raman polarization and fourth-order (spontaneous Raman polarization) on chromophore Q'. This phase locking is now mediated through interference with fields 1 and S. As a result, the various damped detuning beats and material bilevel and trilevel quantum beats listed in Tables I–III can be generated.

The sub-pulse-width signal transients induced in CSRS and CARS are sensitive to any process that may disrupt the phase coherence between the interfering material-radiation superpositions. This decoupling can occur upon introducing independent field statistics into the nonlinear mixing by increasing the bandwidth of J_1 (ω'_1) or of J_D (ω'_S), or by introducing inhomogeneous material broadening. Thus a static distribution of Bohr frequencies quenches the material-dependent transients, leaving only the purely-light-damped (coherent peak) signal components (see Appendix C).

CONCLUSIONS

The theoretical basis for new signals observed in three-color 4WM interferometry and spectroscopy is derived from a more general treatment of 4WM scattering with correlated fields. In the particular application, two of the incident fields are broadband twin fields of one color, interferometrically separated by τ, and each assigned its own **k** vector. The third incident field, having its own **k** vector and a second color, joins the twin fields in a nonlinear sample. A signal field of a third color is produced, having its **k** vector constrained by phase matching. The spectral width of the nondegenerate incident field is taken as an experimental parameter, as is that of the signal field. Analytic expressions are obtained for the signal intensity as a function of τ and the viewing frequency ω_S. Fundamental to the generation of these responses is the introduction of material correlation through the action of mutually coherent fields in the time development of the scattering amplitudes on separate chromophores. As a result, two-chromophore coherences arise from the phase locking of the Rabi detuning oscillations of the radiation-matter superposition states on each of the individual chromophores. Such two-oscillator or exciplexlike coherences give rise to new resonant features at steady state. It is shown that for a homogeneous ensemble of chromophores certain of these resonances possess a width that depends only on the bandwidths of the nondegenerate field and the signal field in the fast modulation limit of the matter-bath stochastic processes.

The different oscillating transients seen in the interferograms, such as radiation-matter detuning beats and matter-matter quantum beats, as well as the zero-frequency terms, decay at a rate given by one, or a combination of, the material and/or the radiation linewidths. It is shown how the relative strength of various signal components is sensitive to the dephasing that is introduced by going to a nonzero bandwidth of the nondegenerate field or the detector field (or both). When the spectral width of both the signal filter and nondegenerate field is made submaterial linewidth, the fourth-wave signal is dominated by new Rabi detuning oscillations Δ^{Q}, Δ'^{Q}, and Δ''^{Q} involving a ground-electronic-state Raman mode, an excited-electronic-state Raman mode, and a vibronic mode, respectively. These signal transients, though bichromophoric in origin, carry precise mode frequency and dephasing rate information for a given pair of states on a single chromophore. Under such excitation conditions and in the absence of interchromophore coherence transfer, the interference of all nearby super-

posed modes, manifested in the interferograms as material quantum beats, or detuning beats involving Bohr frequencies on separated chromophores, is suppressed.

In comparing long-pulsed incoherent excitation with short-pulse coherent excitation in general 4WM measurements, the issue of the relevant time scales for measuring material response arises. The τ dependence of the interferograms presented in this paper are based on phase-sensitive amplitude correlation of the intervening fields. Since the temporal resolution is limited to the coherence time of the superposition field, both broadband incoherent fields and short-pulsed coherent fields of equal bandwidth will probe the same short-time dynamics. However, measurements using long-pulsed incoherent (nonbandwidth limited) excitation fields are accumulative in nature and result in a real-time averaging of the material response over the long-pulse envelope. Spectral diffusion processes and possibly additional scattering pathways due to slow transfer among material states may influence the line shape in a manner that is absent when short pulses are used. The use of long-pulse incoherent fields also allows a higher permutation symmetry of the driving fields in the mixing, thus enabling correlation among a greater number of scattering channels.

If static inhomogeneity of material Bohr frequencies survives on the time scale of the long pulse, and if it exceeds the homogeneous width, then the new Rabi detuning oscillations are quenched, leaving only the coherent peak of the radiation fields in the 4WM signal.

The analytic results presented in this paper describe signal features in the coherent Raman 4WM spectroscopies which are in excellent agreement with experimental results (paper II). However, consideration must be given to the applicability of such Markovian models (for material dynamics and field noise) in describing ultrafast responses in condensed-phase systems. We hope to explore numerically, how non-Markovian behavior affects the damping of the various new oscillatory transients and the spectral widths of the new resonances seen in these 4WM experiments. With regard to the new spectral features, does the rigorous cancellation of the material homogeneous linewidths, associated with the $\Delta^{Q}=0$, $\Delta'^{Q}=0$, and $\Delta''^{Q}=0$ resonances, occur for general line-broadening mechanisms? We already know that in the Markov limit of homogeneous broadening, were the width of one of these new resonances to exceed that conveyed by the signal filter and the nondegenerate field, one would have a new way to characterize the degree of inhomogeneity.

The absence of any contribution from the twin broadband fields to the spectral width in much of the resonant substructure, as well as to the damping parameter of several signal transients, indicates their ability to destructively interfere. Their constructive interference gives rise to many of the broadband resonances and fast transients. Interference, constructive or destructive, is a measure of the degree of coherence between the driving fields. In need of further theoretical (and experimental) investigation, however, is how the shape of the coherence profile influences the optical mixing process. For example, it was seen how a change in the spectral densities of the fields from Lorentzian to Gaussian removes the narrow resonance at $\Delta_R=0$. Also, the interferometric oscillations at Δ_R vanish. Many of the oscillatory signal features listed in Tables I–III (e.g., the vibrational-vibronic trilevel quantum beats) do not contribute significantly to the signal regardless of the Lorentzian widths Γ_1 and Γ_S. Perhaps different spectral densities and signal filter functions can selectively enhance certain signal components or introduce entirely new transient and spectral features. Phase-amplitude pulse shaping is the logical outcome of such considerations.[36–38] Another approach (not considered here) which has the potential for unlocking new phase-sensitive optical phenomena involves two-color heterodyne detection. In general, three- or four-color 4WM involving correlated and/or uncorrelated input fields will generate a signal field phase coherent with its predecessor fields. Gating of the signal field with one or more of the input fields through, for example, frequency mixing in a nonlinear crystal, will directly probe optical responses originating with the zero-point intervention contained in the general eight-field correlator [Eq. (1.13)]. Such techniques have been utilized in the detection of squeezed light.

Comparative studies of nonlinear optical measurements using broadband incoherent laser fields and coherent short-pulse fields will prove to be complementary in probing condensed-phase dynamics. Use of long-pulse incoherent fields will isolate those signals that are phase sensitive to the driving fields. We have seen how such signals can have contributions that arise from interesting field-mediated interchromophore correlation, which for the coherent Raman spectroscopies excited with incoherent light is the only source for the τ dependence when the input fields are maintained in constant temporal overlap. Therefore these measurements offer the potential for observing new transients due to the interference from different time-ordered scattering channels that cannot function when only ultrashort coherent pulses are used. Furthermore, excitation with ultrashort pulses examines stochastic processes over short accumulation times. Such pulses, when used in coherent Raman spectroscopies, produce phase-sensitive field mediated interchromophore correlation similar to that which occurs in incoherent excitation. But in addition, signal transients appear that are based on a phase-insensitive intensity correlation. Here the chromophore itself mediates between fields which are not cotemporal and otherwise noninterfering. Such material transients do not occur when incoherent light is used whose temporal width greatly exceeds the material relaxation rate constants.

ACKNOWLEDGMENTS

We wish to thank Professor Roger Loring and Dr. Joe Melinger for many valuable discussions relating to this topic. We also thank several members of the A. C. Albrecht research group for critically reading several sections of this manuscript. Our gratitude also goes to the National Science Foundation (Grant No. CHE-8617960) and the Materials Science Center for Cornell University for support of this work.

APPENDIX A

Stochastic interactions between the driven chromophore states (the states of $\hat{H}_M$) and the thermalized excitations of the material bath (the states of $\hat{H}_B$) are represented by the function $F^Q(t)$ [Eq. (1.42) for the qth channel]. Chromophore resonances at the fundamentals, or at the difference frequencies, of the (optical) excitation fields are considered. Possible resonances at sum frequencies are neglected. The random modulation of vibrational Bohr frequencies, resonant at second order of the driving fields, is taken to be statistically independent of the random modulation of the vibronic resonances generated at first and third orders. This amounts to the assumption that vibronic pure dephasing is decoupled from vibrational pure dephasing, regardless of whether the vibrational resonance is in the excited electronic state or in the ground electronic state. For the special situation having nearly degenerate electronic states, a vibronic resonance is possible at second order and the decoupling of its pure dephasing from that of other vibronic resonances is problematical. This special case is not treated here.

The uncoupling of stochastic modulations in the electronic space from that in the vibrational space permits a factoring of $F^Q(t)$ into an electronic (e) and a vibrational (v) part:

$$F^Q(\tau_1,\tau_2,\tau_3)=F_e^Q(\tau_1,\tau_2,\tau_3)F_v^Q(\tau_2)\ , \tag{A1}$$

where

$$F_e^Q(\tau_1,\tau_2,\tau_3)=\left\langle \exp\left[i\int_{\tau_2+\tau_3}^{\tau_1+\tau_2+\tau_3}d\tau\,\delta\omega_{fn}(\tau)\right] \times\exp\left[\pm i\int_0^{\tau_3}d\tau\,\delta m_{ng}(\tau)\right]\right\rangle_{B_Q} \tag{A2}$$

and

$$F_v^Q(\tau_2)=\left\langle \exp\left[i\int_0^{\tau_2}d\tau\,\delta\omega_{mn}(\tau)\right\rangle_{B_Q}\right. . \tag{A3}$$

Here the labels m and n (f and g) refer to vibrational levels of the excited (ground) electronic surface. Following the usual approach, a Gaussian stochastic process with zero mean is assumed. Since the stochastic interactions are adiabatic, this assumption is equivalent to a second-order cumulant truncation of $F^Q(t)$ in terms of the $\delta\omega$'s.

Equation (A3) involves a single exponential average and can be written as

$$F_v^Q(\tau_2)=\exp\left[-\int_0^{\tau_2}d\tau\int_0^{t}d\tau' w_{mn}(\tau,\tau')\right]\ , \tag{A4}$$

where

$$w_{mn}(\tau,\tau')=\langle\delta\omega_{mn}(\tau)\delta\omega_{mn}(\tau')\rangle_{B_Q}\ . \tag{A5}$$

In order to simulate a distribution of dynamical processes, the frequency modulation $\delta\omega_{mn}$ can be written as a sum of statistically independent random variables,

$$\delta\omega_{mn}=\sum_i \delta\omega_{mn}^i\ . \tag{A6}$$

Following the development in Refs. 25–27 and making use of the correlation function in Eq. (2.9), we can write Eq. (A4) as

$$\exp\left[-\int_0^{\tau_2}d\tau\int_0^{\tau}d\tau'\sum_i w_{mn}^i(\tau,\tau')\right] =\prod_i{}^{v}\exp\left[-\frac{\delta_i^2}{\Lambda_i^2}(e^{-\Lambda_i\tau_2}-1+\Lambda_i\tau_2)\right]\ . \tag{A7}$$

The ith independent stochastic process is characterized by its amplitude δ_i and its correlation time Λ_i^{-1}.

Electronic pure dephasing, described by the first factor Eq. (A1), involves two exponential terms [Eq. (A2)]. The two different vibronic Bohr frequency modulations are assumed correlated by virtue of the fact that they belong to the same pair of electronic potential surfaces. Correlation between the random variables $\delta\omega_{fn}^i$ and $\delta\omega_{ng}^i$ will be given in terms of $\delta\omega_e^i$, the modulation of the excited-state electronic surface relative to the ground electronic surface. The electronic pure dephasing function can be written as

$$\begin{aligned}F_e^Q(\tau_1,\tau_2,\tau_3) =&\exp\left[-\int_0^{\tau_1}d\tau\int_0^{\tau}d\tau' w_{fn}(\tau,\tau')\right.\\ &-\int_0^{\tau_3}d\tau\int_0^{\tau}d\tau' w_{ng}(\tau,\tau')\\ &\left.\mp\int_{\tau_2+\tau_3}^{\tau_1+\tau_2+\tau_3}d\tau\int_0^{\tau_3}d\tau' w_e(\tau,\tau')\right]\ .\end{aligned} \tag{A8}$$

Correlation of the stochastically modulated vibronic frequencies across the two different time intervals τ_1 and τ_3 is represented by the third double integral. The effects of such "vertex" terms in various nonlinear mixing processes has been investigated in Ref. 29 under the more general context of arbitrary field strengths. Here this component can be rewritten as

$$\begin{aligned}&\int_{\tau_2+\tau_3}^{\tau_1+\tau_2+\tau_3}d\tau\int_0^{\tau_3}d\tau' w_e(\tau,\tau')\\ &=\left[\int_0^{\tau_1+\tau_2+\tau_3}d\tau+\int_0^{\tau_2}d\tau-\int_0^{\tau_2+\tau_3}d\tau\right.\\ &\quad\left.-\int_0^{\tau_1+\tau_2}d\tau\right]\int_0^{\tau}d\tau' w_e(\tau,\tau')\ .\end{aligned} \tag{A9}$$

Using Eqs. (A5)–(A7) for multiple stochastic processes, but now applied to the electronic problem, Eq. (A8) [with (A9)] becomes

$$F_e^Q(\tau_1,\tau_2,\tau_3)=\prod_i{}^{e}\left\{\exp\left[-\left[\frac{\delta_{fn}^i}{\Lambda_{fn}^i}\right]^2(e^{-\Lambda_{fn}^i\tau_1}-1+\Lambda_{fn}^i\tau_1)\right]\exp\left[-\left[\frac{\delta_{ng}^i}{\Lambda_{ng}^i}\right]^2(e^{-\Lambda_{ng}^i\tau_3}-1+\Lambda_{ng}^i\tau_3)\right] \times\exp\left[\pm\left[\frac{\delta_e^i}{\Lambda_e^i}\right]^2 e^{-\Lambda_e^i\tau_2}(1-e^{-\Lambda_e^j\tau_1})(1-e^{-\Lambda_e^i\tau_3})\right]\right\}\ . \tag{A10}$$

The limiting behavior of any given stochastic process can be explored for both the electronic and the vibrational pure dephasing. Each time interval between field intervention points can be characterized by an accumulation time $\tau_{\rm acc}$. Such an accumulation time is determined by the pulse width [the local intensity functions $e^{+}_{\lambda,\lambda'}(\tau_i)$ in Eq. (2.14)] or the effective ground-state recovery time of some optically pumped channel, should it exceed the interval between successive pulses. Thus the fast-modulation limit for the ith stochastic process is obtained if $(\Lambda^i)^{-1} \ll \tau_{\rm acc}$ over the interval in which it is active. In order for such stochasticity to be manifested in the measured dynamics, the condition $\delta^i/\Lambda^i \ll 1$ must be met. Therefore if we take $(\Lambda^i)^{-1} \ll \tau_{\rm acc}$ and $\delta^i/\Lambda^i \ll 1$ for the ith stochastic process during all time intervals, correlation across the τ_1 and τ_3 time intervals is reduced to unity. The resulting contribution of this stochastic electronic process [Eq. (A10)] to the integrand in Eq. (2.14) can be approximated as

$$\exp\left[-\frac{(\delta^i_{fn})^2}{\Lambda^i_{fn}}\tau_1\right]\exp\left[-\frac{(\delta^i_{ng})^2}{\Lambda^i_{ng}}\tau_3\right]. \tag{A11}$$

In the slow-modulation limit $(\Lambda^i)^{-1} \gg \tau_{\rm acc}$ is assumed, and when $\delta^i/\Lambda^i \gg 1$, the ith stochastic process retains a contribution from the cross frequency correlators. Over most of the integration time in Eq. (2.14), electronic pure dephasing from the ith process can be approximated as

$$\exp\left[-\frac{(\delta^i_{fn}\tau_1)^2}{2}\right]\exp\left[-\frac{(\delta^i_{ng}\tau_3)^2}{2}\right] \times\exp[-(\delta^{i^2}_e)\tau_1\tau_3]\,. \tag{A12}$$

In general, $\tau_{\rm acc}$ need not be the same for the three time intervals, particularly if it is determined by pulse-to-pulse accumulation of material dynamics. For example, if the accumulation time during the τ_2 interval is such that $(\Lambda^i_e)^{-1} \ll \tau_{\rm acc}$ (fast modulation), but for the τ_1 and τ_3 intervals $(\Lambda^i)^{-1} \gg \tau_{\rm acc}$ (slow modulation), then the electronic pure dephasing process loses any contribution from the cross frequency correlators that give rise to the third exponential term in Eq. (12).

Equation (2.15) is obtained from Eq. (A10) if one assumes identical self and cross correlators for the vibronic frequency modulations $[w^i_{fn}(\tau,\tau')=w^i_{ng}(\tau,\tau')=w^i_e(\tau,\tau')]$. This condition is realized in the case of degenerate 4WM where identical vibronic coherences (to within a phase factor) are generated at first and third orders of the field-matter interaction. For two-color 4WM, the assumption leading to Eq. (2.15) suggests that vibronic pure dephasing is determined by the modulation of the excited (adiabatic) electronic surface relative to the ground state. In general, however, correlation between different vibronic frequency modulations must be distinguished, as suggested by Eq. (A10).

APPENDIX B

Certain equations that are only alluded to in the text are given in more detail in this appendix.

The fifth and sixth signal components on the rhs of Eq. (3.19) represent the purely-light-related transients which define the short-time response in the interferograms. The first of these terms, $I^{\alpha\beta}_{\Gamma_{2+2+1+S}}(\tau)$, is the analog of Eq. (3.15) for Lorentzian spectral densities of the nondegenerate field $J_1(\omega'_1)$ and signal field $J_D(\omega'_S)$. The unlike chromophore component $[G(\alpha,\beta)$ in Eq. (3.15)] can be written here as

$$\begin{aligned}
G(\alpha,\beta)=&\frac{e^{-\Gamma_{2+2+1+S}|\tau|}}{[(\Delta_R)^2+(\Gamma_{1+S})^2][(\Delta_R)^2+(\Gamma_{2+2+1+S})^2]}\\
&\times\left[\left[\frac{\mathrm{Re}[B(\Delta,\Gamma)_1]\cos(\Delta_R\tau)+\mathrm{Im}[B(\Delta,\Gamma)_1]\sin(\Delta_R|\tau|)}{[(\Delta^\alpha_S)^2+(\Gamma^\alpha_{fg-2-S})^2][(\Delta^\beta_1)^2+(\Gamma^\beta_{fg-2-1})^2]}\right]\right.\\
&+\left[\frac{\mathrm{Re}[B(\Delta,\Gamma)_2]\cos(\Delta_R\tau)+\mathrm{Im}[B(\Delta,\Gamma)_2]\sin(\Delta_R|\tau|)}{[(\Delta^\alpha_S)^2+(\Gamma^\alpha_{fg+2-S})^2][(\Delta^\beta_1)^2+(\Gamma^\beta_{fg+2-1})^2]}\right]\\
&+\left[\frac{\mathrm{Re}[B(\Delta,\Gamma)_3]\cos(\Delta_R\tau)+\mathrm{Im}[B(\Delta,\Gamma)_3]\sin(\Delta_R|\tau|)}{[(\Delta^\alpha_1)^2+(\Gamma^\alpha_{fg-2-1})^2][(\Delta^\beta_1)^2+(\Gamma^\beta_{fg+2+1})^2]}\right]\\
&+\left[\frac{\mathrm{Re}[B(\Delta,\Gamma)_4]\cos(\Delta_R\tau)+\mathrm{Im}[B(\Delta,\Gamma)_4]\sin(\Delta_R|\tau|)}{[(\Delta^\alpha_1)^2+(\Gamma^\alpha_{fg+2-1})^2][(\Delta^\beta_1)^2+(\Gamma^\beta_{fg-2+1})^2]}\right]\\
&+\left[\frac{\mathrm{Re}[B(\Delta,\Gamma)_5]\cos(\Delta_R\tau)+\mathrm{Im}[B(\Delta,\Gamma)_5]\sin(\Delta_R|\tau|)}{[(\Delta^\alpha_S)^2+(\Gamma^\alpha_{fg-2-S})^2][(\Delta^\beta_S)^2+(\Gamma^\beta_{fg+2+S})^2]}\right]\\
&+\left.\left[\frac{\mathrm{Re}[B(\Delta,\Gamma)_6]\cos(\Delta_R\tau)+\mathrm{Im}[B(\Delta,\Gamma)_6]\sin(\Delta_R|\tau|)}{[(\Delta^\alpha_S)^2+(\Gamma^\alpha_{fg+2-S})^2][(\Delta^\beta_S)^2+(\Gamma^\beta_{fg-2+S})^2]}\right]\right],
\end{aligned} \tag{B1}$$

from which $G(\beta,\alpha)$, $G(\alpha,\alpha)$, and $G(\beta,\beta)$ can be obtained. The weighting of the sines and cosines is given by the complex functions, whose real and imaginary parts can be written as

$$\mathrm{Re}[B(\Delta,\Gamma)_1]=(\Delta_R^2+\Gamma_{1+S}\Gamma_{2+2+1+S})(\Delta_S^\alpha\Delta_1^\beta+\Gamma_{fg-2-S}^\alpha\Gamma_{fg-2-1}^\beta)-2\Delta_R\Gamma_{2+1+S}(\Delta_1^\beta\Gamma_{fg-2-S}^\alpha-\Delta_S^\alpha\Gamma_{fg-2-1}^\beta) \tag{B2}$$

and

$$\mathrm{Im}[B(\Delta,\Gamma)_1]=2\Delta_R\Gamma_{2+1+S}(\Delta_S^\alpha\Delta_1^\beta+\Gamma_{fg-2-S}^\alpha\Gamma_{fg-2-1}^\beta)+(\Delta_R^2-\Gamma_{1+S}\Gamma_{2+2+1+S})(\Delta_1^\beta\Gamma_{fg-2-S}^\alpha-\Delta_S^\alpha\Gamma_{fg-2-1}^\beta)\ , \tag{B3}$$

respectively. Equations (B2) and (B3) can be abbreviated as $B(\Delta,\Gamma)_1=B(\Delta_S^\alpha,\Delta_1^\beta,\Gamma_{fg-2-S}^\alpha,\Gamma_{fg-2-1}^\beta)$ from which the terms

$$B(\Delta,\Gamma)_2=B(\Delta_S^\alpha,\Delta_1^\beta,\Gamma_{fg+2-S}^\alpha,\Gamma_{fg+2-1}^\beta),\quad B(\Delta,\Gamma)_3=B(\Delta_1^\beta,\Delta_1^\alpha,\Gamma_{fg-2-1}^\beta,\Gamma_{fg+2+1}^\alpha)\ ,$$

$$B(\Delta,\Gamma)_4=B(\Delta_1^\beta,\Delta_1^\alpha,\Gamma_{fg-2+1}^\beta,\Gamma_{fg+2-1}^\alpha),\quad B(\Delta,\Gamma)_5=B(\Delta_S^\alpha,\Delta_S^\beta,\Gamma_{fg-2-S}^\alpha,\Gamma_{fg+2+S}^\beta)\ ,$$

$$B(\Delta,\Gamma)_6=B(\Delta_S^\alpha,\Delta_S^\beta,\Gamma_{fg+2-S}^\alpha,\Gamma_{fg-2+S}^\beta)$$

are obtained.

The second purely-field-damped transient is not seen in the δ-function limit of $J_1(\omega_1')$ and $J_D(\omega_S')$. This signal component is a zero-frequency transient and can be written as

$$I_{\Gamma_{2+2}}^{\alpha\beta}\approx e^{-2\Gamma_{2+2}|\tau|}(y_\alpha^2[\Gamma_1K_1(\alpha,\alpha)+\Gamma_SK_2(\alpha,\alpha)+\Gamma_1\Gamma_SK_3(\alpha,\alpha)]+y_\beta^2[\Gamma_1K_1(\beta,\beta)+\Gamma_SK_2(\beta,\beta)+\Gamma_1\Gamma_SK_3(\beta,\beta)]$$
$$+y_\alpha y_\beta\{\Gamma_1[K_1(\alpha,\beta)+K_1(\beta,\alpha)]+\Gamma_S[K_2(\alpha,\beta)+K_2(\beta,\alpha)]+\Gamma_1\Gamma_S[K_3(\alpha,\beta)+K_3(\beta,\alpha)]\})\ . \tag{B4}$$

For the unlike chromophore cross terms, we have

$$K_1(\alpha,\beta)=\frac{1}{[(\Delta_R)^2+(\Gamma_{1-S})^2][(\Delta_R)^2+(\Gamma_{1+S})^2]}$$

$$\times\left[\frac{k_1(\Delta,\Gamma)_1}{[(\Delta_S^\alpha)^2+(\Gamma_{fg-2+S}^\alpha)^2][(\Delta_S^\beta)^2+(\Gamma_{fg-2-S}^\beta)^2]}+\frac{k_1(\Delta,\Gamma)_2}{[(\Delta_S^\alpha)^2+(\Gamma_{fg-2+S}^\alpha)^2][(\Delta_S^\beta)^2+(\Gamma_{fg+2-S}^\beta)^2]}\right.$$
$$\left.+\frac{k_1(\Delta,\Gamma)_3}{[(\Delta_S^\alpha)^2+(\Gamma_{fg+2+S}^\alpha)^2][(\Delta_S^\beta)^2+(\Gamma_{fg-2-S}^\beta)^2]}+\frac{k_1(\Delta,\Gamma)_4}{[(\Delta_S^\alpha)^2+(\Gamma_{fg+2+S}^\alpha)^2][(\Delta_S^\beta)^2+(\Gamma_{fg+2-S}^\beta)^2]}\right]\ . \tag{B5}$$

The function $k_1(\Delta,\Gamma)_1$ is given by

$$k_1(\Delta,\Gamma)_1=k_1(\Delta_S^\alpha,\Delta_S^\beta,\Gamma_{fg-2+S}^\alpha,\Gamma_{fg-2-S}^\beta)$$
$$=[(\Delta_R)^2+\Gamma_{1-S}\Gamma_{1+S})(\Delta_S^\alpha\Delta_S^\beta+\Gamma_{fg-2+S}^\alpha\Gamma_{fg-2-S}^\beta)-2\Delta_R\Gamma_S(\Delta_S^\alpha\Gamma_{fg-2-S}^\beta-\Gamma_{fg-2+S}^\alpha\Delta_S^\beta)]\ , \tag{B6}$$

where the remaining $k_1(\Delta,\Gamma)_i$ terms can be written as $k_1(\Delta,\Gamma)_2=k_1(\Delta_S^\alpha,\Delta_S^\beta,\Gamma_{fg-2+S}^\alpha,\Gamma_{fg+2-S}^\beta)$, $k_1(\Delta,\Gamma)_3=k_1(\Delta_S^\alpha,\Delta_S^\beta,\Gamma_{fg+2+S}^\alpha,\Gamma_{fg-2-S}^\beta)$, and $k_1(\Delta,\Gamma)_4=k_1(\Delta_S^\alpha,\Delta_S^\beta,\Gamma_{fg+2+S}^\alpha,\Gamma_{fg+2-S}^\beta)$. In Eq. (B4), $K_2(\alpha,\beta)$ can be obtained from $K_1(\alpha,\beta)$ under the following parameter interchange:

$$K_2(\alpha,\beta)=\hat{T}(\Delta_S^\alpha\rightarrow\Delta_1^\alpha,\Delta_S^\beta\rightarrow\Delta_1^\beta,\Gamma_S-\Gamma_1)K_1(\alpha,\beta)\ , \tag{B7}$$

and $K_3(\alpha,\beta)$ is given by

$$K_3(\alpha,\beta)=\frac{2}{[(\Delta_S^\alpha)^2+(\Gamma_{fg-2+S}^\alpha)^2][(\Delta_S^\alpha)^2+(\Gamma_{fg-2-S}^\alpha)^2][(\Delta_1^\alpha)^2+(\Gamma_{fg-2+1}^\alpha)^2][(\Delta_1^\alpha)^2+(\Gamma_{fg-2-1}^\alpha)^2]}$$
$$\times\left[\mathrm{Re}[k_3(\Delta,\Gamma)]\left[\frac{\Gamma_{fg+fg-2-2}^{\alpha\beta}}{[(\Delta_{fg-fg}^{\alpha\beta})^2+(\Gamma_{fg+fg-2-2}^{\alpha\beta})^2]}+\frac{\Gamma_{fg+fg}^{\alpha\beta}}{[(\Delta_{fg-fg}^{\alpha\beta})^2+(\Gamma_{fg+fg}^{\alpha\beta})^2]}\right]\right.$$
$$\left.+\mathrm{Im}[k_3(\Delta,\Gamma)]\left[\frac{\Delta_{fg-fg}^{\alpha\beta}}{[(\Delta_{fg-fg}^{\alpha\beta})^2+(\Gamma_{fg+fg-2-2}^{\alpha\beta})^2]}+\frac{\Delta_{fg-fg}^{\alpha\beta}}{[(\Delta_{fg-fg}^{\alpha\beta})^2+(\Gamma_{fg+fg}^{\alpha\beta})^2]}\right]\right]$$
$$+(\mathcal{T}_{\Gamma_{fg-2\pm S}^Q\rightarrow\Gamma_{fg+2\pm S}^Q}+\mathcal{T}_{\Gamma_{fg-2\pm1}^Q\rightarrow\Gamma_{fg+2\pm1}^Q})\ , \tag{B8}$$

The real and imaginary parts of $k_3(\Delta,\Gamma)$ are written as

$$\mathrm{Re}[k_3(\Delta,\Gamma)]=(\Delta_S^\alpha-\Gamma_{fg-2+S}^\alpha\Gamma_{fg-2-S}^\alpha)(\Delta_1^\alpha-\Gamma_{fg-2+1}^\alpha\Gamma_{fg-2-1}^\alpha)-4\Delta_1^\alpha\Delta_s^\alpha(\Gamma_{fg-2}^\alpha)^2 \tag{B9}$$

and

$$\mathrm{Im}[k_3(\Delta,\Gamma)]=2[\Delta_s^\alpha\Gamma_{fg-2}^\alpha(\Delta_1^\alpha-\Gamma_{fg-2+1}^\alpha\Gamma_{fg-2-1}^\alpha)+\Delta_1^\alpha\Gamma_{fg-2}^\alpha(\Delta_S^\alpha-\Gamma_{fg-2+S}^\alpha\Gamma_{fg-2-S}^\alpha)]\ , \tag{B10}$$

respectively.

In Sec. III C, we presented electronically resonant CSRS signal transients oscillating at the detunings Δ^{Q} and Δ'^{Q} from electronically ground- and excited-state Raman modes, respectively. The signal components given in Eqs. (3.49) and (3.56) as $F_{AC^*}(\alpha,\beta)+F_{CA^*}(\alpha,\beta)$ and $F'_{AC^*}(\alpha,\beta)+F'_{CA^*}(\alpha,\beta)$, respectively, are defined here. The former component can be written as

$$
\begin{aligned}
F_{AC^*}(\alpha,\beta)+F_{CA^*}(\alpha,\beta)=&L^{1}_{AC^*+CA^*}(\Delta,\Gamma)L^{2}_{AC^*+CA^*}(\Delta,\Gamma)e^{-\Gamma^{\alpha\alpha}_{fg+fg+1+S}|\tau|}\\
&\times\left\{\left[\mathrm{Re}[U_1(\Delta,\Gamma)]\left[\frac{\mathrm{Im}[U_2(\Delta,\Gamma)]}{|U_2(\Delta,\Gamma)|^2}+\frac{\mathrm{Im}[U_3(\Delta,\Gamma)]}{|U_3(\Delta,\Gamma)|^2}\right]\right.\right.\\
&-\mathrm{Im}[U_1(\Delta,\Gamma)]\left[\frac{\mathrm{Re}[U_2(\Delta,\Gamma)]}{|U_2(\Delta,\Gamma)|^2}+\frac{\mathrm{Re}[U_3(\Delta,\Gamma)]}{|U_3(\Delta,\Gamma)|^2}\right]\\
&+\mathrm{Re}[U_4(\Delta,\Gamma)]\left[\frac{\mathrm{Im}[U_5(\Delta,\Gamma)]}{|U_5(\Delta,\Gamma)|^2}+\frac{\mathrm{Im}[U_6(\Delta,\Gamma)]}{|U_6(\Delta,\Gamma)|^2}+\frac{\mathrm{Im}[U_6(\Delta,\Gamma)]}{|U_6(\Delta,\Gamma)|^2}\right]\\
&\left.-\mathrm{Im}[U_6(\Delta,\Gamma)]\left[\frac{\mathrm{Re}[U_5(\Delta,\Gamma)]}{|U_5(\Delta,\Gamma)|^2}+\frac{\mathrm{Re}[U_6(\Delta,\Gamma)]}{|U_6(\Delta,\Gamma)|^2}\right]\right]\cos(\Delta^{\alpha}\tau)\\
&+\left[\mathrm{Re}[U_1(\Delta,\Gamma)]\left[\frac{\mathrm{Re}[U_2(\Delta,\Gamma)]}{|U_2(\Delta,\Gamma)|^2}+\frac{\mathrm{Re}[U_3(\Delta,\Gamma)]}{|U_3(\Delta,\Gamma)|^2}\right]\right.\\
&+\mathrm{Im}[U_1(\Delta,\Gamma)]\left[\frac{\mathrm{Im}[U_2(\Delta,\Gamma)]}{|U_2(\Delta,\Gamma)|^2}+\frac{\mathrm{Im}[U_3(\Delta,\Gamma)]}{|U_3(\Delta,\Gamma)|^2}\right]\\
&+\mathrm{Re}[U_4(\Delta,\Gamma)]\left[\frac{\mathrm{Re}[U_5(\Delta,\Gamma)]}{|U_5(\Delta,\Gamma)|^2}+\frac{\mathrm{Re}[U_6(\Delta,\Gamma)]}{|U_6(\Delta,\Gamma)|^2}\right]\\
&\left.+\mathrm{Im}[U_4(\Delta,\Gamma)]\left[\frac{\mathrm{Im}[U_5(\Delta,\Gamma)]}{|U_5(\Delta,\Gamma)|^2}+\frac{\mathrm{Im}[U_6(\Delta,\Gamma)]}{|U_6(\Delta,\Gamma)|^2}\right]\right]\sin(\Delta^{\alpha}|\tau|)\Bigg\}\,. \qquad \text{(B11)}
\end{aligned}
$$

In the above equation, $L^{1}_{AC^*+CA^*}(\Delta,\Gamma)$ is identical to $L^{1}_{AA^*}(\Delta,\Gamma)$ given in Eq. (3.52) and $L^{2}_{AC^*+CA^*}(\Delta,\Gamma)$ is written as

$$
L^{2}_{AC^*+CA^*}(\Delta,\Gamma)=\frac{1}{[(\Delta^{\alpha}_{nf-S})^2+(\Gamma^{\alpha}_{nf+S})^2][(\Delta^{\beta}_{nf-S})^2+(\Gamma^{\beta}_{nf-S})^2][(\Delta^{\alpha}_{mg-1})^2+(\Gamma^{\alpha}_{mg+1})^2]}\,. \qquad \text{(B12)}
$$

The complex functions $U_i(\Delta,\Gamma)$ are given in terms of their real and imaginary parts as

$$
\begin{aligned}
\mathrm{Re}[U_1(\Delta,\Gamma)]=&\mathrm{Re}[A(\Delta,\Gamma)][\Delta^{\alpha}_{mg-1}(\Delta^{\alpha}_{nf-S}\Delta^{\beta}_{nf-S}+\Gamma^{\alpha}_{nf+S}\Gamma^{\beta}_{nf-S})+\Gamma^{\alpha}_{mg+1}(\Gamma^{\alpha}_{nf+S}\Delta^{\beta}_{nf-S}-\Gamma^{\beta}_{nf-S}\Delta^{\alpha}_{nf-S})]\\
&+\mathrm{Im}[A(\Delta,\Gamma)][\Delta^{\alpha}_{mg-1}(\Gamma^{\alpha}_{nf+S}\Delta^{\beta}_{nf-S}-\Gamma^{\beta}_{nf-S}\Delta^{\alpha}_{nf-S})-\Gamma^{\alpha}_{mg+1}(\Delta^{\alpha}_{nf-S}\Delta^{\beta}_{nf-S}+\Gamma^{\alpha}_{nf+S}\Gamma^{\beta}_{nf-S})]\,, \qquad \text{(B13)}\\
\mathrm{Im}[U_1(\Delta,\Gamma)]=&\mathrm{Im}[A(\Delta,\Gamma)][\Delta^{\alpha}_{mg-1}(\Delta^{\alpha}_{nf-S}\Delta^{\beta}_{nf-S}+\Gamma^{\alpha}_{nf+S}\Gamma^{\beta}_{nf-S})+\Gamma^{\alpha}_{mg+1}(\Gamma^{\alpha}_{nf+S}\Delta^{\beta}_{nf-S}-\Gamma^{\beta}_{nf-S}\Delta^{\alpha}_{nf-S})]\\
&-\mathrm{Re}[A(\Delta,\Gamma)][\Delta^{\alpha}_{mg-1}(\Gamma^{\alpha}_{nf+S}\Delta^{\beta}_{nf-S}-\Gamma^{\beta}_{nf-S}\Delta^{\alpha}_{nf-S})-\Gamma^{\alpha}_{mg+1}(\Delta^{\alpha}_{nf-S}\Delta^{\beta}_{nf-S}+\Gamma^{\alpha}_{nf+S}\Gamma^{\beta}_{nf-S})]\,, \qquad \text{(B14)}\\
U_2(\Delta,\Gamma)=&(\Delta^{\beta\alpha}_{ng-fg-S}\Delta^{\alpha\beta}+\Gamma^{\beta\alpha}_{ng-fs-S})+i(\Delta^{\beta\alpha}_{ng-fg-S}\Gamma^{\beta\alpha}_{fg-fg-S-1}-\Gamma^{\beta\alpha}_{ng-fg-S}\Delta^{\alpha\beta})\,, \qquad \text{(B15)}\\
U_3(\Delta,\Gamma)=&(\Delta^{\beta\alpha}_{ng+fg-1}\Delta^{\beta\alpha}_{fg-fg}+\Gamma^{\beta\alpha}_{nf+fg+1}\Gamma^{\beta\alpha}_{fg+fg})+i(\Delta^{\beta\alpha}_{ng+fg-1}\Gamma^{\beta\alpha}_{fg+fg}-\Gamma^{\beta\alpha}_{ng+fg+1}\Delta^{\beta\alpha}_{fg-fg})\,, \qquad \text{(B16)}\\
U_4(\Delta,\Gamma)=&\hat{T}(\Gamma^{\alpha}_{nf+S}\rightarrow\Gamma^{\alpha}_{nf-S},\Gamma^{\beta}_{nf-S}\rightarrow\Gamma^{\beta}_{nf+S})U_1(\Delta,\Gamma)\,, \qquad \text{(B17)}\\
U_5(\Delta,\Gamma)=&(\Delta^{\beta}_{mg-1}\Delta^{\alpha\beta}-\Gamma^{\beta}_{nf-fg-1}\Gamma^{\alpha\beta}_{fg-fg-S-1})+i(\Delta^{\alpha\beta}\Gamma^{\beta}_{ng-fg-1}+\Gamma^{\alpha\beta}_{fg-fg-S-1}\Delta^{\beta}_{mg-1})\,, \qquad \text{(B18)}
\end{aligned}
$$

and

$$
\begin{aligned}
U_6(\Delta,\Gamma)=&(\Delta^{\beta}_{mg-1}\Delta^{\alpha\beta}_{fg-fg}-\Gamma^{\beta}_{ng-fg-1}\Gamma^{\alpha\beta}_{fg+fg})\\
&+i(\Delta^{\alpha\beta}_{fg-fg}\Gamma^{\beta}_{ng-fg-1}+\Gamma^{\alpha\beta}_{fg+fg}\Delta^{\beta}_{mg-1})\,. \qquad \text{(B19)}
\end{aligned}
$$

Finally, the $F'_{AC^*}(\alpha,\beta)+F'_{CA^*}(\alpha,\beta)$ component of Eq. (3.56) is similar to form to Eq. (B11) and can be written in terms of the following parameter change:

$$
\begin{aligned}
F'_{AC^*}(\alpha,\beta)+F'_{CA^*}(\alpha,\beta)=&\hat{T}(\omega^{Q}_{fg}\rightarrow\omega^{Q}_{mn},\Gamma^{Q}_{fg}\rightarrow\Gamma^{Q}_{mn})\\
&\times[F_{AC^*}(\alpha,\beta)+F_{CA^*}(\alpha,\beta)] \qquad \text{(B20)}
\end{aligned}
$$

for both $Q=\alpha$ and β.

APPENDIX C

The effects of inhomogeneous broadening of the material resonances on the τ dependence of fourth-wave signal is treated by distributing, at the amplitude level, the material Bohr frequencies, or equivalently, their detunings. Here we write the polarization correlation function of Eq. (1.16), without the spatial factor, as

$$C(t',s';\tau)=\left\langle\left\langle\int d\Delta_j^{\alpha} g(\Delta_j^{\alpha})\hat{p}^{(3)}(\Delta_j^{\alpha},t';\tau)\right\rangle_{\alpha'} \times\left\langle\int d\Delta_k^{\beta} g(\Delta_k^{\beta})\hat{p}^{(3)}(\Delta_k^{\beta},s';\tau)\right\rangle_{\beta'}^{\dagger}\right\rangle_R . \tag{C1}$$

The averages $\langle\ \rangle_{Q'}$ are over degrees of freedom of the material bath except for those that leave a static distribution of Bohr frequencies on the experimental time scales. Consider the electronically nonresonant CSRS process (Δ_j^Q and $\Delta_k^Q \rightarrow \Delta_1^Q$ and Δ_S^Q) for a Gaussian distribution of vibrational Bohr frequencies where

$$g(\Delta_j^Q)=\frac{1}{\sqrt{2\pi}\delta^Q} e^{-(\Delta_j^Q/\delta^Q)^2} , \tag{C2}$$

$g(\Delta_S^Q)=g(\Delta_1^Q)$, and δ^Q ($Q=\alpha,\beta$) is the inhomogeneous width for the ensemble of chromophore type Q. Considering Lorentzian spectral densities for all intervening fields, and assuming a broad inhomogeneous distribution ($\delta^Q \gg \Gamma_{fg}^Q$), Eq. (3.19) is now written as

$$I^{\alpha\beta}(\tau)=I'^{\alpha\beta}_{\Gamma_{2+2+1+S}}(\tau)+I'^{\alpha\beta}_{\Gamma_{2+2}}(\tau)+I_c'^{\alpha\beta} , \tag{C3}$$

where

$$I^{\alpha\beta}_{\Gamma_{2+2+1+S}}(\tau)\approx\Gamma_2\{y_\alpha^2 G'(\alpha,\alpha)+y_\beta^2 G'(\beta,\beta) +y_\alpha y_\beta[G'(\alpha,\beta)+G'(\beta,\alpha)]\} . \tag{C4}$$

The cross term between unlike chromophores is given by

$$G'(\alpha,\beta)=\frac{e^{-\Gamma_{2+2+1+S}|\tau|}}{[(\Delta_R)^2+(\Gamma_{1+S})^2][(\Delta_R)^2+(\Gamma_{2+2+1+S})^2]} \times\left\{\exp\left[\left[\frac{\Gamma_{fg+2+1}^{\alpha}}{\delta^{\alpha}}\right]^2\right]\exp\left[\left[\frac{\Gamma_{fg+2+S}^{\beta}}{\delta^{\beta}}\right]^2\right] \times\{[(\Delta_R)^2+\Gamma_{1+S}\Gamma_{2+2+1+S}]\cos(\Delta_R\tau)+2\Delta_R\Gamma_{2+1+S}\sin(\Delta R|\tau|)\}+\mathcal{T}(\Gamma_1\leftrightarrow\Gamma_S)\right\} , \tag{C5}$$

where $\mathcal{T}(\Gamma_1\leftrightarrow\Gamma_S)$ represents identical terms with Γ_1 replaced by Γ_S and vice versa, from which $G'(\alpha,\alpha)$, $G'(\beta,\beta)$, and $G'(\beta,\alpha)$ can be obtained. The second term on the rhs of Eq. (C3) is similar to the purely-light-damped (Γ_{2+2}) signal component given in Eq. (B4), except the material-dependent Lorentzian line shapes are replaced with Gaussian line shapes, width δ^Q. The (constant) background signal generated from the intensity correlation of the field is represented by the third term in Eq. (C3). Significantly, all contributions from the material-dependent transients given in Eq. (3.19), including the detuning oscillations, are absent.

In the electronically resonant case inhomogeneous broadening of the material states also eliminates the detuning oscillations and quantum beats associated with electronically resonant CSRS discussed in Sec. III C. Thus a static distribution of material Bohr frequencies tends to disrupt the phase coherence between the superposition states on different chromophores driven by conjugate broadband fields, and as a result, diminishes the destructive (or constructive) interference; the net field-induced coupling is weakened, and eventually destroyed for a sufficiently broad static distribution of Bohr frequencies.

[1] A. M. Weiner, S. DeSilvestri, and E. P. Ippen, J. Opt. Soc. Am. B **2**, 654 (1985).

[2] J. K. Steehler and J. C. Wright, J. Chem. Phys. **83**, 3188 (1985); **83**, 3200 (1985); M. T. Riebe and J. C. Wright, *ibid.* **88**, 2981 (1988).

[3] D. P. Weitekamp, K. Duppen, and D. A. Wiersma, Phys. Rev. A **27**, 3089 (1983).

[4] K. Duppen, D. P. Weitekamp, and D. A. Wiersma, Chem. Phys. Lett. **106**, 147 (1984); **108**, 551 (1984).

[5] K. J. Vink, S. Deboer, J. J. Plijter, A. J. Hoff, and D. A. Wiersma, Chem. Phys. Lett. **142**, 433 (1987).

[6] S. Velsko and R. H. Hochstasser, J. Phys. Chem. **89**, 2240 (1985).

[7] P. M. Felker, B. F. Henson, T. C. Corcoran, L. L. Conell, and G. V. Hartland, Chem. Phys. Lett. **142**, 439 (1987); P. M. Felker and G. V. Hartland, *ibid.* **134**, 503 (1987); G. V. Hartland and P. M. Felker, J. Chem. Phys. **91**, 5527 (1987).

[8] G. Eyring and M. D. Fayer, J. Chem. Phys. **81**, 4314 (1987); K. Nelson, R. Casalegno, R. J. D. Miller, and M. D. Fayer, *ibid.* **77**, 1144 (1982).

[9] T. Hattori and T. Kobayashi, Chem. Phys. Lett. **133**, 230 (1987).

[10] C. Kalpouzos, W. T. Lotshaw, D. McMorrow, and G. A. Kenny-Wallace, J. Phys. Chem. **91**, 2028 (1987).

[11] C. L. Schosser and D. D. Dlott, Phys. Rev. B **30**, 2149 (1984); J. Chem. Phys. **80**, 1369 (1984): J. Kosic, R. E. Cline, and D.

D. Dlott, Chem. Phys. Lett. **103**, 109 (1983).
[12]D. DeBeer, E. Usadi, and S. R. Hartmann, Phys. Rev. Lett. **60**, 1262 (1988).
[13]I. A. Walmsley, M. Mitsunaga, and C. L. Tang, Phys. Rev. A **38**, 4681 (1988); M. J. Rosker, F. W. Wise, and C. L. Tang, Phys. Rev. Lett. **57**, 321 (1986).
[14]Y.-X. Yan, E. B. Gamble, Jr., and K. A. Nelson, J. Chem. Phys. **83**, 5391 (1985).
[15]S. Ruhman, A. G. Joly, B. Kohler, L. R. Williams, and K. A. Nelson, Rev. Phys. Appl. **2**, 1717 (1987).
[16]J. E. Golub and T. W. Mossberg, J. Opt. Soc. Am. B **3**, 554 (1986); Opt. Lett. **11**, 431 (1986).
[17]R. Leonhardt, W. Holzapfel, W. Zinth, and W. Kaiser, Chem. Phys. Lett. **133**, 373 (1987).
[18]J. Chesnoy and A. Mokhtari, Phys. Rev. A **38**, 3566 (1988).
[19]K. Wynne, M. Muller, and J. D. W. Van Voorst, Phys. Rev. Lett. **62**, 3031 (1989).
[20]G. V. Hartland, B. F. Henson, and P. M. Felker, J. Chem. Phys. **91**, 1478 (1989).
[21]B. Fluegel, N. Peyghambarian, G. Olbright, M. Lindberg, S. W. Koch, M. Joffre, D. Hulin, A. Migus, and A. Antonetti, Phys. Rev. Lett. **59**, 2588 (1987).
[22]M. Joffre, D. Hulin, A. Migus, A. Antonetti, C. Benoit a la Guillaume, N. Peyghambarian, M. Lindberg, and S. W. Koch, Opt. Lett. **13**, 276 (1988).
[23]M. A. Dugan, J. S. Melinger, and A. C. Albrecht, Chem. Phys. Lett. **147**, 411 (1988).
[24]J. S. Melinger and A. C. Albrecht, J. Phys. Chem. **91**, 2704 (1987).
[25]M. Aihara, Phys. Rev. B **25**, 53 (1982).
[26]S. Mukamel, Phys. Rev. A **28**, 3480 (1983).
[27]S. Mukamel and R. F. Loring, J. Opt. Soc. Am. B **3**, 595 (1986).
[28]Y. Prior and A. Ben-Rueven, Phys. Rev. A **33**, 2362 (1986).
[29]H. Tsunetsugu and E. Hanamura (unpublished).
[30]H. R. Zaidi, Phys. Rev. A **36**, 3897 (1987).
[31]A. M. Levine, N. Chencinski, W. M. Schreiber, A. N. Weiszmann, and Y. Prior, Phys. Rev. A **35**, 2550 (1987).
[32]P. F. Fracassi, L. Angeloni, and R. G. Della Valle, Chem. Phys. **115**, 169 (1987).
[33]M. S. Kumar and G. S. Agarwal, Phys. Rev. A **33**, 1817 (1986).
[34]S. L. Palfrey and T. F. Heinz, J. Opt. Soc. Am. B **2**, 167 (1985).
[35]W. Vogel, D.-G. Welsch, and B. Wilhelmi, Phys. Rev. A **37**, 3825 (1988).
[36]W. S. Warren, J. Chem. Phys. **81**, 5437 (1984).
[37]W. S. Warren and M. A. Banash, *Coherence and Quantum Optics V,* edited by L. Mandel and E. Wolf (Plenum, New York, 1984), p. 959.
[38]W. S. Warren and Ahmed H. Zewial, J. Chem. Phys. **78**, 2279 (1983); **78**, 2298 (1983).
[39]N. Morita and T. Yajima, Phys. Rev. A **30**, 2525 (1984).
[40]A. Asaka, H. Nakatsuka, M. Fujiwara, and M. Matsuoka, Phys. Rev. A **29**, 2286 (1984).
[41]R. Beach and S. R. Hartmann, Phys. Rev. Lett. **53**, 663 (1984).
[42]T. Hattori, A. Terasaki, and T. Kobayashi, Phys. Rev. A **35**, 715 (1987).
[43]G. S. Agarwal, and C. V. Kunasz, Phys. Rev. A **27**, 996 (1983).
[44]Y. Prior, I. Schek, and J. Jortner, Phys. Rev. A **31**, 3775 (1985).
[45]A. G. Kofman, A. M. Levine, and Y. Prior, Phys. Rev. A **37**, 1248 (1988).
[46]T. W. Mossberg, Opt. Lett. **7**, 77 (1982).
[47]M. D. Reid, A. Lane, and D. F. Walls, in *Proceedings of the Fourth International Symposium on Quantum Optics,* edited by J. D. Harvey and D. F. Walls (Springer, New York, 1985).
[48]D. A. Holm, M. Sargent III, and B. A. Capron, Opt. Lett. **11**, 443 (1986).
[49]R. E. Slusher, B. Yurke, P. Grangier, A. La Porta, D. F. Walls, and M. Reid, J. Opt. Soc. Am. B **4**, 1453 (1987).
[50]R. Loring (private communication).
[51]P. Stehle, Phys. Rep. **156**, 67 (1987).
[52]E. Hanamura, Solid State Commun. **51**, 697 (1984).
[53]S. Mukamel and E. Hanamura, Phys. Rev. A **33**, 1099 (1986).
[54]J. Perina, *Coherence of Light,* 2nd ed. (Reidel, Dordrecht, 1985); *Quantum Statistics of Linear and Nonlinear Optical Phenomena* (Reidel, Dordrecht, 1984).
[55]S. Mukamel, Phys. Rep. **93**, 1 (1982).
[56]J. Knoester and S. Mukamel, Phys. Rev. A **39**, 1899 (1989).
[57]K. Faid and R. Fox, Phys. Rev. A **34**, 4286 (1986).
[58]J. Budimir and J. L. Skinner, J. Stat. Phys. **49**, 1029 (1987).
[59]J. H. Eberly and K. Wodkiewicz, J. Opt. Soc. Am. **67**, 1252 (1977).
[60]K. Wodkiewicz and J. H. Eberly, Phys. Rev. A **32**, 992 (1985).
[61]G. S. Agarwal, Phys. Rev. A **25**, 3195 (1982).
[62]G. S. Agarwal, C. V. Kunasz, and J. Cooper, Phys. Rev. A **36**, 143 (1987).
[63]G. S. Agarwal, Phys. Rev. A **37**, 4741 (1988).
[64]P. Tchenio, A. De Barre, J.-C. Keller, and J.-L. Le Gouet, Phys. Rev. A **38**, 5235 (1988).
[65]A. G. Hofman, R. Zaibel, A. M. Levine, and Y. Prior, Phys. Rev. Lett. **1**, 251 (1988); Phys. Rev. A **41**, 6434 (1990).
[66]M. C. Wang and G. E. Uhlenbeck, Rev. Mod. Phys. **17**, 323 (1945).
[67]R. Kubo, J. Math. Phys. **4**, 174 (1963).
[68]Y. S. Bai and M. D. Fayer, Chem. Phys. **128**, 135 (1988).
[69]S. Mukamel, J. Chem. Phys. **71**, 2884 (1979).
[70]D. Lee, Ph.D. thesis, Cornell University, 1983; see also D. Lee and A. C. Albrecht, in *Advances in Infrared and Raman Spectroscopy,* edited by R. J. Clark and R. E. Hester (Wiley-Heyden, New York, 1985), Vol. 12.
[71]M. T. Riebe and J. C. Wright, J. Chem. Phys. **88**, 298 (1988); J. K. Steehler and J. C. Wright, *ibid.* **83**, 3188 (1985); **83**, 3200 (1985); R. J. Carlson and J. C. Wright, Chem. Phys. Lett. **140**, 101 (1987).
[72]A. Ben-Reuven and S. Mukamel, J. Phys. A **8**, 1313 (1975).
[73]V. Mirahi, Y. Prior, and S. Mukamel, Opt. Lett. **8**, 145 (1983).
[74]J. S. Melinger and A. C. Albrecht, J. Chem. Phys. **84**, 1247 (1986).
[75]Z. W. Li, C. Radzewicz, and M. G. Raymer, J. Opt. Soc. Am. B **5**, 2340 (1988).
[76]W. Zinth, M. C. Nuss, and W. Kaiser, Phys. Rev. A **30**, 1139 (1984); Opt. Commun. **44**, 262 (1983).
[77]Y. Prior, A. R. Bogdan, M. Dagenais, and N. Bloembergen, Phys. Rev. Lett. **46**, 111 (1981).